FLEXURAL BEHAVIOR OF UNGROUTED POST-TENSIONED CONCRETE MASONRY

JOHN MARIO GARCÍA GIRALDO

Thesis submitted to the Office of Research and Graduate Studies in partial fulfilment of the requirements for the Degree of Doctor in Engineering

Advisor:

RICARDO LEÓN BONETT DÍAZ

Medellín – Colombia, (June, 2016)

FLEXURAL BEHAVIOR OF UNGROUTED POST-TENSIONED CONCRETE MASONRY AND THEIR APPLICATION IN SOIL RETAINING WALLS

JOHN MARIO GARCÍA GIRALDO

Members of the Committee:

ANDREA PENNA.

JUAN DIEGO JARAMILLO FERNÁNDEZ.

ALBERT RICARDO ORTIZ LASPRILLA

Thesis submitted to the Office of Research and Graduate Studies in partial fulfilment of the requirements for the Degree of Doctor in Engineering

Medellín – Colombia, (June, 2016)

To my family and friends, especially my wife Liliana and our baby Alejandro, for their unconditional love and support, they are a blessing from God and their encouragement was crucial throughout all stages of my research project.

ACKNOWLEDGEMENTS

This project would not have been possible without the financial contributions made by the University of Medellin, and by direct industry sponsors Prefabricados Adoquin-Ar, Area Ingenieros Consultores, Andres Felipe Caballero and Ingeconcreto, who generously provided their products, services, facilities and other resources needed for the successful completion of this investigation. Thanking especially their managers, Engineer Juan P. Arbelaez and Engineer Hector Urrego, for their valuable technical comments and suggestions. Also to the undergraduate civil engineering students of the University of Medellin for their unconditional cooperation in the experimental work, and in the numerical processing of the results - especially Juan Manuel Maya who accompanied the whole experimental process and whose support was crucial in successfully carrying out this work. Gratitude extends to Colciencias and Enlazamundos for the financial support received covering part of the costs of my doctoral studies.

To my supervisors and friends, Professor Ricardo Bonett and Professor Christian Ledezma, without them it would not have been possible. Their encouragement, assistance, dedication and patience ensured post-tensioned masonry became more than just a passion, extending into my academic life.

Finally, a sincere thank you to Professor Arturo Schultz who provided guidance, assistance and helped ensure my exchange trip to the University of Minnesota was so successful, I will always remember his many valuable teachings both academically and in life itself.

Content

LIST OF TABLES XI

LIST OF FIGURES XII

NOTATION XIV

RESUMEN XVI

ABSTRACT XVII

CHAPTER 1. INTRODUCTION 1

1.1 INTRODUCTION 1
1.2 OBJECTIVES 1
1.3 HYPOTHESIS 1
1.4 METHODOLOGY 1
1.5 CONTENT 2
1.6 SCOPE 3
1.7 DECLARATION 3
1.8 DISCLAIMER 3
1.9 LIST OF PUBLICATIONS 4
1.9.1 JOURNAL ARTICLES 4
1.9.2 BOOK CHAPTERS 7
1.9.3 CONFERENCE PAPERS 8
1.9.4 PATENTS 10
1.9.5 ACADEMICALS INTERNSHIPS 12
1.10 AUTHOR'S CONTRIBUTION 12

CHAPTER 2. LITERATURE REVIEW 13

ABSTRACT 14
2.1 INTRODUCTION 14
2.2 HISTORICAL DEVELOPMENT OF POST-TENSIONED MASONRY 15
2.3 WORLDWIDE APPLICATIONS OF POSTTENSIONED MASONRY 16
2.4 POST-TENSIONED MASONRY CODES PROVISIONS 19

2.5 ADVANTAGES AND LIMITATIONS OF THE POST-TENSIONED MASONRY 20
2.6 PRESTRESSED MASONRY PATENTS 21
2.6.1 PROTO-II™ 21
2.6.2 INTEGRA™ WALLS SYSTEM. 21
2.6.3 DUR-O-WAL SURE-STRESS™ WALL SYSTEM. 22
2.6.4 VSL SYSTEM 22
2.7 CASES OF POST-TENSIONED MASONRY IN COLOMBIA AND CHILE 22
2.8 PREVIOUS RESEARCH CONDUCTED ON POST-TENSIONED MASONRY 24
2.8.1 BEAMS 24
2.8.2 OUT-OF-PLANE LOADING 24
2.8.3 IN-PLANE LOADING 25
2.8.4 SLABS 25
2.8.5 COLUMNS 25
2.9 SUMMARY OF CONCLUSIONS 26

CHAPTER 3. ANALYTICAL MODEL FOR COMPRESSION BEHAVIOR OF HOLLOW CONCRETE BLOCKS 27

ABSTRACT 28
3.1 INTRODUCTION 28
3.2 PROBLEM DESCRIPTION 28
3.3 STATE OF THE ART OF EMPIRICAL MODELS FOR CONCRETE 28
3.4 EXPERIMENTAL ASPECTS 29
3.4.1 GEOMETRY 29
3.4.2 CONSTITUTIVE MATERIALS 29
3.4.3 METHODOLOGY OF THE EXPERIMENTAL PROGRAM 29
3.4.4 TEST SETUP 29
3.4.5 INSTRUMENTATION 30
3.5 TEST RESULTS 30
3.5.1 STRESS-STRAIN CURVES 30
3.5.2 TYPES OF FAILURE 31
3.5.3 MODULUS OF ELASTICITY 31
3.6 CORRELATION BETWEEN STRAIN AT THE MAXIMUM STRESS AND THE COMPRESSION STRENGTH 32
3.7 EXPERIMENTAL RESULTS VERSUS EXISTING ANALYTICAL MODELS 32
3.8 PROPOSED ANALYTICAL MODEL 33
3.9 DISCUSSION AND CONCLUSIONS 34

CHAPTER 4. STRESSES AT ULTIMATE STATE OF UNBONDED TENDONS IN UNGROUTED POST-TENSIONED MASONRY BEAMS 35

ABSTRACT **36**
4.1 INTRODUCTION **36**
4.2 REVIEW OF ANALYTICAL EXPRESSIONS AND CODE EQUATIONS TO ESTIMATE TENDON STRESS AT ULTIMATE STATE **37**
4.3 PROPOSED METHODOLOGY TO ESTIMATE THE TENDON STRESS INCREASE BASED ON BEAM DEFLECTION **38**
4.3.1 REVISED (RATIONAL) DERIVATION OF η AND K 40
4.3.1.1 PARAMETER η 40
4.3.1.2 PARAMETER K 40
4.3.1.3 PARAMETER ηK 40
4.3.2 EFFECT OF INELASTIC BEHAVIOR ON η AND K TENDON STRESS PARAMETERS 40
4.3.3 DEFINE THE CURVATURE DUCTILITY 41
4.3.3.1 ELASTIC STATE 41
4.3.3.2 INELASTIC STATE 41
4.3.4 ELIMINATING NEUTRAL AXIS DEPTH - TOTAL TENDON STRESS 43
4.3.5 SELECTION OF EFFECTIVE WIDTH FOR HOLLOW SECTIONS 43
4.3.6 MASONRY STRAIN DUCTILITY FACTOR 44
4.4 EXPERIMENTAL PROGRAM **44**
4.4.1 TEST SPECIMENS 45
4.4.2 MATERIAL PROPERTIES 46
4.4.2.1 HOLLOW CONCRETE BLOCKS 46
4.4.2.2 MORTAR AND CONCRETE 47
4.4.2.3 PRESTRESSING STEEL 47
4.4.3 TEST SETUP AND INSTRUMENTATION 47
4.5 EXPERIMENTAL RESULTS **47**
4.5.1 FAILURE MODE 48
4.5.2 LOAD-DEFLECTION RESPONSE 48
4.5.3 POST-TENSIONED MASONRY CODES ACCURACY 49
4.6 DISCUSSION AND CONCLUSIONS **53**

CHAPTER 5. FLEXURAL BEHAVIOR OF UNGROUTED POST-TENSIONED CONCRETE MASONRY BEAMS, WITH UNBONDED ECCENTRIC TENDONS **54**

ABSTRACT **55**
5.1 INTRODUCTION **55**
5.2 RESEARCH SIGNIFICANCE **55**
5.3 EXPERIMENTAL PROGRAM **56**
5.3.1 BEAM CONSTRUCTION 56
5.3.2 MATERIAL PROPERTIES 56
5.3.2.1 CONCRETE BLOCK AND MASONRY 56
5.3.2.2 ANCHORAGE AND DEVIATOR BLOCKS 57

5.3.2.3 Prestressing steel 58
5.3.4 Specimen details 58
5.3.5 Test configuration and instrumentation 59
5.4 Experimental results 60
5.4.1 Load deflection response 60
5.4.2 Cracking patterns 61
5.4.3 Failure mode 62
5.4.4 Effect of design variable factors 63
5.4.5 Masonry strength effect 63
5.4.6 Initial tendon prestress effect 63
5.5 Cyclic behavior 64
5.5.1 Cyclic versus monotonic behavior 64
5.5.2 Tendon stress increase 65
5.5.3 Stiffness degradation 65
5.6 Codes results 66
5.7 Conclusions 67

CHAPTER 6. STRUCTURAL TESTING OF UNGROUTED POST-TENSIONED CANTILEVER WALLS UNDER CYCLIC TRANSVERSE LOAD 68

Abstract 69
6.1 Introduction 69
6.2 Experimental setup 69
6.2.1 Materials properties 70
6.2.2 Details of specimens 70
6.2.3 Load history and instrumentation 71
6.3 Test results 73
6.3.1 Load-displacement curves 74
6.3.2 Failure modes 75
6.3.3 Tension bars measurements 76
6.3.4 Patterns of displacements measurements 78
6.4 Discussion 80
6.4.1 Cyclic and monotonic test 80
6.4.2 Effect of masonry strength 80
6.4.3 Effect of initial prestress 80
6.4.4 Initial stiffness and stiffness degradation 81
6.4.5 Residual post-tensioning force ratio 81
6.4.6 Residual displacement 82
6.5 Codes results 82
6.6 Discussion and conclusions 85

CHAPTER 7. CONCLUSIONS 86

CHAPTER 8. FUTURE RESEARCH 89

8.1 INTRODUCTION 90
8.2 MATERIALS AND ELEMENTS 90
8.3 ANALYSES AND DESIGN METHODS 90
8.4 BEHAVIOR OF THE STRUCTURAL SYSTEM 91
8.5 CONSTRUCTION PROCEDURE 91

REFERENCES 92

LIST OF TABLES

Table 3. 1 Stress-strain laws for concrete. 29
Table 4. 1 Summary of equations for tendon stress increment at failure in post-tensioned concrete beams 38
Table 4. 2. Summary of expressions to estimate the tendon stress increment in prestressed concrete masonry codes. 38
Table 4. 3. Comparisons of calculations between complete and simplify cross section. 44
Table 4. 4. Test beams details 45
Table 4. 5. Summary of test results 49
Table 4. 6. Summary of proposed methodology and code results 50
Table 5. 1. Compressive strength of masonry materials 57
Table 5. 2. Test beam details 59
Table 5. 3. Summary of test results 60
Table 5. 4. Worldwide code expressions 66
Table 5. 5. Summary of code calculations versus experimental results. 67
Table 6. 1. Masonry, mortar and concrete properties. 70
Table 6. 2. Tested walls properties 71
Table 6. 3. Test results 73
Table 6. 4. Initial stiffness 81
Table 6. 5. Worldwide code expressions to calculate ultimate tendon stress 83
Table 6. 6. Summary of code calculations for ultimate tendon stress versus experimental results 84
Table 6. 7. Summary of code calculations for ultimate moment versus experimental results 84

LIST OF FIGURES

Figure 2. 1 Monadnock Masonry Building, Chicago (Ganz, 1990). 14
Figure 2. 2. Tunnel under River Thames, England, 1825 (ABS ZERO) 15
Figure 2. 3. Worldwide applications of post-tensioned masonry. 18
Figure 2. 4 Post-tensioned masonry walls patents (Wight, 2006). 22
Figure 2. 5. Applications of Post-tensioned Masonry in Colombia 23
Figure 3. 1 . Experimental Setup of the tested samples. 30
Figure 3. 2. Coupler of displacement frame 30
Figure 3.3. Stress-strain curves of all tested blocks 30
Figure 3. 4. Diagonal crack, typical in low strength blocks. 31
Figure 3.5. Modulus of elasticity versus compression strength, of tested concrete blocks.. 31
Figure 3.6. Correlation between strain at maximum stress ($\boldsymbol{\varepsilon b}$) and the compression strength of the block ($\boldsymbol{fb'}$). 32
Figure 3. 7. Normalized stress-strain curves for a) $\boldsymbol{fb'}$=10MPa and b) $\boldsymbol{fb'}$=30MPa. 32
Figure 3. 8. Experimental data versus analytical models in concrete blocks a) low strength (fb′=10MPa) and b) high strength (fb′=30MPa). 33
Figure 3. 9. Analytical model versus experimental results for a) Low strength ($\boldsymbol{fb'}$=10MPa), b) High strength ($\boldsymbol{fb'}$=30MPa). 34
Figure 4. 1 Deflection beam shape 39
Figure 4. 2. Idealized curvature diagram 41
Figure 4. 3. Block geometry (a) Restraining block section (b) Block section (c) Cross section assumed (Dimensions: mm) 46
Figure 4. 4. Stress-strain curve in tested hollow concrete blocks (Garcia et al., 2013). 46
Figure 4. 5. Test setup 47
Figure 4. 6. Typical failure mode. 48
Figure 4. 7. Beam behavior curves of Beam 17 and Beam22 48
Figure 4. 8. Ultimate tension and tendon force increase expressions versus experimental results 52
Figure 5. 1. Beams construction 56
Figure 5. 2. Concrete Blocks. a) Hollow block b) Simplified cross section c) Deviator and anchorage blocks (units: mm) 58
Figure 5. 3. Test setup and instrumentation 60
Figure 5. 4. Typical load–deflection response (B-17) 61
Figure 5. 5. Normalized load–deflection beams 61
Figure 5. 6. Cracking patterns B-13 a) $0P_u$, b) $0.25P_u$, c) $0.5P_u$, d) $0.75P_u$, e) P_u, and f) Unload 62
Figure 5. 7. Typical failure mode a) Beam B-10, b) Beam B-21 62
Figure 5. 8. Effect of masonry strength a) B-17 vs B-21 b) B-1 vs B-11 63
Figure 5. 9. Effect of initial tendon prestress a) B-13 vs B-14 b) B-21 vs B-22 64
Figure 5. 10. Cyclic versus monotonic a) Low strength masonry b) High strength masonry 64

Figure 5. 11. Tendon stress increase a) Cyclic load B-11 b) Monotonic load B-13 and B14 65
Figure 5. 12. Normalized stiffness reduction 65
Figure 6. 1. Applied load history. 72
Figure 6. 2 Applied moment diagram 72
Figure 6. 3 Test specimen and instrumentation 73
Figure 6. 4. Load-Displacement curve. 74
Figure 6. 5. Envelope Load-Displacement curves 75
Figure 6. 6. Typical failure mode 75
Figure 6. 7. Rocking mechanism a) Lateral view b) Back view 76
Figure 6. 8. Load-Tendon Force curve 77
Figure 6. 9. Tendon force increment. 78
Figure 6. 10. Displacement profiles wall 4 a) Measurement profiles b) Experimental profiles 79
Figure 6. 11. Monotonic versus Cyclic curve. 80
Figure 6. 12. Low strength versus High strength curve. 80
Figure 6. 13. Incidence of initial prestress 81
Figure 6. 14. Normalized stiffness reduction. 81
Figure 6. 15. Residual tendon prestress ratio 82
Figure 6. 16. Residual displacement 82

NOTATION

The following symbols are used in this Thesis

A_{ps}= area of unbonded tendons;
A_n= net area of the concrete block section;
a= effective compression stress block depth;
b= width of beam section;
b_{eff}= effective width of beam section;
c= neutral axis depth;
d= distance from extreme compression fiber to centroid of prestressing tendon;
E_b= secant elasticity moduli of concrete block as per MSJC proposal;
E_c= secant elasticity moduli of concrete at maximum resistance $E_c = \frac{f_c'}{\varepsilon_c}$
E_i= initial tangent elasticity moduli corresponding to $\varepsilon = 0$.
E= elastic modulus of the beam cross section;
E_{ps}= modulus of elasticity of prestressing steel;
e= constant tendon eccentricity;
e_{mid}= tendon eccentricity at mid-span beam;
f_b'= maximum hollow concrete block compressive strength;
f_b= compression stress of the concrete block;
f_m'= maximum masonry compressive strength;
f_j' = maximum mortar compressive strength;
f_c= compression stress of the concrete;
f_c'= maximum compression stress of concrete;
f_{pe}= effective initial prestressing stress;
f_{pe}= initial tendon stress;
$f_{ps,u}$= prestressing steel stress at ultimate state;
f_{ps}= prestressing steel stress;
f_{pu}= ultimate prestressing steel stress;
h = overall depth of the section beam section;
S_d= distance between deviators (restraints) ;
T_{cr}= cracking tendon load;
T_i= effective initial tendon load;
T_u= ultimate tendon load;
t = width of vertical partitions of block unit;
t_{eff}= effective width as the sum of the vertical partitions;
W= weight of hollow concrete block;
Z= shear span or the distance between the point of maximum moment and point of contra flexure;
α= compression stress block magnitude factor;
β= compression stress block depth factor;
$\Delta\varepsilon_{cps}$= maximum strain increase in concrete;
$\Delta\varepsilon_{psb}$= maximum strain increase in equivalent amount of bonded prestressing steel beyond ε_{pe};
$\Delta\varepsilon_{psu}$= maximum strain increase in unbonded prestress steel beyond ε_{pe};
$\Delta f_{ps,u}$= ultimate tendon stress increment;
Δf_{ps}= tendon stress increment;
ΔL= tendon length increment;
ΔT= tendon tension force increment;
ΔT_u= maximum tendon load increment at ultimate;
δ_c= deformation at compression zone;
$\delta_{mid,cr}$= mid-span deflection at cracking state;
$\delta_{mid,u}$= mid-span deflection at ultimate state;
δ_{mid}= mid-span deflection;
ε_{ce}= effective strain in concrete;
ε_{cu}= concrete strain in the top fiber at ultimate;

I= moment of inertia of the beam section;
K= load type coefficient;
L= tendon length;
L_a= distance between the applied loads;
L_f= tendon length after loading;
L_l= effective span of the beam;
L_o= tendon length before loading;
L_{NA}= length of the neutral axis in the deformed shape;
L_p= plastic hinge length;
$M(x)$= bending moment along the span due to exterior load;
M_{max}=bending moment at mid-span section;
M_u= ultimate moment of resistance;
N= New Zealand code parameter;
n_p= number of plastic hinges;
n_b= correlation between the initial tangent elasticity modulus and the maximum secant modulus in the concrete block
n= correlation between the initial tangent elasticity modulus and the maximum secant modulus in concrete;
P= applied beam load;
P_{cr}= cracking load;
P_u= ultimate beam load;
P_v= additional force;

ε_{mu}= masonry strain in the top fiber at ultimate;
ε_{pe}= effective initial strain in unbonded prestressing tendon;
ε_{psb}= ultimate strain in bonded prestressing steel;
ε_{psu}= ultimate strain in unbonded prestressing steel;
ε_b= unitary deformation in the concrete block corresponding to f_b'
ε_c= unitary deformation in the concrete block corresponding to f_c'
ε = unitary deformation in hollow concrete block.
θ= beam rocking rotation at mid-span;
θ_{end}= beam rotation at end;
ϕA_{ps}= diameter of prestressing steel;
ϕ_u= curvature at the mid-span section at ultimate load increment;
$\phi(x)$= curvature along beam length;
Ω= bond reduction coefficient;
Ψ = compression shortening factor;
ω= beam angle of curvature;
η= deflection shape parameter;
λ = slenderness ratio; and
ρ= beam radius of curvature.

RESUMEN

Desde tiempos remotos, la mampostería ha sido pieza clave para la civilización humana en temas relacionados con la construcción de sus viviendas, como pilar fundamental de los grandes imperios de la historia y que en la actualidad es empleada por la mayoría de culturas a lo largo de todo el mundo. Sin embargo, su bajo desempeño para resistir esfuerzos de tracción, comparado con materiales como el acero y el hormigón reforzado la ha marginado en su uso a la construcción de pequeñas edificaciones y en elementos no estructurales. Por esta razón, se hace necesario la implementación de nuevas técnicas que mejoren el desempeño de la mampostería convencional y aprovechar mejor sus numerosas bondades para la construcción de grandes proyectos de ingeniería. Una de las técnicas para contrarrestar los esfuerzos de tracción en la mampostería es el postensado, que mediante la inclusión de un pre-esfuerzo de compresión permite mejorar notablemente el comportamiento estructural de la mampostería.
De esta manera, este trabajo doctoral ha planteado la necesidad de estudiar el desempeño estructural a flexión de la albañilería postensada sin relleno de grouting para aprovechar sus ventajas significativas en ahorros de tiempo y materiales de construcción, así como su posible futura implementación para la construcción de muros de contención de tierras.

Para establecer el comportamiento a flexión de la mampostería postensada sin relleno de grouting, se realizaron una serie de ensayos en laboratorio a escala real sobre elementos tipo vigas simplemente apoyadas, y muros en voladizo con carga fuera del plano del muro. En el protocolo de los ensayos se estableció el estudio del efecto en la variación de los principales parámetros que controlan en diseño a flexión de la mampostería postensada, entre ellos la magnitud del tensionamiento inicial de la barra, la resistencia de la mampostería, y la excentricidad del cable, entre otras. Los resultados obtenidos muestran el adecuado comportamiento de este sistema estructural bajo cargas de flexión y su gran viabilidad para ser empleado como sistema estructural en la construcción de muros de contención de tierras. Se observa en todos los ensayos ejecutados que la curva carga-deflexión presenta un comportamiento aproximadamente bilineal, y adicionalmente existe una relación aproximadamente lineal entre el incremento de la tensión del cable y la deformación máxima del elemento estructural, premisa que permitió definir una metodología simple de cálculo para estimar la capacidad última a flexión en esta tipología estructural. Igualmente se observa que algunas expresiones propuestas en los principales códigos de diseño de mampostería postensada en el mundo predicen adecuadamente la capacidad máxima de carga de este tipo de elementos. Estos resultados, al igual que las experiencias constructivas adquiridas en el desarrollo de esta tesis de doctorado han promovido nuevas temáticas de investigación que se espera sean desarrolladas a corto y mediano plazo, e igualmente permitan continuar con la dinámica de investigación en esta línea de conocimiento.

ABSTRACT

Since ancient times, masonry has been the basis of human civilization in every aspect related to the construction of houses, as a cornerstone of the great empires of the ancient world and is used by diverse cultures all around the world. However, their poor structural performance in supporting tensile stresses compared with other materials such as steel and reinforced concrete, has marginalized the use of masonry to small buildings and nonstructural elements. It is for this reason that it is necessary to implement new techniques that improve the structural performance of conventional masonry and thus make the best use of their multiple benefits in the construction of large engineering projects. One of the most often used techniques to counteract tensile stresses effects is post-tensioning, that consists of the inclusion of a pre-compression force which considerably enhances the structural behavior of masonry. Thus, this dissertation raised the need to study the structural behavior of ungrouted post-tensioned masonry in bending to use their comparative advantages in aspects which include labor, time, and building costs, as well as their future implementation in the construction of retaining walls.

For establishing the flexural behavior on ungrouted post-tensioned masonry, a series of full scale laboratory tests were conducted on simple supported beams and cantilever walls subject to out-of-plane lateral loading. The test protocol established the importance of studying the effect in the variation of the main design parameters that control the bending behavior of post-tensioned masonry, including the initial prestress, masonry strength, and tendon eccentricity, among others. The results obtained show an adequate performance of this structural system under bending loads and its great versatility for use in the construction of retaining walls. One of the observations in the study was that the load-deflection curve exhibits an approximately bilinear behavior in all conducted tests, and additionally there was a linear relationship between the tendon stress increase and maximum deflection, a premise that allowed a new methodology to estimate ultimate flexural capacity in ungrouted post-tensioned masonry to be established. It was also observed that some proposal expressions on main worldwide design codes in post-tensioned masonry predict the ultimate load capacity of ungrouted masonry adequately.

These results combined with the observations obtained from wall and beam construction during this doctoral thesis have allowed innovative ideas and new research areas to be developed. These ideas are expected to be developed in the short and medium term to allow applied research in this specific area to progress dynamically in the future.

CHAPTER 1. INTRODUCTION

"Pre-stressed brickwork should not be seen as a direct substitute for concrete but as a material that has considerable benefits when used in appropriate structural forms". (Remo Pedreschi, 2004)

1.1 Introduction

Through countless human civilizations masonry has been recognized as a competent and widely used building material. Precasting, ungrouted and prestressing are techniques that increase productivity in the construction of buildings and infrastructure under strict material quality control, labor savings and reducing costs. Thanks to all these advantages, ungrouted post-tensioned masonry can be conceived as a technique used in the construction of retaining walls that makes it so attractive and more competitive than conventional retaining wall structures such as reinforced concrete and reinforced earth retaining walls. These are of great use in countries such as Colombia and Chile.

This study has been undertaken intended to help fill the knowledge gap on the use of ungrouted elements in several worldwide post-tensioned masonry codes, to verify their equations and the accuracy of their theories in order to calculate the ultimate state in flexural behavior for ungrouted elements. Simultaneously, new analytical expressions are presented which may better explain the ultimate flexural behavior for ungrouted elements in post-tensioned masonry, and thus establish a better correlation between the main design variables in its structural behavior and the ultimate flexural capacity. This enables effective implementation and regulation of this structural system.

1.2 Objectives

To evaluate the structural behavior of ungrouted post-tensioned masonry elements under bending loads, and the possible use of this structural system for the construction of retaining walls, guaranteeing the minimum standards of quality.

As specific objectives, this thesis seeks to:

- Evaluate the most relevant mechanical properties of structural elements that make up post-tensioned masonry, in order to determine their constitutive laws that enable the development of numerical models.
- Development of a full-scale experimental testing program in post-tensioned masonry elements subjected to bending loads, and to identify the mechanical behavior of this structural system.

1.3 Hypothesis

- Through conventional laboratory tests, it is possible to establish the most relevant mechanical properties of materials that make up post-tensioned ungrouted masonry, such as hollow concrete blocks, high strength threaded bars, and contact elements which are input parameters to predict the structural behavior in masonry assembly.
- Full scale laboratory tests can be used to determine the structural behavior of ungrouted post-tensioned masonry under bending loads.

1.4 Methodology

Due to limited information available concerning ungrouted post-tensioned masonry, this research has been especially developed to generate a new experimental database that allows for understanding the flexural behavior of this structural system, as well as the influence of the main design parameters in their mechanical behavior. The first part of this research work was centered on the compilation of information taken from published scientific literature, postgraduate theses, technical proceedings, patents and non-scientific literature stored in different databases.

Subsequent to literature review, most of the research takes place in the experimental evaluation of mechanical properties of both constituent materials and structural elements, and the proposed experimental stage has been divided into three main phases. In the first of these phases, a detailed study of the mechanical properties of the constituent materials of ungrouted post-tensioned concrete masonry is conducted. Various tests were carried out, the uniaxial compression test was done to determine the stress-strain curve, and the other tests included the friction coefficients test, the indirect tensile test, among others.

The second experimental phase was focused on the analysis of the structural behavior of simply supported ungrouted post-tensioned masonry beams. A set of monotonic and cyclic tests were developed with the aim to establish the effects of the variation in the main design variables that control the flexural behavior in post-tensioned masonry. Among the parameters considered in this study include masonry

strength, tendon eccentricity, initial prestress and beam length.

The third experimental phase was focused on the structural behavior of cantilever ungrouted post-tensioned masonry walls, with variations in the initial prestress loading, cross section (single whyte and diaphragm wall), masonry strength, and the height of the wall. For this experimental phase, additional instrumentation to measure the wall curvature and determine plastic length was provided. The applied lateral force simulated an approximately triangular distributed load emulating an equivalent earth pressure.

After each experimental phase, all the collected data was carefully processed and analyzed independently comparing their structural response with theories proposed in the literature adapted by main worldwide codes. Equally, based on the analysis of collected information, a new methodology to predict tendon stress increase in ungrouted post-tensioned concrete masonry was proposed, this new methodology can be used to determine the ultimate flexural capacity of structural elements under bending loads.

1.5 Content

The focus in this thesis is on the flexural behavior of post-tensioned concrete masonry elements with unbounded tendons and ungrouted wall cavities, particularly the response on simple support beams and out-plane cantilever walls. Material properties of post-tensioned concrete masonry were investigated in relation to their strength and strain capacity. A group of 40 beams and 12 cantilever walls has been tested at the Structural Laboratory of the University of Medellin, in order to observe the influence of the main design parameters in the structural behavior of ungrouted post-tensioned masonry.

The organization of this thesis has been developed in the following eight (8) chapters, it is important to specify that Chapters 2 through 6 were developed in a paper format as individual articles. This way to present the thesis means that each chapter is independent of the others, and can be read separately. In spite of the structure of this format, it is also possible to find related information between the chapters due to the connectivity across the entire contents of the thesis.

Chapter 2– Literature Review: Presents a complete summary of the historical development of post-tensioned masonry in the world, from its origins up until the present day discoveries. Particularly mentioned are the main worldwide applications, code provisions, advantages and limitations, patents, some cases of prestressed masonry in Colombia and Chile, and the principal historical progresses in investigation. The conclusions identify the many advantages offered by this structural system, and the need for further research with the focus on some related topics that require more scientific development.

Chapter 3– Analytical model for compression behavior of hollow concrete blocks: Reports a summary of information collected from a careful study of several uniaxial compression tests in standard hollow concrete blocks to determine the stress-strain curve for two different masonry strengths. The results show a direct relationship between compression behavior in simple concrete and masonry units, where both the shape of the stress-strain curve and the ultimate strain of the masonry unit are directly dependent on the magnitude of masonry strength.

Chapter 4– Stresses at ultimate state of unbonded tendons in ungrouted post-tensioned masonry beams: Proposes a new methodology to calculate tendon stress increase at ultimate state in unbonded tendons. This new methodology is based on beam deflection principles and founded on the basic theories of mechanics of materials. The results of this new theory show a better approximation to experimental results than proposed expressions in the main worldwide post-tensioned masonry codes, given that most of these equations are based on adapted strain compatibility theories, with the use of empirical parameters for their effective implementation.

Chapter 5– Flexural behavior of ungrouted post-tensioned concrete masonry beams with unbonded eccentrically tendons: Contains a detailed analysis of the structural behavior of an ungrouted post-tensioned masonry beam group, with unbonded tendon and flexural failure. A parametric analysis to study the influence of the main design variables, and accuracy of the prediction equations proposed by the main worldwide prestressed masonry codes at ultimate state was performed. All beams showed a bilinear load-displacement behavior, and some code

expressions predict properly the ultimate state of ungrouted post-tensioned masonry beams.

Chapter 6– Structural Behavior of Ungrouted Post-tensioned Cantilever Wall under Cyclic out of Plane Load: Make known a summary of the experimental results of seven cantilever post-tensioned ungrouted walls in flexure subject to out of plane loads. The effect of the initial prestress and masonry strength was included in the design parameters analyzed in this study. The results show a flexural failure in all walls by the formation of one plastic hinge at the bottom of the wall in the flexural compression zone. Damage is limited to a small area, and the remaining portion of the wall presented negligible destruction. Some worldwide code expressions predicted the ultimate state in ungrouted post-tensioned masonry cantilever walls relatively well.

Chapter 7– Summary of Conclusions: This chapter shows the main results and conclusions obtained from both analytical and experimental development in the doctoral thesis. Also, it provides a detailed description of the main observations during the experimental and analytical phases of the structural behavior of ungrouted post-tensioned masonry in bending. Furthermore, some recommendations for both design and construction for these types of structures are included.

Chapter 8– Suggestions for Future Research: As a motivation for the future, this chapter lists some ideas for upcoming research on applications of ungrouted post-tensioned masonry - providing guideline suggestions to follow in each of them. It is hoped that this list will provide a dynamic increase in ungrouted post-tensioned masonry research, as well as in the inclusion of ungrouted post-tensioned masonry in all worldwide design codes.

1.6 Scope

The general purpose of this experimental and analytical thesis was to understand the structural behavior of ungrouted post-tensioned concrete masonry elements under bending loads, and the effect on flexural response of the following design parameters, including: geometry, material properties, loading type, tendon profile, steel ratio, initial prestress. To achieve this objective, a complete test program was carried out to establish the mechanical properties of the constituent materials, as well as the structural behavior of full-size simple supported beams and cantilever walls. The results and conclusions were based on observed behavior, and compared with some theories and code expressions. All these activities will finally determine the feasibility of use of this structural system in the construction of retaining walls and a variety of other infrastructure and building projects.

1.7 Declaration

This thesis is the result of research work undertaken in the Faculty of Engineering at the University of Medellin-Colombia for a post graduate in Engineering. It is declared that all the work, ideas and the results of this thesis have been carried out and achieved by the author himself and by his own initiative, under the supervision of Professor Ricardo León Bonett Díaz.

1.8 Disclaimer

This thesis was prepared by the Faculty of Engineering at the University of Medellin-Colombia, and describes the development of ungrouted post-tensioned concrete masonry in flexure. The opinions, conclusions and recommendations presented herein are those of the author and do not necessarily reflect those of the University of Medellin-Colombia or any of the sponsoring parties of this project.

1.9 List of publications

1.9.1Journal articles

revista de la construcción
Journal of Construction
Volumen 12 N°3 | DICIEMBRE 2013 | ISSN 0717-7925 | ISSN ELECTRÓNICO 0718-915X
PONTIFICIA UNIVERSIDAD CATÓLICA DE CHILE
ESCUELA DE CONSTRUCCIÓN CIVIL
FACULTAD DE INGENIERÍA

Modelo analítico del comportamiento a compresión de bloques huecos de concreto

Analytical Model for Compression Behavior of Hollow Concrete Blocks

John Mario García Giraldo (Autor Principal)
jmgarcia@udem.edu.co
Universidad de Medellín, Facultad de Ingeniería
Programa de Ingeniería Civil, Colombia
Carrera 87 # 30-65 Medellín Colombia
Fono: 57-4-3405333, Fax: 57-4-3405555

Christian Ledezma Araya (Autor Oficial de Contacto)
Pontificia Universidad Católica de Chile, Chile
ledezma@ing.puc.cl

Ricardo León Bonett Díaz
Universidad de Medellín, Colombia
rbonett@udem.edu.co

Código: 0106
Fecha de Aceptación: 1 de diciembre de 2013.

Revista EIA, ISSN 1794-1237 / Año XI / Volumen 11 / Edición N.22 / Julio-diciembre 2014 / pp. 119-131
Publicación semestral de carácter técnico-científico / Escuela de Ingeniería de Antioquia —EIA—, Envigado (Colombia)

LA INFRAESTRUCTURA DE PUENTES EN LAS VÍAS SECUNDARIAS DEL DEPARTAMENTO DE ANTIOQUIA

JOHN MARIO GARCÍA GIRALDO[1]
JAIME OSPINA GIRALDO[2]
EDIR AMPARO GRACIANO GÓMEZ[3]

Ingeniería Civil

doi: http://dx.doi.org/10.16925/in.v9i17.804

Evaluación técnica de los puentes en la infraestructura vial del departamento de Antioquia

John Mario García[1], Jaime Ospina Giraldo[2], Edir Amparo Graciano[3]

[1] Profesor de la Facultad de Ingeniería, Programa de Ingeniería Civil, Universidad de Medellín, Colombia
Correo electrónico: jmgarcia@udem.edu.co
[2]Profesional Universitario de la Secretaría de Obras Públicas de Antioquia, Colombia
[3]Consultora independiente, ex-directora de Desarrollo Físico de la Secretaría de Infraestructura Física de Antioquia, Colombia

Recibido: 10 de septiembre del 2014. Aprobado: 18 de noviembre del 2014.

1.9.2 Book chapters

“Uso de Ceniza Volante como Adición Mineral y Remplazo del Cemento Portland en la Fabricación del Concreto Hidráulico”
García, J.M. and others

Book:
“Innovación y Transferencia de Conocimiento en Ingeniería”

“Uso estructuras de contención discontinuas en suelos con cohesión para estabilidad de laderas”
García, J.M.

1.9.3 Conference papers

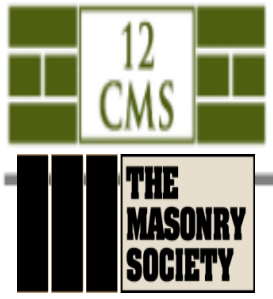

12th Canadian Masonry Symposium
Vancouver, British Columbia, June 2-5, 2013

Experimental and Analytical Model for Compression Behavior in Hollow Concrete Block

García, J.M., Ledezma, C., and Bonett, R.L

Evaluación técnica de los puentes en la infraestructura vial del departamento de Antioquia

John Mario García[1], Jaime Ospina Giraldo[2], Edir Amparo Graciano[3]

El uso de la mampostería postensada en el mundo y su aplicación para la repotenciación de edificaciones en América latina

García, J.M., Bonett, R.L., and Ledezma, C

Flexural behavior of ungrouted post-tensioned masonry beams with eccentric, unbonded tendons

García, J.M., Bonett, R.L., Ledezma, C., and Schultz, A

1.9.4 Patents

Invention patent: "Sistema constructivo de muros de contención en mampostería postensada con elementos no adheridos". (in Spanish) (Submission date: 9 June 2015).

Awards and recognition

International exchange program scholarships by the Municipio de Medellín

Doctoral scholarships

Honorable Mention Paper Award

12th North American Masonry Conference
Honorable Mention Paper Award

The Masonry Society presents a 12NAMC Honorable Mention Paper Award to

Flexural Behavior of Ungrouted Post-Tensioned Masonry Beams with Eccentric, Unbonded Tendons

Published in the 12NAMC Proceedings published in 2015 by TMS, and authored by:

John Mario Garcia Giraldo, Ricardo Leon Bonett Diaz, Christian Ledezma Araya, Arturo E Schultz

Michael Schuller, 12NAMC Co-Chair

Phillip J. Samblanet, TMS Executive Director

3970 Broadway, Suite 201-D * Boulder, CO 80304 * Phone 303-939-9700 * Fax 303-541-9215 * Website: www.masonrysociety.org

1.9.5 Academicals internships

1.10 Author's contribution

The most important results obtained in the course of this doctoral research have contributed significantly to the generation of new knowledge. These contributions are subdivided into theoretical and practical contributions according to their particular focus.

Theoretical contribution:

- An update to the state of the art post-tensioned masonry.
- A new expression to estimate the stress-strain curve in hollow concrete block masonry units.
- A methodology to calculate the tendon stress increase in unbonded elements.
- An upgraded conception and analysis design of ungrouted post-tensioned masonry in bending.
- The creation of a new test database of the structural flexural behavior of ungrouted post-tensioned masonry.

Practical implications:

- The creation of a new structural system for the construction of retaining walls in post-tensioned masonry with vertical anchors in the foundation soil.
- The drafting of a production manual for the construction of retaining walls in post-tensioned masonry with vertical anchors.
- The conception of a new design manual for retaining walls in ungrouted post-tensioned masonry walls.

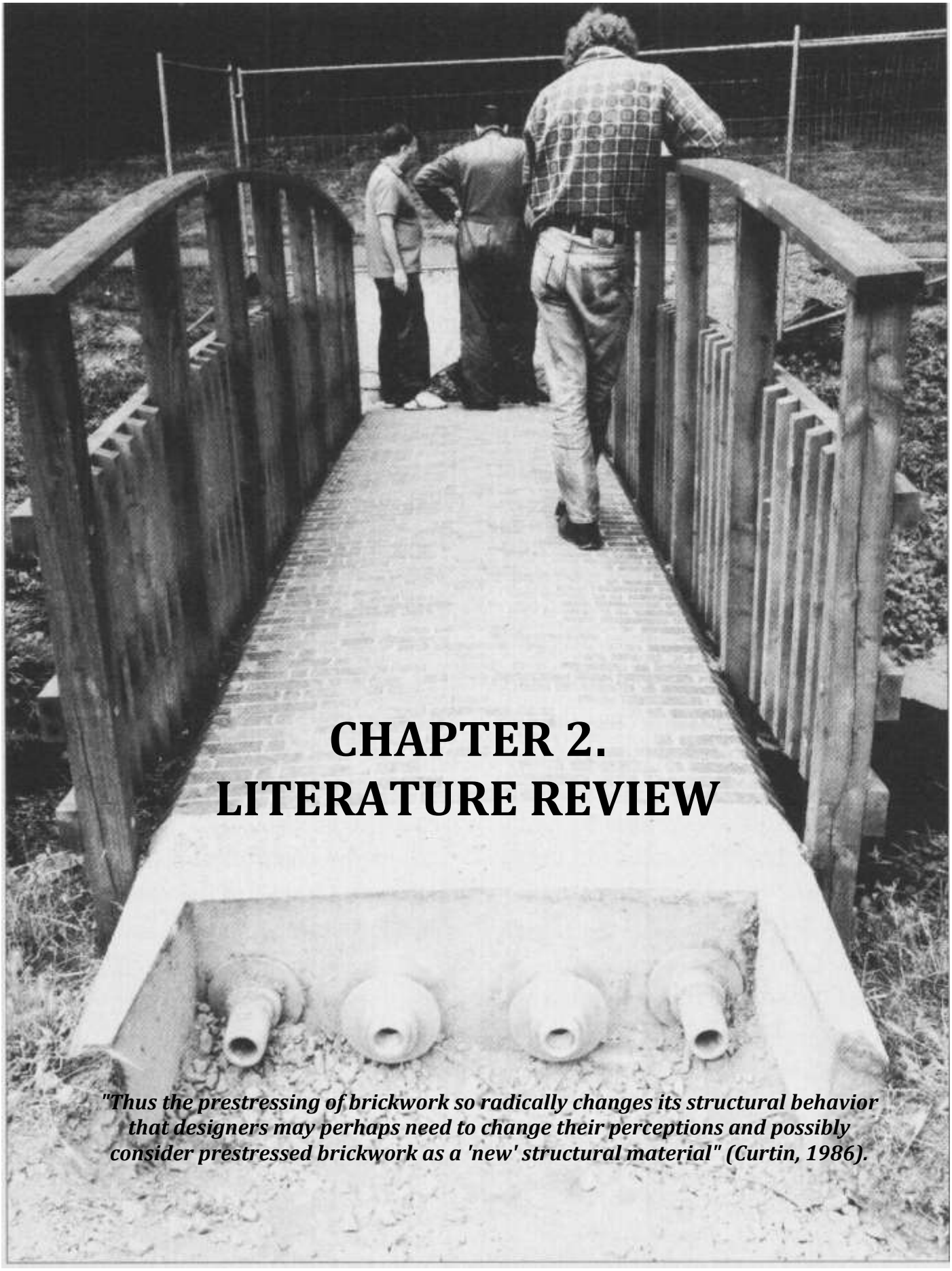

CHAPTER 2.
LITERATURE REVIEW

"Thus the prestressing of brickwork so radically changes its structural behavior that designers may perhaps need to change their perceptions and possibly consider prestressed brickwork as a 'new' structural material" (Curtin, 1986).

Abstract

A general review, and a detailed literature review analysis of the historical evolution, research development, and practical application of post-tensioned masonry spanning various periods in structural engineering, was undertaken as part of this thesis. This chapter provides a summary about the historical development of prestressed masonry, principal applications of post-tensioned masonry, worldwide code provisions, advantages and limitations of prestressed masonry as well as patents. Also included are some cases of post-tensioned masonry in Colombia and Chile, as well as a short overview of the previous studies of the structural performance of this construction system. The review of the literature shows the structural and construction benefits of post-tensioned masonry, such as: enhancement of shear and flexural strength, decrease of cracking to serviceability state, reduction of waste, and optimization of construction costs. These advantages, combined with the benefits of prefabrication, make this construction system an attractive solution and an excellent alternative to be used in the construction of complementary structures on road infrastructure.

Keywords: Masonry, post-tensioned, literature review, advantages, limitations.

2.1 Introduction

Since ancient times, masonry has been the predominant building material in different cultures around the world, and qualifies as the oldest man made construction material (Schultz and Scolforo, 1991). The first sunbaked clay bricks have been attributed to the Sumerians as long ago as 3,500 B.C. (Baker, 1981). Since then, masonry has been the cornerstone material in famous worldwide heritage constructions, including the Tower of Babel, the Temples at Ur, the Pharos lighthouse in Alexandria, Stonehenge in England, the Great Wall of China, and the Pyramids of Egypt. Furthermore it has been prominently featured in the housing and monuments of the ancient Mayan and Aztec cultures, as well as the earliest European explorers in North America, among others (Ganz, 1990; Drysdale et al., 1999; Lissel, 2001).

Masonry offers a number of advantages as a building material: It is easy to implement and economic in construction, highly durable, has high thermal and acoustic insulation, fire resistant, natural appeal and low maintenance costs. However, due to its low tensile strength and the emergence of reinforced concrete in the steel industrialization, masonry currently takes second place. Today, in most cases masonry is used in nonstructural elements and in poor construction practices as a secondary structural material (Schultz and Scolforo, 1991). The Monadnock Building in Chicago, built in the year 1891 (Fig. 2.1), is considered the last great building to be constructed with traditional masonry architecture in the United States before the industrialization of steel. It is a 16 story high structure, with 1.8m thick walls and very big footings in its foundation (Ganz, 1990).

Figure 2. 1 Monadnock Masonry Building, Chicago (Ganz, 1990).

Despite the decline of masonry at the end of the 1800s, the economic crisis in India in 1920 created the need to use different materials as a substitute for steel and reinforced concrete. Most research on reinforced masonry for the construction of walls, slabs, beams and columns had already been carried out but it took until 1940 for European engineers and architects, led by Haller in Switzerland, to begin experimental studies on the design of masonry walls. This led to a renaissance of masonry design and construction, despite little formal research undertaken in structural masonry during a number of decades in comparison with reinforced concrete (Ganz, 1990).

The development of this research has focused primarily on the characterization of ungrouted post-tensioned masonry to be used as a structural component in road infrastructure. Latin America is a region with a significant deficit in its highway

network, and Colombia is obviously no exception to these conditions, because according to recent statistics the lag in the development of road infrastructure reach values close to 30 years has been observed, minimizing its trade competitiveness compared with other industrialized countries.

Ungrouted post-tensioned masonry proves to be an excellent alternative to the construction of road infrastructure in undeveloped regions. Its structural, architectural and constructive advantages make this new structural system a promising alternative to overcome the deficit in terms of road infrastructure in Latin America.

2.2 Historical development of Post-tensioned Masonry

The structural properties of masonry can be enhanced by different techniques such as reinforcement, confinement and prestressing, all of which focus on optimizing its low tensile strength. Post-tensioned masonry combines one of the most recent techniques with the oldest construction material (Ganz, 2003). Conceptually post-tensioned masonry is a simple technique used to increase tensile strength in masonry using prestress. Prestressing reduces or eliminates tension stress from the external load; reduces crack formation; and increases flexural capacity, flexural stiffness and shear strength (Schultz and Scolforo, 1991). (Lissel, 2001) defines post-tensioned masonry as a new building process that provides a simple, economical, durable, innovative and attractive architectural design.

The first countries where post-tensioned masonry was developed were England, Australia and New Zealand (Bean, 2007). Although many structural designers consider post-tensioned masonry a new structural technique, historical records show that the first innovative application of post-tensioned masonry dates back to 1825, developed in England, for the construction of a tunnel under the River Thames (Fig. 2.2). Post-tensioned masonry occurs by the heating of steel bars inside walls through bonfires, which when cooled produces pre-compression in the masonry. This tunnel structure was 15m in diameter, had 21m high caissons with 0.75m thick walls reinforced with 25 mm diameter rods (Biggs, 2003; Foti and Monaco, 2000; Wight, 2006; Ganz, 1990).

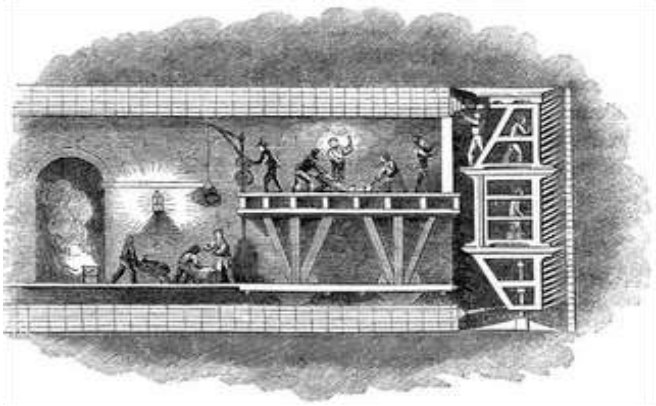

Figure 2. 2. Tunnel under River Thames, England, 1825 (ABS ZERO)

Some authors affirm that British engineers were the first pioneers of post-tensioned masonry, when they started to apply this system in the construction of different types of structures by the end of the 1950s; however, the first application of post-tensioned masonry in the United States was reported by a patent of P.H. Jackson in 1886, it was used to develop a prefabricated roof and floor system, and followed by Lee in 1893, Brinkman in 1902, Lund in 1912 and Henderson in 1926 (Schultz and Scolforo, 1991; Devalapura et al., 1997). According to the records, England is the first country to document the application of post-tensioned masonry since the Victorian era. Engineer Haller was the first to implement a post-tensioned floor with ceramic tiles, followed by a variety of applications: water tanks, storage silos, retaining walls, houses, buildings, tall and slender walls, meeting halls, schools, churches, pedestrian and vehicular bridges, abutments, heritage preservations, and structural rehabilitation, among others (Ganz, 2003; Dawe and Aridru, 1993). Another pioneer of post-tensioned masonry in England was the engineer J. Felix Samuely, who reported in 1953 the implementation of prestressing techniques on 10 m high masonry brick piers in the construction of a high school building in the United Kingdom (Shrive, 1988). With this application, Samuely discovered an increase in cracking moment under flexural loads. Likewise, engineer Curtin, with his remarkable research and developments in post-tensioned masonry between 1975 and 1986, can be considered another of the great forerunners of worldwide post-tensioned masonry (Devalapura et al., 1997).

The first prestressed masonry structures in the United States of America were designed by the engineering consulting firm Bryan and Dozier, which was

extensive experience in the design of major works in worldwide engineering. One of the first applications of post-tensioned masonry in the United States was the bleacher seating at Fayetteville High School football stadium, Tennessee. It was constructed in the summer of 1950 with a cost of about half the price of reinforced concrete, following this, a small bridge of 21 m length of prestressed masonry was built in Madison County, Tennessee in October 1950; the total cost of the structure was estimated to be 20% less than conventional bridges. Actually, there are eleven prestressed masonry bridges in Tennessee, all of them constructed between 1950 and 1956. One of them receives significant truck volume, and the state inspection records show that all the bridges are in good condition. However, leaching is a common problem and there was also, some slight spalling and breaking out in the corners of a few blocks, as well as longitudinal cracks running through the bottom of the blocks (Bennett, 2008).

In South America, an innovative architectural technique used in post-tensioned masonry arose with the work of Uruguayan engineer Eladio Dieste, who for more than 50 years designed and constructed over one hundred buildings with new forms of prestressed masonry structures. (Pedreschi, 2004). Other significant research and projects in post-tensioned masonry in South America have been developed in Brazil, by the engineer Guilherme Parsekian.

Post-tensioned masonry already shows great potential for contemporary masonry buildings. Nevertheless, there must be continual research development on its mechanical properties, design analysis, and behavior before engineers, architects, and builders can incorporate it safely and economically in construction (Drake, 2004). Post-tensioned masonry should not be considered a direct substitute for prestressed concrete, but seen as an alternative solution that has considerable benefits when used in appropriate structural forms (Pedreschi, 2004).

All these worldwide developments have shown not only the great potential of the post-tensioned masonry to be used in structural and architectonics applications, but also leave the doors open to imagination and innovation in regard to future developments where this structural system is used, as well as the new questions needing answers about their mechanical behavior and the prediction of its mechanical behavior. All these new questions, lead the generation of new research areas, which includes the research topic that will be discussed in this doctoral thesis.

2.3 Worldwide applications of Posttensioned Masonry

Before the appearance of the first post-tensioned masonry design regulations, a large number of practical applications were developed with excellent results. Several projects have been built using post-tensioned masonry with excellent structural results, most of them were developed in countries such as England, Australia and the United States. Developments and applications of post-tensioned masonry that which have been constructed to date, have generally employed grouted clay elements with bonded tendons. The developments in post-tensioned masonry is reflected in a wider spectrum of applications such as: bridges, houses, buildings, retaining walls, tanks, grain silos, seismic retrofit, unconventional structures, among others. Some of the most important worldwide projects in post-tensioned masonry are mentioned below:

- Grain silos, England, between 1952 y 1965 (Fig. 2.3a).
- Vehicular bridge, United States, 1951 and 1954 (Fig. 2.3aa) (Fig. 2.3b).
- Apartment complex, New Zealand, Christchurch, 1970 and Colombia, Bogota, 2001 (Fig. 2.3c).
- Emblematic building, Salvation army citadel, England, 1980 (Fig. 2.3d), Oak Tree Lane community center, England (Fig. 2.3w)
- Rushden Fire Station, England, Northamptonshire County, 1985 (Fig. 2.3e).
- Columns, United Kingdom, Braintree (Fig. 2.3q).
- Post-tensioned stone blockwork, India.
- Retaining wall, England, Trent Valley, 1987, Canada, University of Calgary, 2002 (Fig. 2.3f) and Brazil (Fig. 2.3v).
- NCMA Lifestyle 2000 house, United States, Maryland, 1990 (Fig. 2.3g).
- Retrofitting of existing buildings. Australia, General post office, 1990 (Fig. 2.3h) and United States, Holy cross Church, 1992 (Fig. 2.3i).
- Cylindrical water tank, United Kingdom, 1967 (Fig. 2.3w)
- Waste water treatment tanks, United States, Virginia, 1990.
- Pedestrian Bridge, England, Tring, 1991 (Fig. 2.3j).

- Abutments at Glinton by Pasited States, Virginia, 1998 (Fig. 2.3k).
- Berlin Technical Museum, Germany, 1998 (Fig. 2.3l).
- External re-strength old masonry wall (Fig. 2.3t).
- Sound walls, United States, Denver, 2000 (Fig. 2.3m).
- Free-standing barrel vault, Bus station, Salto, Uruguay (Fig. 2.3ac).
- Repair of commercial buildings, England, Peterborough, 1991 (Fig. 2.3s).
- Commercial shopping, Montevideo, Uruguay (Fig. 2.3ab).
- Industrial center building, Switzerland, Altendorf, 1993 (Fig. 2.3n).
- Roanoke Building School, United States, Michigan, 2000.
- Post-tensioned masonry building, USA (Fig. 2.3r).
- Post-tensioned masonry roof, Brazil and Uruguay (Fig. 2.3u), (Fig. 2.3ae).
- Tallest Leadership in Energy and Environmental Design (LEED) building, United States, Tucson Arizona, 2013 (Fig. 2.3o).
- Two story house include bidirectional slab, Colombia, University of Medellin, 2014 (Fig. 2.3p).
- Masonry water tower, Uruguay (Fig. 2.3af).
- Football stadium bleachers, United States, 1950.
- Bus shelter, Salto, Uruguay.

a) Grain silos (Curtin et al., 1982)

b) Vehicular bridge (Wight, 2006)

c) Apartment complex Colombia (Torres, 2001)

d) Salvation army citadel (Wight, 2006)

e) Rushden Fire Station, (Allen, 1986)

f) Retaining wall U. of Calgary (Lissel et al., 2005)

g) NCMA Lifestyle 2000 house (Crigler, 1991)

h) Retrofitting, Australia, (Ganz, 2003)

i) Retrofitting United States (Ganz, 2003)

j) Pedestrian Bridge, (Ganz, 2003)

k) Abutments (Halsall, 1991)

l) Berlin Technical Museum, (Wight, 2006)

m) Sound walls (Woodham, 2001)

n) Industrial center building, (Ganz, 2003)

o) Tallest LEED building (Robertson & Scott, 2014)

p) Two story-bidirectional slab house. (Bonett, 2012)

q) Ambulance Garage Columns (Shaw, 1988)

r) PM building, USA (Biggs, 2003)

s) Supermarket repaired with PM (Biggs, 2003)

t) External cables to re-strength old masonry (Jansen and Tilly, 1999)

u) PM roof at the Federal University of Piaui - Brazil (Parsekian et al., 2007)

v) Cantilevered concrete masonry earth-retaining (Parsekian et al., 2007)

w) Oak Tree Lane community center (Curtin, 1990)

x) Prestressed circular water tank (Sinha, 2002)

y) Bus shelter The Seagull petrol station, Salto, Uruguay (Sinha, 2002)

z) Football stadium bleachers, Tennessee (Bennett, 2008)

aa) Vehicular bridge, Tennessee, USA (Bennett, 2008)

ab) Shopping, Montevideo, Uruguay (Pedreschi, 2004).

ac) Bus station, Salto, Uruguay (Pedreschi, 2004).

ad) Industrial building, Refresco del Norte, Salto Uruguay (Pedreschi, 2004).

ae) Roof over offices, agro-industry Massaro, Uruguay (Pedreschi, 2004).

af) Masonry water tower, Uruguay (Sinha, 2002).

Figure 2. 3. Worldwide applications of post-tensioned masonry.

2.4 Post-tensioned Masonry codes provisions

After completing a large number of investigations into enhanced masonry materials and design procedures, the first masonry building code was developed in Switzerland in 1943 (Ganz, 1990). Subsequent to this great achievement in Europe, the first masonry code in the United States was developed in 1966 (MSJC, 2005). Few countries in the world have a special code to design post-tensioned masonry, this is due to a pronounced lack of knowledge in their real structural behavior and gaps in their design philosophy that limit its use to areas of low seismic intensity (Biggs, 2003). Apparently, codes expressions to estimate shear strength of prestressed masonry are deficient to predict the shear failure according to the different results in several experimental test. Therefore, further investigation about shear strength in post-tensioned masonry is needed (Lissel, 2001).

Actually, prestressed masonry codes typically provide design expressions to calculate masonry strength at the ultimate limit state. Although code provisions in prestressed masonry have been around since 1985, with the inclusion of the British Standards BS 5628-85 relating to prestressed masonry walls, many of them are overly conservative. Research has shown that some post-tensioned masonry structures are resisting greater loads than that permitted by the worldwide design codes (Lissel, 2001). The use of post-tensioned masonry was implemented much later in countries such as Canada, USA, Australia, Switzerland and Germany. Many of these countries made their first code incursion during the 1990's. Currently, some of the main codes and provisions for designing post-tensioned masonry in the world are: Great Britain (BS 5628-2, 2005), Australia (AS 3700, 2011), USA (MSJC, 2013), New Zealand (NZS 4230, 2004), Canada (CSA S304, 2014), European Union: Eurocode 6 (CEN, 2005) and Brazil (ABNT 15812-1, 2010 and ABNT 15961-1, 2011). Unbonded post-tensioning masonry has also been referred to as a viable seismic retrofit solution and was also included in FEMA 547-06 (FEMA, 2006) and in ASCE/SEI 41-06 (ASCE, 2006) (Ismail and Ingham, 2012). Most of these regulations have been developed on the experience gained in previous research and experimental processes. However, unlike reinforced concrete, there is still a great lack of information regarding the structural behavior of prestressed masonry. This lack of knowledge leads too much uncertainty in the design methods, which is reflected in higher safety factors and significant levels of uncertainty, because a large percentage of design expressions have been developed from empirical methods or using correlations derived from experimentation.

The vast range of engineering and practical activities surrounding the use of post-tensioned masonry in the United Kingdom started arousing public interest in construction during the early 1970s, leading to the initiation of a code provision for prestressed masonry structure in 1978 (Haseltine, 1982). Subsequently, the first provisions for the design of post-tensioned masonry were published by the British Standards Institution in 1985 (Schulz and Scolforo, 1991). These provisions were the culmination of the work of many design and empirical engineers that began in the 1800s. During the late 1950s, many British engineers working in prestressed masonry, laid the ground work for building code provisions regarding this technique. During the late 1970s, this work was reviewed for inclusion in the general masonry code. In 1985 prestressed masonry was included in the general masonry code BS 5628 part 2, entitled "'Code of Practice for the use of Masonry, Structural use of Reinforced and Prestressed Masonry". This code has been updated several times over the years and the current version was released in 2005. Many British Standard expressions were taken from masonry and concrete codes used at that time and provisions adopted based on design recommendations and research by Curtin, Phipps, and their associates (Lissel, 2001; Laursen, 2002; Wight, 2006).

The Swiss code (SIA VI77, 1995) also addresses prestressed masonry. The European Code first included prestressed masonry in EC 6-95 (CEN, 1995), later updated in EC 6-05 (CEN, 2005). In the Australian code, based primarily on the British code and Australian research, the prestressed masonry design standard appears for the first time in 1998, with the title of AS 3700, and was updated last in 2011. This code limited construction with post-tensioned masonry in non-seismic regions, or a special design with elastic response can be implemented for the seismic forces in earthquakes zones. In The United States, the Standard for prestressed masonry was included for the first time in a draft amendment in 1999, and the provisions were based primarily on prestressed concrete theory. This standard was recognized in the edition of the MSJC 'Building Code

Requirements for Masonry Structures' in TMS 402-02 (MSJC, 2002), and as several already have done, this typically followed the provisions outlined in BS 5628 in terms of prestressed masonry. MSJC recognizes the use of prestressed masonry for ductile seismic design. It is conceptually parallel with the design of prestressed concrete, prestressed masonry was included for the first time in the New Zealand Masonry Standard, NZS 4230 "Design of Reinforced Concrete Masonry Structures" in the 2004 edition, in the form of a normative appendix. The Canadian code CSA S304.1 "Design of Masonry Structures" prestressed masonry is superseded in 2002, including the version in 2004 (Laursen, 2002; Wight, 2006; Lissel, 2001).

For countries such as Colombia and Chile, prestressed masonry is not mentioned in official design codes, therefore special permission is required to use post-tensioned masonry on any type of structure. Hopefully, this thesis will mark the start of prestressed masonry in standards and design codes in these countries, as well as the beginning of a line of investigation to promote new practical and theoretical approaches within this structural system.

2.5 Advantages and limitations of the Post-tensioned Masonry

This structural technique provides efficient masonry structural optimization that improves many of the inherent properties of traditional masonry, in addition to reducing the adverse effects of its low tensile strength. Several investigations have been conducted to support the structural behavior of this construction system to establish its benefits and restrictions. The following are some of the most important results and conclusions about post-tensioned masonry:

- The use of precast materials make for a more flexible construction in this structural system, and allow it to be dismantled just as quickly as it was assembled, moved and rebuilt in another place.
- Lighten buildings, through the reduction of steel and concrete in structures. This represents a more efficient use of materials and a reduction in project costs (Schultz and Scolforo, 1991). Spacing of the bars is optimized, expediting the laying of the masonry units (Laursen and Ingham, 1999; Drake 2004).
- Reduced water infiltration, due to post-tensioning producing a densification in the materials and crack closure by compression stress imposed on the system. (Biggs, 2001).
- Increased out of plane strength in walls, especially in low-rise buildings supporting low dead loads. (Schultz and Scolforo, 1991).
- Reduced construction time and waste, in addition to its aesthetic properties. (Wight, 2006). Provides many economic advantages in the construction process: economy, material availability, simplicity of construction, and low construction costs (Ganz, 1990b; Schultz and Scolforo, 1991; Ganz, 2003; Drake, 2004)
- Increased ultimate flexural strength by significantly reducing tensile stresses (Foti and Monaco, 2000).
- Unlike pre-tensioned masonry, post-tensioned masonry does not have prestressing losses due to elastic deformation of the masonry, and its construction is much more efficient as it does not require the use of grout (Schultz and Scolforo, 1991).
- The structural system provides corrosion protection for bars inside hollow blocks, by reducing cracks through which water infiltrates, thus avoiding its contact with prestressed steel (Biggs, 2001).
- Shrinkage deformations are generally compensated by the block strain expansion due to block moisture and creep deformations produced by the serviceability load (Ganz, 1990).
- Reduction in maintenance due to the durability of the system (Bean, 2003; Ganz, 2003; Drake, 2004).
- Post-tensioning system with threaded rods does not require skilled labor (Torres, 2001).
- A large percentage of the energy introduced into the system is stored as potential energy or strain energy of elastic deformation, this energy is recovered almost completely during the unloading of the structural element (Ganz, 1990). Apparent ductile response over large displacements and a tendency to return to its initial state after unloading (self-centering behavior), is of great value in earthquake areas (Laursen and Ingham, 1999; Korany et al., 2001; Rosenboom and Kowalsky, 2003).
- Precast materials ensure effective quality control before the construction process, allowing materials testing prior use.
- The system has a high capacity for thermal and acoustic insulation, and leads to a reduction in energy costs due to the superior insulating properties (Schultz and Scolforo, 1991; Bean, 2003; Drake, 2004).
- Zero cracks under service loads, with a more efficient use in thinner elements, and taller walls (Schultz and

Scolforo, 1991; Drysdale et al., 1999; Laursen and Ingham, 1999; Subasic, 2001).

- Due to the shear strength increment by applied prestress, shear reinforcement may be removed in some cases (Laursen and Ingham, 1999).
- The pre-compression works as an active force to prevent or reduce the tension force that occurs in the masonry (Hassanli et al., 2015).
- The system maintains its integrity even in large displacements, without considerable damage (Hassanli et al., 2015).
- Localized damage and cost effective. In severe events such as large earthquakes, the damage is limited to a small portion in the toe of the wall, which can be repaired easily and with minimal cost (Hassanli, 2015).
- The construction of post-tensioned masonry is easy, cheap and fast (Hassanli, 2015).
- Post-tensioned masonry has very similar behavior to prestressed concrete (Pedreschi, 2004)
- Full grouting is not necessary; cost savings present in material and labor compared to reinforced masonry (Drysdale et al., 1999; Woodham and Hamilton, 2003).
- Shorter construction schedule dependence, operation is scheduled relative to other construction tasks (Laursen and Ingham, 1999; Drake, 2004)

Despite the multiple benefits of the post-tensioned masonry, there are some shortcomings in the structural behavior of the system which may limit its utility for some specific types of buildings:

- There is no adequate numerical model to simulate the structural response of post-tensioned masonry.
- Prestress losses in time, make the long-term structural behavior prediction in post-tensioned masonry difficult.
- Few countries in the world have codes or standards that govern the design and regulations of post-tensioned masonry (Foti and Monaco, 2000).
- Construction method and bonding patterns in post-tensioned masonry make it more difficult to incorporate shear and flexural reinforcement (Pedreschi, 2004).
- Little is known about the ductility capacity and energy dissipation of the post-tensioned masonry (Laursen, 2002).
- There are no efficient parameters to determine the characteristics of energy dissipation in post-tensioned masonry.
- Grouting of the masonry cavity after the post-tensioning process can be difficult (Pedreschi, 2004).
- For structures with high levels of compression loads, post-tensioned masonry is not recommended for use, due to the fact that a large fraction of compression capacity is absorbed by the prestressing force (Foti and Monaco, 2000).

2.6 Prestressed masonry patents

Development of some new construction methods in post-tensioned masonry have led to innovative patents based on this modern building methodology. Some of these patents are listed below:

2.6.1 Proto-II™

The Proto-II™ wall system (Fig. 2.4a) is one of the most frequently used systems in the United States for concrete masonry. It is mainly used on fences, retaining walls and noise barriers. This patent is backed up by many experimental laboratory tests and has been used for more than two decades. At least 28 million square meters installed in more than 16000 kilometers of walls have been built with this methodology. After an earthquake in Northridge, California on January 17th 1994, this system demonstrated excellent structural behavior with less than 1% of wall failures when compared to the total number of failures in masonry walls caused by earthquakes. The top anchorage system consists of a rectangular support plate, a nut of ½ inch in outer diameter, and a post-tension rod which is tightened using a wrench with a specific torque, until a Proto- II™ Direct Tension Indicator (DTI) washer collapse with a tolerance of ± 3% of the design force. Twelve years after implementing a Proto-II™ wall system, no corrosion problem in the prestressing bar has been reported and the prestress loss incurred over time can be compensated for, by over-tensioning the tendons (Wight, 2006)

2.6.2 Integra™ walls system.

The Integra™ post-tensioned system (Fig. 2.4b) has been used to build more than 10,000 housing units since its invention in 1984. This patent system consists of a specially designed specific masonry unit which has open ends and a core web. The system usually is partially grouted with 5/8 in prestressing bars which pass through a specially moulded bearing block used on the last course. Each bar is anchored in

the reinforced concrete foundation and passes through a slot up into the wall. Tendon restraint can be used to ensure a fixed position, inside the wall during all loading processes. Ungrouted cells can be filled with a special polyurethane to provide optimum thermal and acoustic insulation. The post-tensioning system consists of high tensile steel rods connected to a ½ in. bearing plate, standard washers, a nut and a special 7400 lb DTI washer for the applied post-tensioned load control. This prestress load provides an assumed design force of approximately 5000 lb after losses. This building system offers benefits such as cost savings by reduced labor and material costs, as the amount of grout is reduced by up to 95% (Wight, 2006).

2.6.3 Dur-O-Wal Sure-Stress™ wall system.

The Dur-o-Wal Sure-Stress™ system can be used with a wide variety of masonry units currently available for commercial use. The system is composed of a foundation anchor, a tendon, a restraint plate, a coupler, a bearing plate, a load indicating washer, a nut, and a lateral top restraint anchor to attach the top of the wall to the bottom. Usually reinforced cells are grouted. If additional corrosion protection is necessary for exterior walls in areas of high humidity levels, the bars can be protected with a hot dipped galvanized coating (Wight, 2006).

2.6.4 VSL System

The VSL system (Fig. 2.4c) from Switzerland uses 15 mm high tensile mono-strands with a plastic coating and plastic duct or galvanized steel to provide a complete corrosion protection in unbonded tendons. The VSL system consists of a self-activating dead-end anchorage at the bottom of the wall and a prefabricated concrete element attached to the anchorages at both the top and bottom of the wall. The post-tensioned high tensile cable is strengthened generally up to 75% its maximum strength (Wight, 2006).

a) Proto-II™

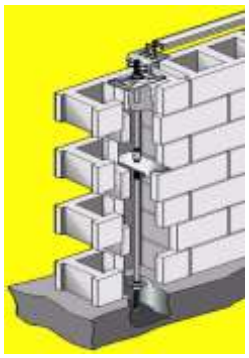

b) Dur-o-Wal

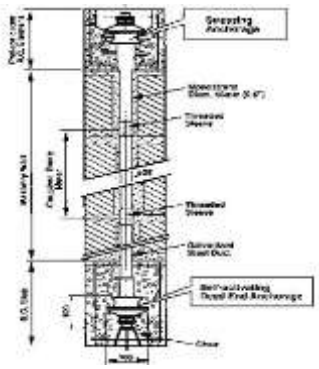

c) VSL

Figure 2. 4 Post-tensioned masonry walls patents (Wight, 2006).

2.7 Applications of Post-tensioned Masonry in Colombia and Chile

Post-tensioned masonry is gradually gaining recognition as a profitable and safe masonry system worldwide. It is currently widely used in Europe and is becoming more common in the United States, but has had little reception in South America particularly in countries such as Colombia and Chile. Structural design codes in these countries lack specific regulations to govern this structural methodology.

A low-cost housing apartment complex in Bogota built in the early 2000's, was the first case of applied post-

tensioned masonry in Colombia. It is called "Urbanizacion Mazuren" located in Ciudad Bolivar town. This kind of structural building is made for the purpose of testing the economic viability of a new, simple construction technology applicable to brick and hollow concrete block masonry, a very common and economic material used in Colombia. As a result of the final construction process, it has been determined that the method is not economically viable in relation to construction of houses up to three floors and that have a large number of walls, that are proven components of both structural and architectural design (Torres, 2001).

Colombian engineer Hector Urrego who works for the consulting, engineering and Design Company "Area Ingenieros Consultores", is considered one of the most important precursors of post-tensioned masonry in Colombia. Urrego designed and constructed one of the first bi-directional slab used in post-tensioned concrete masonry producing excellent results in their structural strength performance.

Its first application was used in the construction of a model house in Medellin-Colombia, and this structural system has been successfully employed as a principal structural system in the construction of two story apartment buildings. This designs should be recognized as the first cases of Post-tensioned Masonry in Colombia. Developed with technical and financial support by the alliance between University of Medellin and the building companies: Porticos S.A.S, Area Ingenieros Consultores S.A.S and Prefabricados Adoquin-Ar.

There are only a few examples of the use of post-tensioned masonry in Colombia, most of them are taking place at the University of Medellin – Colombia under the coordination of Professor Ricardo Bonett-Diaz. Here several full-scale prototypes of conventional structural elements such as beams, slabs, in plane shear walls, out of plane cantilever walls, two stories houses and retaining walls have been developed (Fig. 2.5).

a) Bidirectional slab

b) Beams

c) Shear walls

d) Shake table test

e) Two story house (50m^2)

f) Two story house (98m^2)

Figure 2. 5. Applications of Post-tensioned Masonry in Colombia

The introduction of a new construction process or a new material within Latin-American culture often requires long periods of development, investigation and education. Post-tensioned masonry has good structural behavior, and researchers and designers worldwide, particularly in the United Kingdom, the United States and Australia, have experimented with some structural applications which produced good results. Post-tensioned masonry has been proved to be an excellent alternative to be used in those countries in which it has not already been implemented. In order to accomplish this, close communication is required between designers, builders, material suppliers, and researchers surrounding masonry (Schultz and Scolforo, 1991).

2.8 Previous research conducted on Post-tensioned Masonry

Much of the recent research in post-tensioned masonry worldwide has been conducted in the last four decades, most of them conducted on prestressed clay masonry walls and topics related to design codes and procedures. The studies focused on the influence of the main variables that govern the behavior of post-tensioned masonry, specifically the effect of masonry strength, magnitude of initial prestress, tendon restraint, tendon bonding, reinforced ratio, load typology, bond pattern, and geometric shape, among others. Previous research shows The United States has concentrated its efforts on concrete block masonry due to the advantage of larger cores for posttensioning, unlike the United Kingdom, where brick masonry is more popular. (Devalapura et al., 1997). At present, both types of masonry units are investigated around the world.

Below are some results of the different investigations carried out in in the different types of structural element of prestressed masonry.

2.8.1 Beams

After a series of research interested in prestressed masonry floor systems was carried out, the need to study the behavior of post-tensioned masonry beams is evident (Schultz and Scolforo, 1991). Several investigations into prestressed masonry beams have been widely developed in the last four decades focused on the flexural behavior of these structural elements and the incidence of their main design parameters. Most of them focused on grouted masonry beams and bricks as masonry units, the majority were carried out at the University of Edinburgh under the direction of Professor Sinha. (Pedreschi, 2004).

Some of the results obtained by different projects and research developed are:

- Increase in cracking load and flexural stiffness (Ng and Cerny, 1985 and Neis et al., 1989).
- Presented small deflections and a significant decrease in cracks and there was no advantage to providing only 1/3 ultimate prestress force, additionally, initial prestress affect failure mode (Garwood, 1988).
- Beams with larger steel ratio failed through shear influence and low levels of steel experienced ductile behavior (Sinha , 1994).
- Tendon guide or tendon restrained, increased the ultimate moment capacity of the beams between 1.5 and 3.0 times (Williams and Phipps, 1982; Roumani and Phipps (1983, 1985, 1986 and 1988); Montague and Phipps, 1984; Al-Gahtani and Fairbairn, 1995; Urrego and Bonett, 2011; Phipps and Montague, 1987). The tendon guide shows an increase of 21% and 534% over the ultimate load and midspan deflection respectively. Similarly, ductility and the safety factor increased by 1500% and 163%, respectively (Urrego and Bonett, 2011).
- Flexural behavior of prestressed masonry, showing that post-tensioning has a reasonable ductility and overloading capacity before failure since first cracking. When shear span/depth ratio decreases, shear strength increases (Baqi et al., 1999).

2.8.2 Out-of-plane loading

Walls construction have been one of the most classic application of prestressed masonry. Development and application of prestressed masonry walls began in Australia during mid-1960s (Schultz and Scolforo, 1991). The first scientific research and tests in post-tensioned masonry has been primarily developed in out-of-plane walls, in United Kingdom from the early 1970s (Lissel, 2001).

Some of the results obtained by different projects and research developed are:

- Diaphragm walls have a good increase in lateral load due to prestressing force, post-tensioning serves to increase cracking load, flexural stiffness, ultimate

capacity, and reduce serviceability deflections (Curtin, (1987, 1968 and 1970); Curtin and Howard, 1991).

- Results on out of plane concrete block tests showed the good performance in walls with guided or restrained tendons, the improvement in ultimate load and displacement capacity, and after unloading, displacement was almost completely restored like a "self-centering" behavior (Al-Manaseer and Neis, 1987; Ungstad et al., 1990; Geschwinder and Ostag, 1990).
- The moment at ultimate capacity was controlled by the initial prestress force and the slenderness, magnitude of prestress was more effective at greater slenderness, and less effective with increasing axial load. (Lacika and Drysdale, 1995).
- Initial wall response was linear up to initial cracking, but cracking was observed over a broad range of loading. A large drift of 3 to 5%, before losing their load capacity, was observed. (Bean et al., 2004 and 2007).
- Post-tensioning increased flexural resistance and cracking loads, with a better crack distribution (Mojsilovic and Marti, 2000).
- Prestressing increases bending strength, with apparent ductility, and improves shear resistance. Post-tensioned masonry would attract most innovative designers, adventurous builders and first-class researchers in the new, non-traditional applications of such cost-effective, buildable and durable engineering materials (Curtin, 1990).

2.8.3 In-plane loading

Several studies have been reported on masonry walls subjected to in-plane lateral loads and some of the results obtained by different projects and research developed are:

- Shear strength increases because pre-compression induced by post-tensioned force increases frictional resistance in the bed joints.
- Residual displacements were minimal, but providing that the residual prestressing force is sufficiently large. Results validated the ability of post-tensioned masonry walls to self-center near to the original vertical alignment. (Wight et al., 2007a and 2007b).
- Ductile response was measured, with reliable drift capacity up to 1.5%, with relatively little energy dissipation. Only localized damage occurred in the flexural compression zone, simple to repair. An adequate shear friction between the wall and foundation was provided. (Laursen and Ingham, 2004).
- Prestressing strands return the walls to their initial position, and the lateral force-displacement response may be described by a nearly non-linear elastic relationship. The integrity of the walls is maintained as no plastic hinges form. Consequently minimal structural and non-structural wall damage can be expected. (Laursen and Ingham, 2001).
- Adding shear reinforcement for walls with tendon spacing smaller than 2 m does not improve the shear strength of the walls, however, for spacing between tendons greater than 2 m, even with a small amount of shear reinforcement, the shear strength increases significantly (Ryu et al., 2013).

2.8.4 Slabs

- Post-tensioned masonry slabs show reasonable ductility and overloading capacity before failure since first cracking. (Baqi et al., 1999).
- Restrained blocks observed an increase in strength and midspan deflection of 113% and 304%, respectively by unrestrained blocks. (Bonett y Urrego, 2008 and 2011).
- Slabs show a higher ultimate capacity than traditional masonry systems with an isotropic behavior despite the geometrical differences (Bonett y Urrego, 2008).
- Restrained blocks cause a change in the failure mode, with a brittle failure for unrestrained tendons and a ductile failure for restrained tendons (Bonett y Urrego, 2008).

2.8.5 Columns

- Shaw (1988) discusses the flexural behavior of the free standing masonry columns under self-dead weight gravity loads, and the effect of lateral loads, such as wind forces and accidental impact forces of a vehicle accident.
- Prestress does not significantly alter the load carrying capacity of the column but failure mode and the lateral deflection at failure can be substantially changed for the better. When the post-tensioning tendon is restrained, sideways deflection is reduced significantly and a potential buckling mode of failure can be changed to one of crushing. Applied eccentric load in the opposite direction to the column load, improved load carrying capacity and column deflection and proposed theoretical models show

good agreement with the experimental results. (Phipps and Al-Safi, 2001).

2.9 Summary of conclusions

After conducting an extensive literature review it was possible to compile information about the historical worldwide evolution and principal applications of post-tensioned masonry, which is the subject of the present study. Masonry has been considered as an admirable material throughout history, with a substantial number of building advantages. Post-tensioning counteract the low tensile strength in the masonry reducing tension stress, crack formation; and increases stiffness, flexural capacity and shear strength.

British engineers were the first pioneers of post-tensioned masonry since the Victorian era. In the United States, the bleacher seating at Fayetteville High School football stadium, Tennessee was one of the first applications of post-tensioned masonry. In South America, Uruguayan engineer Eladio Dieste, Brazilian engineer Guilherme Parsekian, and Colombian engineer Hector Urrego, were the precursors of this structural system in this part of the American continent.

Many different post-tensioned masonry projects and applications are in use worldwide. Some of the main applications are: bridges, houses, buildings, retaining walls, tanks, grain silos, seismic retrofit, and unconventional structures, among others.

Almost five (5) worldwide codes currently cover the design of post-tensioned masonry, among them are British (BS 5628-2, 2005), Australian (AS 3700, 2011), American (MSJC, 2013), New Zealand (NZS 4230, 2004), and Canadian (CSA, 2014). For South America, there is not a specific prestressed masonry code and special permission is required to use post-tensioned masonry.

Some of the main advantages of post-tensioned masonry are: To lighten buildings, increased out of the plane strength, reduced construction time and waste, increased ultimate flexural strength, apparent ductile response with self-centering behavior, thermal and acoustic insulation, shear strength increment, and can be repaired easily.

Some of the main limitations of post-tensioned masonry are: there is not an adequate numerical model to simulate the structural response, prestress losses, lack of knowledge about ductility and energy dissipation, and also a lack of worldwide standards.

There are currently more than four patents for post-tensioned masonry, which include Proto-II™ wall system, the Integra™ post-tensioned system, the Dur-o-Wal Sure-Stress™ system, and the VSL system, all related to post-tensioned masonry walls.

In Colombia, engineer Hector Urrego and Professor Ricardo Bonett designed and constructed the first bi-directional slab used in post-tensioned masonry that was used for the construction of a two story apartment building, as well as a series of full-scale prototypes such as beams, slabs, in plane shear walls, and out of plane cantilever walls.

In the last four decades, previous research has been conducted on post-tensioned masonry in different types of structural elements, contributing to having detailed records about the structural behavior of post-tensioned masonry. The main findings in the structural benefits of post-tensioned masonry include: increase in cracking and ultimate load, reduced costs, tendon guide increased the ultimate capacity, it has reasonable ductility, reduced serviceability deflections, after unloading, displacement is almost completely restored, improved shear strength, simple to repair, and changed the failure mode for the better.

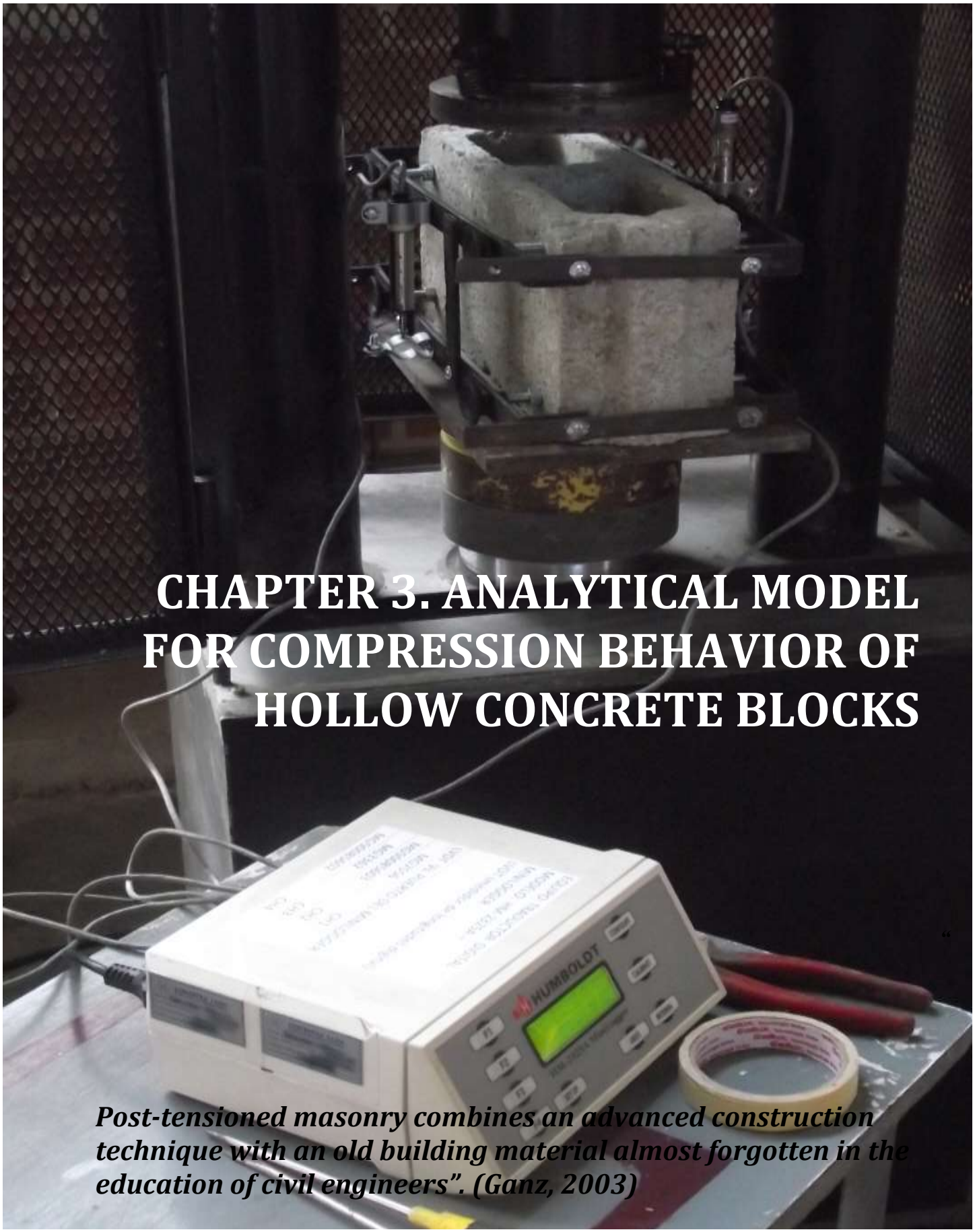

CHAPTER 3. ANALYTICAL MODEL FOR COMPRESSION BEHAVIOR OF HOLLOW CONCRETE BLOCKS

Post-tensioned masonry combines an advanced construction technique with an old building material almost forgotten in the education of civil engineers". (Ganz, 2003)

Abstract

The structural behavior of concrete masonry is directly related to the mechanical properties of its component materials. The compressive strength of masonry is probably the most important parameter in the design of masonry structures, and it depends mainly on the compressive strength of the individual blocks. However, the design code for masonry structures assumes simplified linear-elastic model behavior for the numerical models, which cannot provide an accurate prediction for the real structural behavior of this material, thereby generating a high degree of uncertainty of its displacements. Currently, displacement-based design approaches have been developed taking into account the displacement control, this is one of the most important variables which determines their structural behavior. In this study, a constitutive model has been developed to estimate the behavior of concrete blocks under uniaxial compression stress. This was measured using the correlation between constitutive models and the experimental results of 90 samples of hollow concrete blocks, each classified into one of two groups according to their compression strength levels (10MPa y 30MPa). The results show that models that consider the strength of the blocks within their parameters, are the ones which best correlate to the experimental results.

Keywords: Stress-strain curve; Compression strength; Modulus of Elasticity; Hollow Concrete block; Masonry.

3.1 Introduction

Masonry is a material with non-lineal behavior mainly due to the mechanical anisotropy of its components (Haach, Vasconcelos, Lourenço, & Mohamad, 2010). Therefore, with the exception of very small deformations, it is inaccurate to use elasticity formulations to establish the structural behavior of masonry. Neither exclusive values for the elasticity model when determining the deformations of the system through applying a given amount of load can be assumed. On the contrary, the non-linear behavior of masonry requires structural designs which incorporate the plasticity of its components, this updates the approach of elastic design and eventually reduces the uncertainty of the design, delivering adequate safety factors for these types of structures.

3.2 Problem description

Both, concrete and masonry share certain characteristics, among them include: good compression strength, low tensile strength, as well as fragility. Therefore, it is valid to assume that the accumulated knowledge from the different investigations developed regarding concrete can be extrapolated with appropriate modifications to that of masonry. For example, within the use of similar analytic and empirical expressions.

A fundamental step in the investigation of the mechanical performance of structural concrete masonry, is the adequate knowledge of strength variables of the masonry unit (Jaafar, Thanoon, Najm, Abdulkadir, & Abang, 2006). Unfortunately, there are very few studies on this subject, and most of them have focused on the behavior of the masonry (masonry unit + mortar) without much concern for the behavior of each of the parts independently (Haach et al., 2010). Although the behavior of the masonry unit differs in the case of a masonry prism, low walls or regular walls, the strength parameters of the unit are directly related to the performance of the different geometric configurations of the masonry system (Jaafar et al., 2006). The compression strength is possibly the most important parameter to be determined in masonry units. In addition, the stress-strain curve determines the most important design parameters in masonry, those which serve as a basis to predict the structural behavior of the structural system and to identify the different limits of its mechanical performance.

3.3 State of the art of empirical models for concrete

There are few investigations focusing on establishing the mechanical behavior of the masonry unit; however Jaafar et al. (2006) observed that masonry strength is limited principally by the strength of the masonry unit. The above implies that one of the most efficient ways to improve the mechanical behavior of masonry is to optimize the strength of its components.

Given the similarity which exists between the raw materials for conventional concrete and mortar for prefabricated blocks, there is a relative gap of knowledge on the subject regarding mechanical behavior curves pertaining to hollow concrete blocks, a complete revision has been carried out of the

different expressions for concrete blocks.

A thorough revision of the literature regarding the different stress-strain equations proposed in the concrete literature has been carried out, and their possible application to the experimental values obtained in laboratory testing for hollow concrete blocks (Table 3.1).

3.4 Experimental aspects

The tested blocks were prefabricated pieces made by the vibro-compactation method. The standard which establishes the minimum dimension and mechanical resistance requirements of these elements is the standard ASTM C90 of the American Society of Testing Materials. "Standard Specification for Loadbearing Concrete Masonry Units" (ASTM C90, 2011).

Table 3. 1 Stress-strain laws for concrete**.**

Autor	Equations	N°	Parameters
(Hognestad, 1951)	$\frac{f_c}{f_c'} = \frac{2\varepsilon}{\varepsilon_c} - \left(\frac{\varepsilon}{\varepsilon_c}\right)^2$	(3.1)	f_c', ε_c
(Smith & Young, 1955)	$\frac{f_c}{f_c'} = \left(\frac{\varepsilon}{\varepsilon_c}\right) e^{1-\left(\frac{\varepsilon}{\varepsilon_c}\right)}$	(3.2)	f_c', ε_c
(Sargin, Ghosh, & Handa, 1971)	$\frac{f_c}{f_c'} = \frac{n\left(\frac{\varepsilon}{\varepsilon_c}\right) - \left(\frac{\varepsilon}{\varepsilon_c}\right)^2}{1 + (n-2)\left(\frac{\varepsilon}{\varepsilon_c}\right)}$ where $n = \frac{E_i}{E_c}$	(3.3)	f_c', ε_c, n
(Popovics, 1973)	$\frac{f_c}{f_c'} = \frac{\frac{n}{n-1}\left(\frac{\varepsilon}{\varepsilon_c}\right)}{\frac{1}{n-1} + \left(\frac{\varepsilon}{\varepsilon_c}\right)^{\frac{n}{n-1}}}$ where $n = \frac{E_i}{E_c}$	(3.4)	f_c', ε_c, n

3.4.1 Geometry

The hollow concrete block under study has the shape of a straight prism with two (2) vertical holes, with symmetry in its two main dimensions. Its dimensions are of (390±1)*(140±1)*(190±2) mm, of length, width and height respectively.

The cross section of the block has a gross nominal area of 54600 mm^2 and an average net area of 32800 mm^2 (60% of the total area of the section). The slenderness ratio (height/width) of the samples was 1.36, meaning that correction factors would have to be applied if these results were to be extrapolated to other slenderness ratios (Drysdale, Hamid, & Baker, 1994).

3.4.2 Constitutive materials

Blocks with two levels of compression strength were evaluated: low strength [f_b'=10 MPa in average] and high strength [f_b'=30 MPa in average]. The constitutive materials for both type of blocks are the same, and the only variation is the dosage of the materials mixture. The constitutive materials of the tested blocks and their respective dosage by weight are: low strength blocks [f_b'=10 MPa]: fine sand (5.5%), medium sand (30.1%), thick gravel (46.5%), cement (6.9%), fly ash (5.5%) and water (5.5%). High strength blocks [f_b'=30 MPa]: fine sand (2.7%), medium sand (50.1%), thick gravel (28.2%), cement (12.0%), fly ash (3.9%) and water (3.1%).

3.4.3 Methodology of the experimental program

The concrete blocks were tested under a uniaxial compression force following the parameters established in the Standard ASTM C140 "Standard Test Methods for Sampling and Testing Concrete Masonry Units and Related Units" (ASTM C140, 2011). From these tests, it was possible to obtain the stress-strain curves for all tested masonry units until block failure, after which correlations were then established using some load deformation parameters for this type of material.

3.4.4 Test setup

Each hollow concrete block was loaded monotonically with a controlled speed of 1 kN/s until material failure, and its axial deformation was then monitored. The purpose of this was to obtain its complete history of axial load-deformation, and in this way garner the main parameters which define its mechanical behavior.

For this investigation 90 samples were tested until failure, 60 of these correspond to low strength blocks (f_b'=10 MPa), a conventionally masonry element

widely-used on the construction sector in Colombia, and the remaining 30 samples correspond to high strength blocks (f_b'=30 MPa), whose application is ideal for medium to tall buildings or in structures with high levels of compression stress.

The samples were tested in a servo-hydraulic compression machine with a capacity of 2500 kN and a tolerance of ±1 kN, controlled by a system of digital data acquisition (Figure 3.1).

Figure 3. 1 . Experimental Setup of the tested samples.

3.4.5 Instrumentation

In order to monitor the displacement in the direction of the application of the axial load, two (2) linear variable differential transformer (LVDT's) were placed on each side of the block with a tolerance of ±0.001 mm (Figure 3.2). The fastening frame was secured in order to measure the vertical displacement in adjacent positions to the hollow areas of the concrete block, where it was expected that the most significant strain would occur in accordance to that reported by Barbosa y Hanai (C.S Barbosa & Hanai, 2009).

3.5 Test results

For each tested block were obtained: the load versus axial deformation, stress-strain deformation curves and the main parameters of its elasticity properties, among them: modulus of elasticity (secant and tangent at origin), maximum strain, ultimate stress and its respective strain.

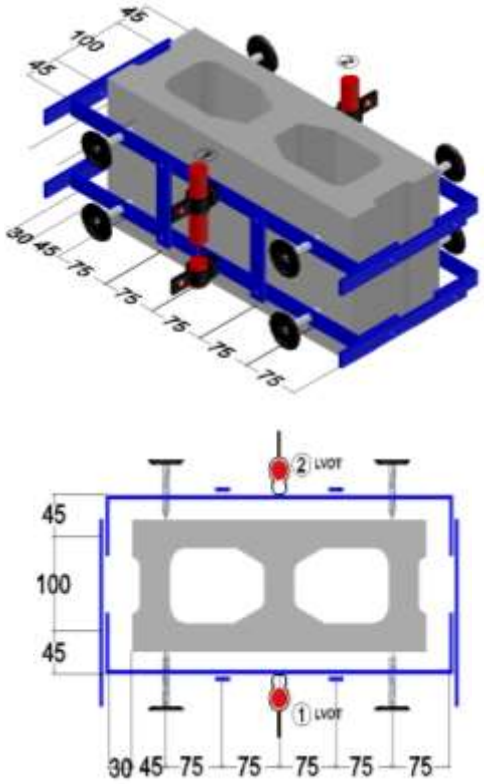

Figure 3. 2. Displacement frame.

3.5.1 Stress-strain curves

Figure 3.3 shows that most of the blocks showed a relatively elastic linear stress-strain behavior up to about 30%-45% of its maximum strength. At this point, the first cracks begin to appear in the interior of the block and gradually increases its inelastic behavior. For a load level close to 90% of its maximum load, a greater level of cracking and ultimate failure with the detachment of a diagonal shear crack wedge was observed in tested specimens.

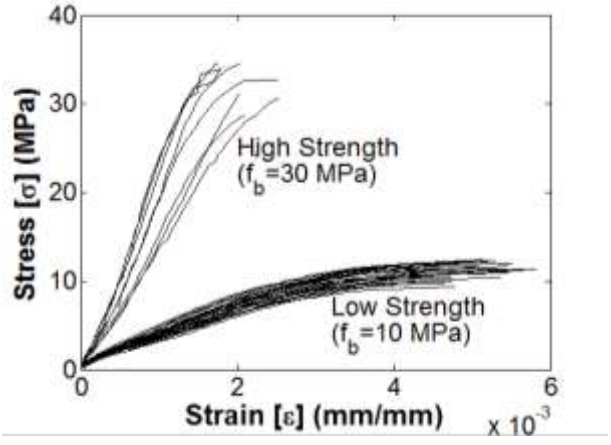

Figure 3.3. Stress-strain curves of all tested blocks

3.5.2 Types of failure

The failure of the compression blocks is characterized by a diagonal crack (Figure 3.4) produced by a combination of different parameters: shear strength, low slenderness of the block, and lateral confinement due to the frictional force generated by the contact between the hollow concrete block and the steel load plates.

Figure 3. 4. Diagonal crack, typical in low strength blocks.

None of the test samples with low strength (f_b'= 10 MPa) showed an explosive rupture. However, the failures occurred together with the prolongation of the diagonal cracks, which appeared generally on the ends of the blocks; similar to that observed by Barbosa and Hanai (2009) in their experimental tests. In the case of the high strength blocks (f_b'= 30MPa), these showed an explosive rupture which makes the detection of a crack pattern before the actual rupture much more difficult. However, initial fissures show a crack pattern similar to low strength blocks.

3.5.3 Modulus of elasticity

The experimental results showed that the stress-strain curves of the masonry units had an approximate linear behavior in the first third of the curve, and afterwards showed a significant nonlinear behavior. The results obtained were analyzed by the methodology of the Masonry Standards Joint Committee (MSJC, 2005), and the American Concrete Institute methodology (American Concrete Institute - ACI-, 2005), in order to establish the modulus of elasticity of the masonry unit. Calculations show that both methodologies obtained similar results, and their differences were less than 10%. Given the similarity in the results, the decision was made to work with the methodology proposed by the MSJC (2005), which is also supported by the Colombian Standards NSR-10 (2010) in their section D.5.2.1.2. This standard establishes the modulus of elasticity secant as the slope of the secant line between 5% and 33% of the maximum compression strength on the stress-strain curve.

Figure 3.5 shows the results obtained by evaluating the correlation between the elasticity module (E_b) calculated in accordance with the parameters established by MSJC (2005), and the maximum compressive strength obtained experimentally in the concrete blocks. Figure 3.5 also reports the experimental values obtained by Kaushik and others (Kaushik, Rai, & Jain, 2007), Haach and others (Haach et al., 2010), Barbosa and Hanai (C.S Barbosa & Hanai, 2009) and by Nwofor (Nwofor, 2012).

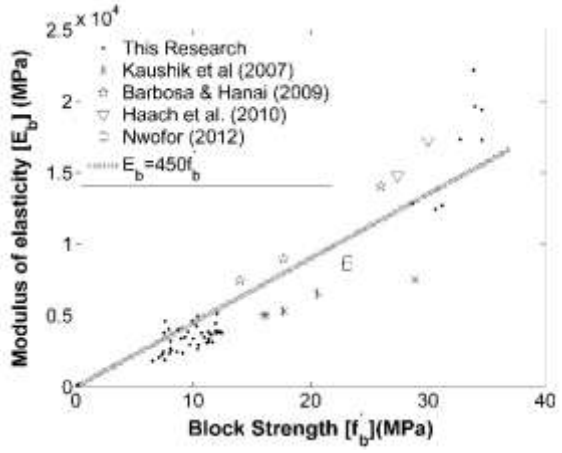

Figure 3.5. Modulus of elasticity versus compression strength, of tested concrete blocks

In the analytical models found in the literature review (Popovics, 1973; Sargin et al., 1971), a characteristic behavior parameter was identified relating to the behavior of the stress-strain curve. This is the relationship between the initial modulus of elasticity tangent (E_i) with respect to the origin of the coordinates on the stress-strain curve, and the modulus of elasticity secant from the origin of the coordinates to the corresponding point of the maximum stress (E_c). The results show that the relationship between the tangent and secant modulus of elasticity versus the compression strength of tested blocks, was similar to that observed in concrete, and the experimental results can be satisfactorily approximated to that expressed in Equation 3.5.

$$\frac{E_i}{E_c} = \frac{20.17\ (MPa)}{f_b'} + 1 \qquad (3.5)$$

The correlation between the modulus of elasticity and compression strength on tested blocks is better reflected in an expression such as $E_b = 450f_b'$. Even so, the tendency observed in the experimental results is not perfectly linear but rather slightly curved.

3.6 Correlation between strain at the maximum stress and the compression strength

Similar to conventional concrete, low strength concrete blocks present values of strain in accordance with its levels of compression strength. As the maximum stress of the block increases, its modulus of elasticity also increases. Additionally, failure point is reached with less deformation in high strength block than low strength blocks (Figure 3.3).

Although there are few researchers who specify a correlation between strain relating to the maximum stress in the concrete (Mohamad, Farid, & A.I.M, 1990; Wee, Chin, & Mansur, 1996), the experimental values obtained in the aforementioned tests show a certain approximate relation between these two variables, as shown in Figure 3.6.

The relationship proposed by Mohamad et al. for conventional concrete (1990) (Eq. 3.6) has a poor correlation with the obtained experimental values, as its calibration was done based on test data as a result of concrete test specimens. In the absence of a greater amount of results, the proposal is to adopt a linear relationship between the low and high strength values (Figure 3.6)

$$\varepsilon_c = 0.0078[f_c'(MPa)]^{-\frac{1}{4}} \quad (3.6)$$

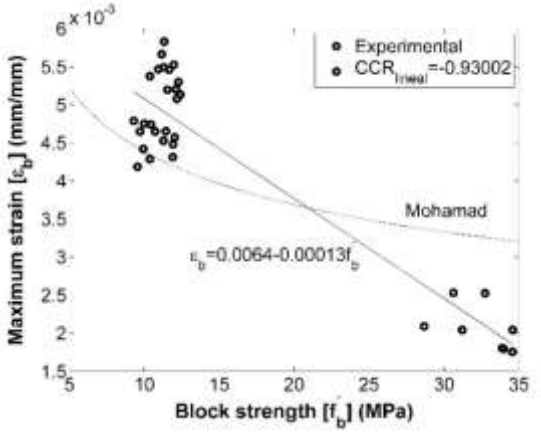

Figure 3.6. Correlation between strain at maximum stress ($\boldsymbol{\varepsilon_b}$) and the compression strength of the block ($\boldsymbol{f_b'}$).

3.7 Experimental results versus existing analytical models

Figure 3.7 shows normalized curves obtained for the tested concrete blocks. These curves indicate that blocks of different resistances have curvature and concavity parameters which differentiate between them, even in spite being of the same material typology and having the same block geometry in both cases.

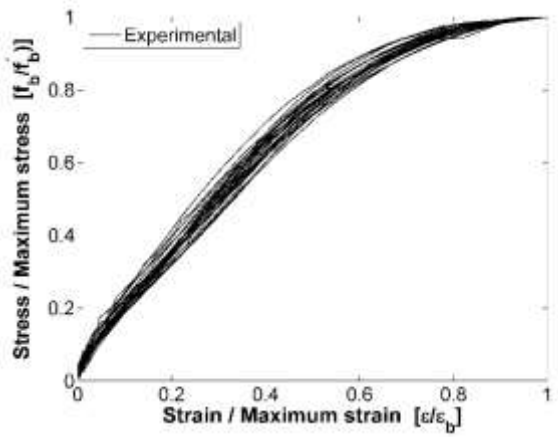

a)

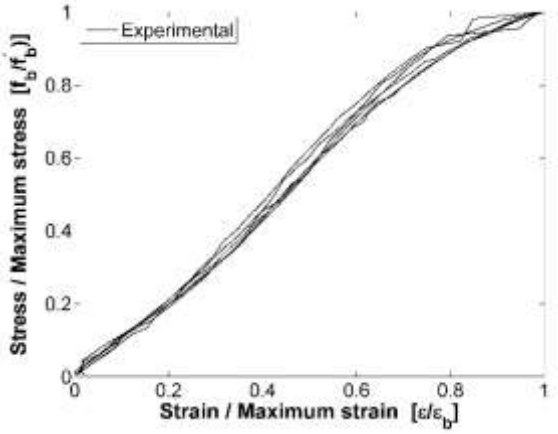

b)

Figure 3. 7. Normalized stress-strain curves for a) $\boldsymbol{f_b'}$=10MPa and b) $\boldsymbol{f_b'}$=30MPa.

The first researchers that established a mathematical correlation between the stress-strain curves for concrete, Hognestad (1951) and Smith and Young (1955), defined the parameters of the curve independently of the magnitude of unit strength. Over time, authors such as Sargin et al. (1971) and Popovics

(1973), noted the variations in the values and shape of the curves under different levels of concrete strength, and due to this observation, they proposed an additional parameters in their formulations in order to incorporate the aforementioned effects.

Figure 3.8 shows a very similar normalized behavior between the test results in hollow concrete blocks and the proposed models for conventional concrete. This figure shows how the experimental results obtained for low strength blocks (f'_b=10MPa) are well correlated with the different analytical models developed in the corresponding literature. The only model which departs slightly from the experimental results is the exponential curve proposed by Smith and Young (1955).

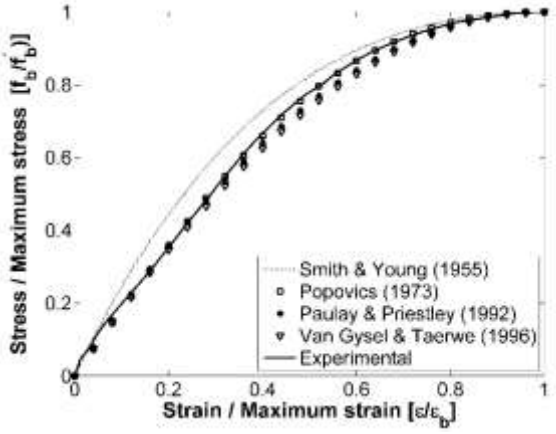

a)

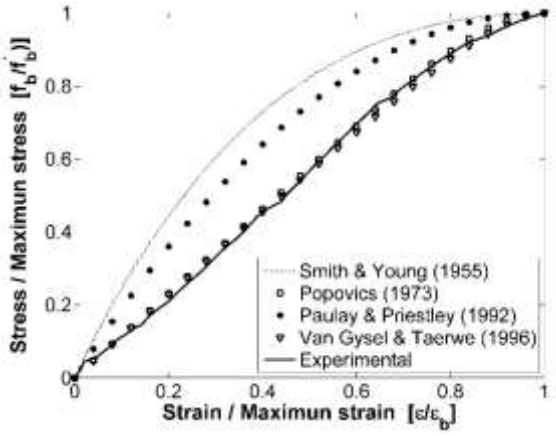

b)

Figure 3. 8. Experimental data versus analytical models in concrete blocks a) low strength (f'_b=10MPa) and b) high strength (f'_b=30MPa).

Likewise, a comparison was made between the proposed normalized curves for conventional concrete and the experimental results for high strength blocks (Figure 3.8b). Figure 3.8 shows that analytical models which consider behavior parameters in their expression, related to the maximum compression strength and maximum strain, are the ones best adjusted to the experimental values. On the other hand, models such as those proposed by Paulay and Priestley (1992) and Smith and Young (1955) don't show a satisfactory correlation with the experimental results for the different masonry strength.

3.8 Proposed analytical model

The experimental results obtained show that the expressions which best match with laboratory results, are those which involve the maximum compression strength and maximum strain within its parameters, this determines the shape of the stress-strain curve. In this manner it was determined to adapt the expression proposed by Popovics (1973), as it correlated best with the experimental results, in addition to its mathematical simplicity. From the extensive testing over 90 concrete blocks, the parameters used by Popovics have been adjusted and thus have been recalibrated using the test results as a starting point (Eq. 3.7).

$$\frac{f_b}{f'_b} = \frac{\frac{n_b}{n_b - 1}\left(\frac{\varepsilon}{\varepsilon_b}\right)}{\frac{1}{n_b - 1} + \left(\frac{\varepsilon}{\varepsilon_b}\right)^{\frac{n_b}{n_b - 1}}} \qquad (3.7)$$

where,

$$n_b = \frac{E_i}{E_c} = \frac{20.17\ (MPa)}{f'_b} + 1$$

The comparison between the experimental results obtained and the proposed curve (Eq. 3.7) can be seen in Figure 3.9, in which a high correlation between the experimental results and the proposed analytical model can be seen, both for concrete blocks of low strength, as well as, for high strength blocks.

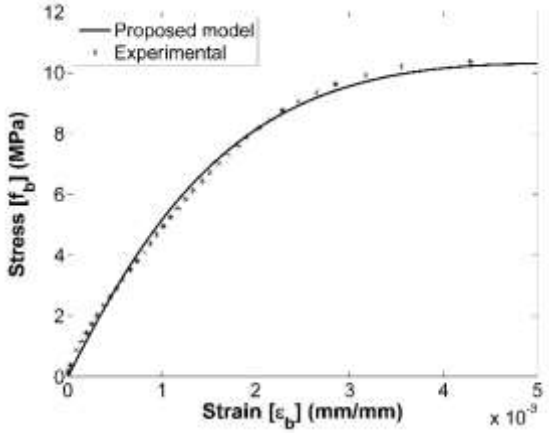

a)

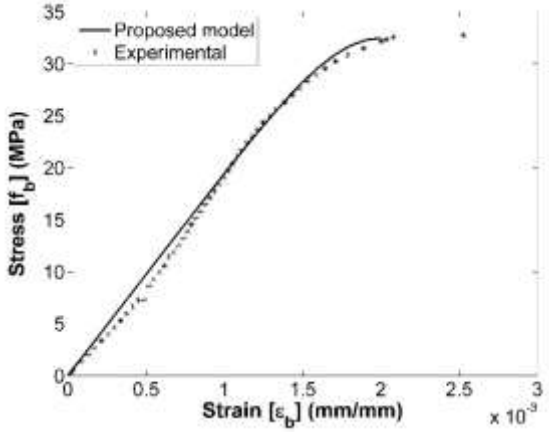

b)

Figure 3. 9. Analytical model versus experimental results for a) Low strength (f'_b=10MPa), b) High strength (f'_b=30MPa).

3.9 Discussion and conclusions

The mechanical behavior of prefabricated hollow concrete blocks has been evaluated experimentally with uniaxial compression loads, in order to obtain the complete stress-strain history and the main design parameters which control the behavior of masonry units. With these results, and considering the similarity between the experimental results and the expression proposed by Popovics (1973), this equation has been adapted to evaluate the normalized stress-strain curve for prefabricated hollow concrete blocks. New empirical correlations were established in order to obtain the parameters related to the structural behavior observed in concrete blocks. The above constitutes a useful tool for the design of masonry structures centered on the displacement based design method.

The two levels of compression strength which were evaluated enabled the identification of the need to employ analytical models which consider the variation in compression strength. The formula proposed by Popovics (1973) complies with this requirement. The results obtained show that for both, conventional concrete, as well as prefabricated hollow concrete blocks, the shape of the stress-strain curve depends on the magnitude of uniaxial compression strength. Although the constructive process of both materials may be different, its structural behavior under uniaxial compression loads is similar.

The expressions used by the design codes in order to obtain the main parameters that affect the behavior of masonry should be revised and validated experimentally. In general, the experimental results show that the values of the modulus of elasticity in the masonry units are below the proposed correlations of worldwide codes for masonry structures. This implies that the deformations of these elements are presently being underestimated. The experimental values obtained in this investigation show that the best correlation between the modulus of elasticity and its compression strength for masonry units is a curve, contrary to the proposal of a linear correlation presented in the majority of the worldwide standards.

CHAPTER 4. STRESSES AT ULTIMATE STATE OF UNBONDED TENDONS IN UNGROUTED POST-TENSIONED MASONRY BEAMS

"With the exception of material phenomena not covered in previous masonry or prestressed concrete research, the next logical step in the development of prestressed masonry is the synthesis of specific structural applications. This requires close communication between designers, builders, materials suppliers and researchers who advocate the use of structural masonry." (Schultz and Scolforo, 1991)

Abstract

An accurate estimation of tendon stress is crucial for calculating the flexural capacity of post-tensioned masonry. Tendon stresses in bonded elements may be calculated based on the concept of strain-compatibility. In unbonded tendons, stresses depend on the relative displacement between the element's anchor points, and strain-compatibility is not totally applicable in calculating stress variations. Post-tensioned masonry codes provide several equations based on modified strain-compatibility approaches, which are used for calculating ultimate-state stress increments in unbonded tendons; many of these equations were obtained through the statistical evaluation of experimental results and finite-element models. Given the uncertainty on several hypotheses of strain-compatibility between the tendon and the adjacent masonry for unbonded elements, which are used by most worldwide masonry codes, a new approach to calculate tendon stress increment has been developed. It is based exclusively on the theory of solid mechanics of beam deflections for the elastic behavior, which includes a plastic hinge with a geometric curvature distribution in the inelastic region. To compare the accuracy of code equations and the proposed methodology, a large database of experimental test results of post-tensioned masonry beams was used. This comparison shows that the proposed equation provides an accurate prediction of tendon stress at ultimate for post-tensioned masonry beams.

Keywords: Unbonded tendon; Stress; Post-tensioning; Masonry; Beams.

4.1 Introduction

The tendon force in a prestressed masonry beam with unbonded tendons balances the external forces and reduces the beam deflection. An exact calculation of the flexural capacity of post-tensioned masonry elements has generated a great challenge over the years, it requires an accurate estimation of the tendon stress at the ultimate state, and it should be validated for realistic designs of post-tensioned masonry structures. This is relatively straightforward for post-tensioned members with bonded tendons due to the strain compatibility, where tendons and the adjacent masonry are "glued" together, which prevents the relative longitudinal displacement from occurring between them. The use of unbonded tendons in post-tensioned masonry is becoming more widespread in the masonry industry, and strain-compatibility is not applicable in determining tendon force increment in ungrouted, unbonded elements. Stress increment in unbonded tendons cannot be estimated through the analysis of a single section, and it depends strongly on the global kinematic compatibility between masonry and tendons, as well as the deformation of the whole assembly (Ozkul et al., 2008). Since the early 1950s, research for post-tensioned concrete beams has been conducted to determinate the stress at the ultimate state in unbonded tendons. The results of these investigations have been adopted by several design provisions such as those in Great Britain (BS 5628-2, 2005), Australia (AS 3700, 2011), USA (MSJC, 2013), New Zealand (NZS 4230, 2004) and Canada (CSA, 2014).

The equations used to calculate tendon stress of unbonded elements at failure state are usually based on a modified strain-compatibility, an approach where equivalent plastic lengths or strain reduction (or bond reduction) factors are used; however, these methodologies are still controversial due to the empirical parameters used in those equations (Yang and Kang, 2011). In this work, a rational expression, based on beam deflection methodology (He and Liu, 2010), is adapted to calculate the tendon stress at ultimate state, this methodology is based exclusively on the theory of solid mechanics of beam deflections to calculate stress increment within the linear elastic range. In the nonlinear range, the methodology is based on the concept of an equivalent plastic hinge that occurs at the section of maximum moment, near to the midspan beam, and use of the principle of curvature distribution on the beam. For simplicity, the geometric curvature in the plastic hinge length of the beam is idealized as an equivalent rectangle for calculating the area under the curvature diagram. This proposed expression involves the key design parameters for this structural system: loading type, initial prestress force, masonry compressive strength, beam length, tendon eccentricity, and prestressed tendons' cross section. This new approach is supported by data acquired through full-scale structural testing of ungrouted post-tensioned masonry beams, as well as by data collected from the literature.

4.2 Review of analytical expressions and code equations to estimate tendon stress at ultimate state

In this section, a summary of studies related to the estimation of tendon stress increment at ultimate state is presented. Over the past four decades, several experimental and theoretical investigations have studied the influence of the principal factors that affect tendon stress increment in unbonded concrete members, and numerous design equations have been proposed with significant scatter in their predictions regarding the experimental results. From both, theoretical and experimental research, the following basic parameters have been found to be the most influential in the tendon stress increment at ultimate: concrete strength, reinforcement cross section, span-depth ratio, and loading type (Guiglia et al., 2012).

The usual expression used to predict the tendon stress in the unbonded tendon for any external load (f_{ps}), results from adding the effective prestress after losses (f_{pe}) and the subsequent stress increment (Δf_{ps}) due to the applied additional bending load (Eq. 4.1):

$$f_{ps} = f_{pe} + \Delta f_{ps} \qquad (4.1)$$

To estimate Δf_{ps}, two types of methods have been proposed: one based on strain reduction, and one based on an equivalent plastic hinge. Baker (1949) introduced the strain or bond reduction method, which includes a bond reduction factor (Ω), defined as the ratio between the strain change adjacent to the unbonded tendons ($\Delta\varepsilon_{psu}$), and the strain change in the equivalent bonded tendons ($\Delta\varepsilon_{psb}$) ($\Omega = \Delta\varepsilon_{psu}/\Delta\varepsilon_{psb}$). Here Ω=1 corresponds to tendons perfectly bonded to the concrete. Actual values of Ω are influenced by the loading type, the cable profile, and the relationship between ends and mid-span eccentricities (Naaman and Alkhairi, 1991).

Alternatively, an equivalent plastic hinge method has been proposed to calculate the tendon stress increment at failure (Wight et al., 2006). This method considers the development of both elastic and inelastic zones along the beam, and its formulation can be derived from rigid-body mechanics. The mechanism of two equal non-deflected rigid bodies connected at the mid-span by a plastic hinge is used to represent the deformed shape of a simply supported beam at failure. A plastic hinge is produced at the maximum moment section, which redistributes any extra load to adjacent regions. The increment of tendon length between the anchorage blocks is due to the deformation in the plastic region.

Several equations have been proposed to calculate stress increment at ultimate ($\Delta f_{ps,u}$) using the previous approaches, and some of them have been adopted by post-tensioned masonry codes (Phipps, 1992; Pannell, 1969). A short summary of some of these expressions is presented in Table 4.1, where some symbols have been modified from the original expressions to provide a standard notation and avoid confusion.

The first design provisions for post-tensioned masonry were published by the British Standards Institution in 1985 (Schulz and Scolforo, 1991), and many of those expressions were taken from masonry and concrete codes used at that time. The use of strain compatibility between the tendon and the adjacent masonry makes the accuracy of code equations questionable, as prior researchers have shown (Bean, 2003; Wight et al., 2006; Bean and Schultz, 2010).

The equations given in five post-tensioned masonry codes allow a direct comparison between estimates of tendon stress at ultimate stage, and experimental results (see Table 4.2). In most codes, the expression to estimate the tendon force at failure comes from the equivalent plastic hinge methodology (Eq. 4.2) using Whitney's rectangular stress distribution (Eq. 4.3). The difference among codes is the assumption regarding the behavior at ultimate stage, and the different empirical parameters obtained from test data and statistical correlations.

$$f_{ps} = f_{pe} + \frac{\mathrm{E_{ps}}}{L}(d - c)\theta \qquad (4.2)$$

$$c = \frac{a}{\beta_1} = \frac{f_{ps}A_{ps} + P_v}{\beta_1\beta_2 f'_m b} \qquad (4.3)$$

Table 4. 1 Summary of equations for tendon stress increment at failure in post-tensioned concrete beams

Reference	Equation	Observations
a) Expressions based on strain or bond reduction method		
Naaman and Alkhairi's (1991)	$\Delta f_{ps,u} = E_{ps}\Omega\varepsilon_{cu}\left(\frac{d}{c}-1\right)$	$\Omega = \frac{1.5}{L/d}$ for single − point loading $\Omega = \frac{3.0}{L/d}$ for two-point or spread loading
Sivaleepunth et al. (2006)		$\Omega = 0.3\frac{L_a}{L} + 0.01\frac{S_d}{d} + 0.1$ for single, two-point or spread loading
b) Expressions based on equivalent plastic hinge length		
Pannell (1969)	$\Delta f_{ps,u} = E_{ps}\varepsilon_{cu}\frac{d-c}{c}\left(\frac{L_p}{L}\right)$	$L_p = 10.5c$
Harajli (1990)		$L_p = L_a + d + 0.1Z$
Au and Du (2004)		$L_p = 10.5c$

Some code assumptions have been investigated by Wight et al. (2006), who observed that code expressions leads to substantial errors for low aspect and axial force ratios (h_e/l_e<10, and f_m/f'_m<0.1, respectively). Similarly, after reviewing the results of 54 laboratory tests on out-of-plane loaded post-tensioned masonry walls, Bean and Schultz (2003), showed that the MSJC-2002 provided over-conservative estimates of tendon force increment, and proposed a modification to the tendon stress equations which establishes differences between restrained and unrestrained tendons that were included in the MSJC-2005 code. The formula found in MSJC-2013 to calculate the tendon stress increment, is based on the research by Bean and Schultz (2010), who indicated that the MSJC-2008 expression was typically conservative with a large variance (COV>0.75).

A summary of code equations is shown in Table 4.2, where some symbols have been modified from the original expressions to provide a standard notation and avoid confusion.

Table 4. 2. Summary of expressions to estimate the tendon stress increment in prestressed concrete masonry codes.

Code	Equations	α	β	ε_{mu}	Observations
British (BS 5628-2, 2005)	$\Delta f_{ps,u} = 700\left(\frac{d}{L}\right)\left[1-1.4\frac{f_{pu}A_{ps}}{f'_m bd}\right]$ (MPa)	0.50	1.00	0.0035	$\theta = \frac{\delta_c}{c} = \frac{\varepsilon_{mu}c}{c} = \varepsilon_{mu}$
Australian (AS 3700, 2011)	$\Delta f_{ps,u} = 700\left(\frac{d}{l_p}\right)\left[1-0.7\frac{f_{pu}A_{ps}}{f'_m bd}\right]$ (MPa)	1.10	0.85	0.0035	$\theta = \frac{\delta_o}{c} = \frac{\varepsilon_{mu}c}{c} = \varepsilon_{mu}$
USA (MSJC, 2013)	$\Delta f_{ps,u} = 0.03\left(\frac{E_{ps}d}{L}\right)\left(1-1.56\frac{f_{ps,u}A_{ps}}{f'_m bd}\right)$	0.80	0.80	0.0025	$\theta = \frac{\delta_o}{c} = \frac{\Psi\varepsilon_{mu}c}{c} = 0.03$
New Zealand (NZS 4230, 2004)	$\Delta f_{ps,u} = 70 + \frac{f'_m bd}{NA_{ps}}$ (MPa)	0.85	0.85	0.0030	N = 100 for $\lambda \leq 35$ N = 300 for $\lambda > 35$
Canadian (CSA, 2014)	$\Delta f_{ps,u} = \frac{E_{ps}}{25L}\sum_{n_p}(d-c)$	0.85	0.80	0.0030	$\theta = \frac{1}{25}$, and more than one gap may open

4.3 Proposed methodology to estimate the tendon stress increase based on beam deflection

A new methodology to calculate tendon stress increment, adapted from beam deflection expressions, is proposed. It is based on linear-elastic mechanics of solids theory, where a linear correlation between tendon stress increments and beam deflection exists during the entire loading stage. The total tendon elongation can be calculated under the following

assumptions: shear deformation is negligible, force along the tendon is constant, a plastic hinge is developed at the ultimate state, and friction between the deviator block, surrounding masonry, and the tendon is negligible.

Stress increment comes from the relative deformation between the tendon anchorages which, in turn, relates to the beam deflection. In the initial condition for the beam, it has been assumed that the cable is deflected, and the beam is deformed by its own weight. The initial cable length, before the additional vertical load is applied, is obtained as $L_o=\rho\omega=$ □ where ρ is the distance from the center of curvature to the neutral axis, and ω is the angle subtended by the arc between the ends of the beam due to beam deflection [Fig. 4.1], assuming that length of neutral axis fiber remains constant during the loading process.

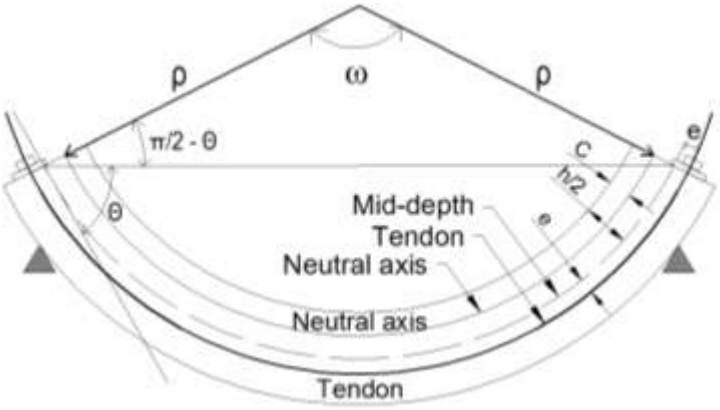

Figure 4. 1 Deflection beam shape

Deviator blocks located at midspan and beam ends make the post-tensioned bar acquire a deformed shape close to that of the deflected beam. The final length, L_f, in the masonry adjacent to the tendon after load is applied is:

$$L_f = \left[\rho - c + \left(\frac{h}{2} + e\right)\right]\omega \qquad (4.4)$$

The total length change in the masonry adjacent to the tendon, ΔL, is:

$$\Delta L = L_f - L_o = \left(\rho - c + \frac{h}{2} + e\right)\omega - \rho\omega = \left(e + \frac{h}{2} - c\right)\omega \qquad (4.5)$$

Noting that the beam is assumed to deflect symmetrically due to the symmetry of both structure and load, the total angle change, ω, is equal to $2\theta_{end}$, and the length change can be expressed as follows:

$$\Delta L = 2q_{end}\left(e + \frac{h}{2} - c\right) \qquad (4.6)$$

The tendon length change can be computed in the elastic regime as:

$$\Delta L = \frac{\Delta T * L}{A_{ps}E_{ps}} = \Delta f_{ps}\frac{L}{E_{ps}} \qquad (4.7)$$

By equating Eq. (4.6) and Eq. (4.7), the tendon stress increment can be written as:

$$\Delta f_{ps} = \frac{2E_{ps}q_{end}}{L}\left(e + \frac{h}{2} - c\right) \qquad (4.8)$$

For a continuous beam in the elastic stage, θ_{end} can be expressed as:

$$\theta_{end} = \eta\frac{\delta_{mid}}{2L} \qquad (4.9)$$

Thus, the tendon stress increment in the elastic stage can be written as follows:

$$\Delta f_{ps} = h\frac{E_{ps}d_{mid}}{L^2}\left(e + \frac{h}{2} - c\right) \qquad (4.10)$$

From the theory of solid mechanics a relationship between midspan deflection (δ_{mid}) and peak bending moment (M_u) can be found for a simply supported beam under a specific load type, giving the following expression:

$$\delta_{mid} = K\frac{M_u L^2}{EI} = KL^2\phi_u = KL^2\frac{\varepsilon_{mu}}{c} \qquad (4.11)$$

Replacing Eq. (4.11) into Eq. (4.10), an adapted expression for the tendon stress increment can be found:

$$\Delta f_{ps,u} = hKE_{ps}e_{mu}\left(\frac{e + h/2}{c} - 1\right) \qquad (4.12)$$

or, equivalently:

$$\Delta T_u = hKA_{ps}E_{ps}e_{mu}\left(\frac{e + h/2}{c} - 1\right) \qquad (4.13)$$

In this way, the tendon stress at the ultimate state can be written as:

$$f_{ps,u} = f_{pe} + \eta K E_{ps} \varepsilon_{mu} \left(\frac{e + h/2}{c} - 1 \right) \quad (4.14)$$

which is equivalent to:

$$T_u = T_i + \eta K A_{ps} E_{ps} \varepsilon_{mu} \left(\frac{e + h/2}{c} - 1 \right) \quad (4.15)$$

Total tendon elongation can be calculated under the following assumptions: the post-tensioned masonry beam is dominated by bending and shear deformation is negligible, stress along the tendon is uniform, and friction between the tendon and the surrounding masonry is negligible.

4.3.1 Derivation of parameters η and K

4.3.1.1 Parameter η

From Eq. (4.8) and Eq. (4.10), the parameter η is obtained:

$$\eta = \frac{2\theta_{end} L}{\delta_{mid}} \quad (4.16)$$

Where θ_{end} is the slope at the end of the beam with length, L, and the maximum deflection, δ_{mid}, occurs at mid-span. The beam is assumed to deflect in a symmetric manner, such that $\theta_{end} = \omega/2$.

The end-slope θ_{end} and the deflection δ_{mid} can be obtained using the Moment-Area method to integrate the curvature relation as shown in Eq. (4.17).

$$\theta_{end} = \frac{1}{2}\omega = \frac{1}{2}\int_0^L \frac{M(X)}{EI} dx = \frac{1}{2} A_{M/EI} \quad (4.17)$$

where $A_{M/EI}$ is the area under the curvature (M/EI) diagram along beam length, L. Similarly, the mid-span deflection, δ_{mid}, is obtained using the tangential deflection, at end of the beam with respect to the mid-span, $\tau_{a/mid}$:

$$\delta_{mid} = \tau_{a/mid} = \int_0^{L/2} x_a \frac{M(X)}{EI} dx = \bar{X}_a \int_0^{L/2} \frac{M(X)}{EI} dx = \bar{X}_a \left(\frac{A_{M/EI}}{2} \right) \quad (4.18)$$

where the area under the curvature diagram for one-half of the beam is equal to one-half of the total area due to symmetry. The position variable x_a originates at one of the ends of the beam, and $\bar{X}_a$ is the distance from that point to the centroid of one-half of the total area of the curvature diagram. Substituting Eq. (4.17) and Eq. (4.18) into Eq. (4.16), the parameter η is obtained for the case of symmetric beams.

$$h = \frac{2q_{end} L}{d_{mid}} = \frac{2L\left(A_{M/EI}/2\right)}{\left(\bar{X}_a A_{M/EI}/2\right)} = \frac{2L}{\bar{X}_a} \quad (4.19)$$

4.3.1.2 Parameter K

The parameter K can be defined on the basis of Eq. (4.11) and Eq. (4.18):

$$K = \frac{EI}{M_{max} L^2} \delta_{mid} = \frac{\bar{X}_a}{2L} \frac{A_{M/EI}}{\left(\frac{M_{max}}{EI}\right) L} \quad (4.20)$$

4.3.1.3 Parameter ηK

From Eq. (4.19) and Eq. (4.20), the product of η and K is

$$\eta K = \left(\frac{2L}{\bar{X}_a}\right) \left[\frac{\bar{X}_a}{2L} \frac{A_{M/EI}}{\left(\frac{M_{max}}{EI}\right) L} \right] = \frac{A_{M/EI}}{\left(\frac{M_{max}}{EI}\right) L} \quad (4.21)$$

These formulas for η and K provide values for these coefficients that largely agree with values suggested in previous research on post-tensioned concrete beams (MacGregor, 1989; Du and Liu, 2003; Roberts-Wollman and Kreger, 2005; Wang, 2005).

4.3.2 Effect of inelastic behavior on η and K tendon stress parameters

Equation (4.21) can be generalized to include inelastic behavior, by including the consideration of the plastic hinge region. The elastic curvatures, M/EI, are replaced with the geometric curvatures, ϕ, that can be defined for both elastic and inelastic beams. Thus, the resulting expression is:

$$hK = \frac{A_f}{f_m L} \quad (4.22)$$

where A_ϕ is the area under the curvature diagram, and ϕ_m is the maximum curvature. For a simply supported, post-tensioned masonry beam, the curvature diagram can be assumed as in Figure 4.2, in which a portion of the curvature diagram is magnified beyond the elastic values, because the cross-section stiffness decreases rapidly when the masonry units separate due to beam bending.

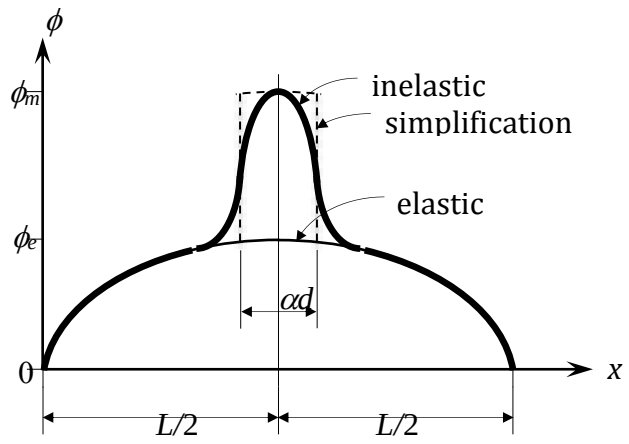

Figure 4. 2. Idealized curvature diagram

This amplification is assumed to occur over an equivalent plastic hinge length at ultimate αd centered about the location of maximum moment when failure state is achieved, were d is the distance from extreme compression fiber to centroid of prestressing tendon, and $d = h/2 + e$. If this region of amplified curvatures is simplified using a rectangular element, then the area under the curvature diagram can be computed as follows:

$$A_{\Phi} = \frac{2}{3}\phi_e L + (\phi_m - \phi_e)\alpha d = \phi_m L\left[\left(\frac{\phi_e}{\phi_m}\right)\left(\frac{2}{3} - \alpha\frac{d}{L}\right) + \alpha\frac{d}{L}\right] \quad (4.23)$$

where ϕ_e is the maximum idealized elastic curvature and ϕ_m is the maximum inelastic curvature. To determine precisely the equivalent plastic hinge length is a difficult task (Harajli, 2006), the parameter α can be obtained from diverse assumptions, and various review investigations classified it proportional to: beam length (Harajli, 1990; Lee et al., 1999; Harajli et al., 2002), neutral axis depth (Tam and Pannell, 1976; Au and Du, 2004; Harajli, 2006), or tendon depth (Naaman and Alkhairi, 1991). Considering that the methodology proposed by Naaman and Alkahari (1991) is best adapted to the laboratory test results conducted in this investigation, a value of α=0.75 was adopted.

Defining the ratio of inelastic to elastic curvature ϕ_m/ϕ_e as the curvature ductility, μ_ϕ, and substituting Eq. (4.23) into Eq. (4.22), the product of η and K can be expressed as a function of the aspect ratio, L/d and the curvature ductility μ_ϕ as follows:

$$\eta K = \frac{1}{\mu_\phi}\left(\frac{2}{3} - \alpha\frac{d}{L}\right) + \alpha\left(\frac{d}{L}\right) \quad (4.24)$$

4.3.3 Define the curvature ductility

4.3.3.1 Elastic state

The elastic curvature, f_e is an idealized quantity because it represents the curvature under maximum moment, M_{max}, but for a section that remains elastic. Under these assumed conditions, the masonry strain in the extreme compressive fiber is approximated using (as) the strain, ε_o in the masonry stress-strain response (relation) at the maximum value of stress. In addition, the neutral axis is assumed to be equal to d.

$$\phi_e \sim \frac{\varepsilon_o}{d} \quad (4.25)$$

4.3.3.2 Inelastic state

For the inelastic state, f_m can be evaluated from the tendon strain at ultimate:

$$f_m = \frac{\varepsilon_{mu}}{c} \quad (4.26)$$

Using Eq. (4.25) and Eq. (4.26) to define μ_f gives the following.

$$\mu_\varphi = \frac{\varepsilon_{mu}/c}{\varepsilon_o/d} = \left(\frac{\varepsilon_{mu}}{\varepsilon_o}\right)\left(\frac{d}{c}\right) = \mu_\varepsilon\left(\frac{d}{c}\right) \quad (4.27)$$

Substituting Eq. (4.27) into Eq. (4.24) and simplifying gives the following:

$$\eta K = \frac{1}{\mu_\varepsilon}\left(\frac{c}{d}\right)\left(\frac{2}{3} - \alpha\frac{d}{L}\right) + \alpha\frac{d}{L} \quad (4.28)$$

Substituting Eq. (4.28) into the revised formula for tendon stress increase gives the following expression:

$$\Delta f_{psu} = E_{ps}\varepsilon_{mu}\left[\frac{2}{\mu_\varepsilon}\left(\frac{c}{d}\right)\left(\frac{2}{3} - \alpha\frac{d}{L}\right) + \alpha\frac{d}{L}\right]\left(\frac{e + h/2}{c} - 1\right) \quad (4.29)$$

Eq. (4.29) can be further rewritten as follows:

$$\Delta f_{psu} = \frac{E_{ps}\varepsilon_{mu}}{\mu_\varepsilon}\left[\left(\frac{c}{d}\right)\left(\frac{2}{3} - \alpha\frac{d}{L}\right) + \alpha\mu_\varepsilon\left(\frac{d}{L}\right)\right]\left(\frac{d}{c} - 1\right) \quad (4.30)$$

Recognizing that $\mu_\varepsilon = \varepsilon_{mu}/\varepsilon_0$, then further simplification gives:

$$\Delta f_{psu} = E_{ps}\varepsilon_o\left[\left(\frac{c}{d}\right)\left(\frac{2}{3} - a\frac{d}{L}\right) + am_e\left(\frac{d}{L}\right)\right]\left(\frac{d}{c} - 1\right) \quad (4.31)$$

To evaluate μ_ε, the value for masonry strain at peak compressive stress, ε_o, is needed. This parameter has been evaluated in many masonry prism compressive tests to be approximately equal to 0.0014 for most masonry. The other parameter needed to evaluate μ_ε is the maximum usable compressive strain for the masonry, ε_{mu}. In the US (MSJC 2013), the code-specified values for ε_{mu}, are equal to 0.0025 and 0.0035 respectively for concrete masonry and fired clay masonry. However, experimental evidence from prisms tests (Kaushik et al., Soto et al.) does not suggest a significant difference between concrete masonry and fired clay masonry.

$$\mu_\varepsilon = \frac{\varepsilon_{mu}}{\varepsilon_o} = \frac{0.0025}{0.0014} = 1.75 \quad (4.32)$$

Equation (4.31) can be implemented with greater accuracy because ε_o, the strain at peak stress in the masonry compressive stress-strain relation, is known more precisely than the compressive strain capacity, ε_{mu} , and the former exhibits less variability than the latter. Moreover, Nazir and Hart (2001) have suggested that ε_o and is related linearly to the compressive strength of masonry, f'_m. In the present study, Nazir and Hart's representation is modified assuming directly proportionality because the strain at peak stress, ε_o, should vanish when f'_m is equal to zero. The strain at peak compressive strain, ε_o, is given by:

$$\varepsilon_o = \frac{f'_m}{E_{mo}} \quad (4.33)$$

where E_{mo} is the secant modulus for the strain-strain relation for masonry in uniaxial compression which connects the origin to the point of peak stress. Nazir and Hart's (2001) uniaxial compression test data for concrete masonry is shown below left along with Eq. (4.33), for which E_{mo} = 11,000 MPa.

The compressive stress-strain data reported by Baqi et al. (1999) is used here to establish a similar relationship for clay masonry in compression. This data is shown in the figure above right along with Eq. (4.33), for which E_{mo} = 5,000 MPa.

Introducing Eq. (4.33) into Eq. (4.31) and rearranging terms gives

$$\Delta f_{psu} = \frac{E_{ps}f'_m}{E_{mo}}\left[\frac{2}{3}\left(\frac{L}{d}\right) + \gamma\right]\left(\frac{d - c}{L}\right) \quad (4.34)$$

Where

$$\gamma = \alpha\left(\mu_\varepsilon\frac{d}{c} - 1\right) \quad (4.35)$$

Of the variables in Eq. (4.33) and Eq. (4.35) for computing Δf_{ps}, E_{ps}, f'_m, L, h and e are known at the time of design, E_{mo} can be estimated knowing the type of masonry, and c can be computed once the total amount of tendon stress is determined. However, to evaluate γ requires knowledge of parameters that define the inelastic behavior of the beam, namely the normalized plastic hinge length, α, and the strain ductility factor, μ_ε. Given that these parameters are difficult, if not impossible to determine without conducting tests or numerical simulations, an approximate constant value for γ is suggested here. The normalized plastic hinge length, α, is assumed to be equal to 0.75 and the neutral axis depth is approximated as d/4. The latter value was selected based on the notion that for most post-tensioned beams, the *d/c* ratio would vary from 2 to 6, with a median value of approximately 4. The strain ductility factor $\mu_\varepsilon = 1.75$ is consistent with a compressive strain capacity, ε_{cu}, equal to 0.0035, and the strain at peak stress, ε_o, of 0.002 (or ε_{cu} = 0.0025 and ε_o = 0.0014). Thus, $\gamma = (0.75)[1.75(4) - 1] = 4.5$, and tendon stress increase is given by:

$$\Delta f_{psu} = \frac{E_{ps}f'_m}{E_{mo}}\left[\frac{2}{3}\left(\frac{L}{d}\right) + 4.5\right]\left(\frac{d - c}{L}\right) \quad (4.36)$$

In summary, the Eq. (4.34) and Eq. (4.35) can (should) be used when sufficient information is available regarding beam response to loading (i.e. α, μ_ε, and *d/c*), otherwise Eq. (4.36) with an approximate constant value for γ = 4.5 is suggested and used in the paper. Additionally, for cases in which E_{mo} cannot be determined nor estimated, values of 11,000 and 5,000 MPa are suggested here for concrete and clay

masonry, respectively.

4.3.4 Eliminating neutral axis depth - total tendon stress

A final measure can be used to further enhance the accuracy of the tendon stress estimates at ultimate. The measure concerns the neutral axis depth, c, and rather than using an iterative approach for its evaluation, c is obtained directly. Equilibrium of internal forces requires that $T_u + N_u = C_m$, and the external axial load on the beam, N_u, is assumed to be equal to zero. Thus, $T_u = A_{ps} f_{ps,u} = A_{ps}\left(f_{se} + \Delta f_{ps,u}\right)$ and $C_m = \left(b_1 f_m'\right)\left(b_2 c\right) b$, where β_1 = 0.8 and β_2 = 0.8 according to the TMS 402-2013. Substituting Eq. (4.36) for Δf_{ps} and solving for neutral axis depth, c, gives:

$$c = \frac{f_{se} + \left(\frac{E_{ps} f_m'}{E_{mo} L}\right)\left[\frac{2}{3}\left(\frac{L}{d}\right) + 4.5\right] d}{\left(0.64 \frac{f_m' b}{A_{ps}}\right) + \left(\frac{E_{ps} f_m'}{E_{mo} L}\right)\left[\frac{2}{3}\left(\frac{L}{d}\right) + 4.5\right]} \qquad (4.35)$$

Substituting Eq. (4.37) into the expression for C_m, noting that $C_m = T_u = A_{ps} f_{ps,u}$, and simplifying gives

$$f_{ps,u} = \frac{T_u}{A_{ps}} = \frac{C_m}{A_{ps}} = \frac{f_{se} + f_m'\left(\frac{E_{ps}}{E_{mo}}\right)\left(\frac{d}{L}\right)\left[\frac{2}{3}\left(\frac{L}{d}\right) + 4.5\right]}{1 + 1.56\left(\frac{E_{ps}}{E_{mo}}\right)\left(\frac{A_{ps}}{bL}\right)\left[\frac{2}{3}\left(\frac{L}{d}\right) + 4.5\right]} \qquad (4.36)$$

And, the tendon stress increase is calculated as the difference of Eq. (4.38) and f_{se}

$$\Delta f_{ps} = \frac{\left[f_m' - 1.56 f_{se}\left(\frac{A_{ps}}{bd}\right)\right]\left(\frac{E_{ps}}{E_{mo}}\right)\left(\frac{d}{L}\right)\left[\frac{2}{3}\left(\frac{L}{d}\right) + 4.5\right]}{1 + 1.56\left(\frac{E_{ps}}{E_{mo}}\right)\left(\frac{A_{ps}}{bL}\right)\left[\frac{2}{3}\left(\frac{L}{d}\right) + 4.5\right]} \qquad (4.39)$$

Eq. (4.3) provides a rational expression to estimate Δf_{ps} based on fundamental concepts of solid mechanics, where equilibrium, stress-strain relations, and deformation compatibility are satisfied. It is pertinent to both elastic and plastic states, and it contains several of the influential factors in the behavior of post-tensioned beams. The proposed expression is an easy and reasonable expression, where the adequacy of the analytical model was verified by comparison against experimental results in the following section. Finally, note from Eq. (4.38) that there is a practical limit beyond which the post-tensioning reinforcement does not produce an increase in tendon stress at ultimate. This occurs when $f_m' \leq 1.56 f_{se}(A_{ps}/bd)$ or $f_{se} A_{ps} \geq 0.64 f_m' bd$.

4.3.5 Selection of effective width for hollow sections

The use of hollow sections in the construction of post-tensioned masonry beams, reduces material consumption, lightens the weight and optimizes structural design of the structure. For sections that are grouted solid with unbonded tendons, Eq. (4.37) and Eq. (4.38) are calculated using the actual width, b, of the section. For hollow sections, they have been tried with a different effective width, b_{eff}, in order to simplify the design procedures and work with an equivalent rectangular cross section. A first proposal of effective width is calculated as the ratio of the net area of the section, A_n, to the overall depth, h, of the section ($b_{eff} = A_n/h$), obtaining thus a direct equivalence in the cross-sectional area of the beam.

The second approach of effective width is calculated as the sum of the vertical partitions, t_{ef}, of a hollow concrete block ($b_{eff} = 2t_{ef}$), assuming the effect of horizontal partitions is negligible. Table 4.3, shows the results obtained to tendon force at ultimate with each approach of effective width and their comparison when all calculations are made using a full hollow block section.

Table 4. 3. Comparisons of calculations of tendon force at ultimate between complete and simplified cross section.

Beam	Complete Hollow Section (kN)	Simplified Section (1) ($b_{eff}=A_n/h$) (kN)	Simplified Section (2) ($b_{eff}=2t_{ef}$) (kN)	Simp. Sec.(1)/ Complete Section	Simp. Sec.(2)/ Complete Section
B-01	116,460	118,570	101,340	1.02	0.87
B-02	97,860	98,550	84,210	1.01	0.86
B-03	108,590	111,100	94,990	1.02	0.87
B-04	100,080	101,090	87,030	1.01	0.87
B-05	107,500	105,830	94,600	0.98	0.88
B-06	109,810	108,840	100,550	0.99	0.92
B-07	114,600	114,030	105,340	1.00	0.92
B-08	129,800	126,920	117,260	0.98	0.90
B-09	201,200	204,730	174,950	1.02	0.87
B-10	182,500	185,520	158,420	1.02	0.87
B-11	182,710	185,740	158,810	1.02	0.87
B-12	169,250	170,000	145,260	1.00	0.86
B-13	186,110	189,570	163,090	1.02	0.88
B-14	173,590	175,010	150,580	1.01	0.87
B-15	172,760	174,040	149,830	1.01	0.87
B-16	114,960	116,760	101,460	1.02	0.88
B-17	114,440	116,320	100,290	1.02	0.88
B-18	111,040	112,760	97,240	1.02	0.88
B-19	102,730	104,080	90,460	1.01	0.88
B-20	127,810	128,740	111,940	1.01	0.88
B-21	179,620	181,980	156,910	1.01	0.87
B-22	164,630	164,600	141,940	1.00	0.86
B-23	162,520	162,180	141,000	1.00	0.87
			Mean	**1.01**	**0.88**
			Standard Deviation	**0.01**	**0.02**
			COV	**0.01**	**0.02**

It can be observed from the results obtained that the proposal simplified section with an effective width of $b_{eff}= A_n/h$, provides a good approximation with complete section values, compared with a simplified section of $b_{eff}= 2t_{ef}$. This approach accurately represents the mechanical behavior of a hollow block section beam used in this research.

The result of this simplification substantially reduces the design calculations, and will be used for the subsequent calculations in this study.

4.4 Experimental program

An experimental program was carried out to evaluate the behavior of unbonded tendon stress increase by external loading on ungrouted prestressed concrete masonry beams under monotonic loading until failure. The test series comprised of twenty-three full-scale beams, tensioned previous to testing using three different magnitudes of tendon prestress induced on the cross section ($0.45f'_b$, $0.33f'_b$ and $0.22f'_b$), three masonry strengths (12 MPa, 18 MPa and 32 MPa), three prestressing tendon areas (177 mm^2, 284 mm^2 and 507 mm^2), two beam lengths (2.4 m and 3.2 m), two loading types (2 points and 4 points) [Fig. 4.4], and two tendon eccentricities (80 mm and 125 mm). Test beams were termed B-n, where n denotes the test number. In these tests, masonry compressive strength (f'_m) was determined by the MSJC-13 unit-strength

method using the tested compressive strengths of the concrete block (f'_b).

Additionally, test data from an experimental investigation carried out by Baqi et al. (1999), were used to verify the accuracy of the code provisions and proposed expressions to estimate tendon stress increase at flexural strength. The experimental program addressed a variety of post-tensioned masonry rectangular beams and one-way slabs, both with a central plain concrete core. Test series comprised twelve full-scale beams and four one-way slabs varying different parameters such as: cross-sectional area, masonry strength, prestressing tendon area, beam length, and tendon eccentricity. Test beams and slabs were termed B_{nm} and S_{nm} respectively, where n denotes the beam or slab number, and m denotes the specimen number. Specimens were prestressed by means of 7 mm diameter wires of high strength steel, with average values of initial modulus of elasticity, yield point (at 1% of strain), and maximum strength of 210 GPa, 1401 MPa, and 1489 MPa, respectively. The beams and slabs dimensions, properties, and posttensioning data are listed in Table 4.4.

4.4.1 Test specimens

The beams were built on the structural laboratory of the Civil Engineering Department at the University of Medellin (Colombia). The specimens were built using one single course bond pattern of hollow concrete blocks, with three (3) restraining blocks, two at the ends of the beams to support the anchorage forces to avoid unwanted local failures, and one at midspan which is used as a deviator block to restrain the tendon movement and keep the lever arm constant between the compression resultant force in the masonry and the traction force in prestressed steel [Fig. 4.3(a)], using a mortar bed typically 10mm thick. One straight threaded bar was placed horizontally along the beam with constant eccentricity guided by restraints in the form of deviator blocks. The average weight of the beams was approximately 756 N/m.

Table 4. 4. Test beams details

	Beam	L_l (m)	L (m)	Point load	f'_m (MPa)	T_i (kN)	e_{mid} (mm)	$\emptyset A_{ps}$ (mm)	A_{ps} (mm²)	L/d
Garcia et al. beams	B-01	2.41	2.62	4	12.00 (*)	75.20	80	25	507	9.53
	B-02	2.40	2.60	4	12.00 (*)	40.37	80	25	507	9.45
	B-03	2.44	2.61	4	12.00 (*)	62.50	80	25	507	9.49
	B-04	2.44	2.61	4	12.00 (*)	30.10	125	25	507	8.16
	B-05	2.30	2.50	2	15.54 (*)	53.65	80	19	284	9.09
	B-06	2.37	2.55	2	15.54 (*)	77.50	80	15	177	9.27
	B-07	2.36	2.56	2	15.54 (*)	84.00	80	15	177	9.31
	B-08	2.38	2.56	2	21.09 (*)	79.17	80	15	177	9.31
	B-09	2.40	2.57	4	21.09 (*)	145.50	80	25	507	9.35
	B-10	2.36	2.59	4	21.09 (*)	91.60	80	25	507	9.42
	B-11	2.44	2.63	4	21.09 (*)	93.40	80	25	507	9.56
	B-12	2.40	2.60	4	21.09 (*)	65.40	80	25	507	9.45
	B-13	2.40	2.58	4	21.09 (*)	71.80	125	25	507	8.06
	B-14	2.40	2.61	4	21.09 (*)	47.50	125	25	507	8.16
	B-15	2.43	2.62	4	21.09 (*)	46.70	125	25	507	8.19
	B-16	3.15	3.37	4	12.00 (*)	62.70	125	25	507	10.53
	B-17	3.13	3.34	4	12.00 (*)	75.80	80	25	507	12.15
	B-18	3.15	3.34	4	12.00 (*)	70.00	80	25	507	12.15
	B-19	3.18	3.35	4	12.00 (*)	42.60	125	25	507	10.47
	B-20	3.21	3.40	4	15.54 (*)	45.70	125	25	507	10.63
	B-21	3.14	3.35	4	21.09 (*)	96.00	80	25	507	12.18
	B-22	3.15	3.34	4	21.09 (*)	67.30	80	25	507	12.15
	B-23	3.20	3.36	4	21.09 (*)	42.10	125	25	507	10.50
	Beam	L_l (m)	L (m)	Point load	f'_m (MPa)	T_i (kN)	e_{mid} (mm)	$\emptyset A_{ps}$ (mm)	A_{ps} (mm²)	L/d
Baqi et	B_{11}	3.54	3.64	2	10.00	55.06	75	7	77	14.16

	Beam	L_l (m)	L (m)	Point load	f'_m (MPa)	T_i (kN)	e_{mid} (mm)	$\emptyset A_{ps}$ (mm)	A_{ps} (mm²)	L/d
al.	B_{12}	3.54	3.64	2	10.00	56.00	75	7	77	14.16
beams	B_{21}	3.54	3.64	2	13.20	56.70	75	7	77	14.16
	B_{22}	3.54	3.64	2	13.20	56.50	75	7	77	14.16
	B_{31}	3.54	3.64	2	10.00	64.00	120	7	77	9.97
	B_{32}	3.54	3.64	2	10.00	64.50	120	7	77	9.97
	B_{41}	3.54	3.64	2	13.20	63.80	120	7	77	10.11
	B_{42}	3.54	3.64	2	13.20	62.40	120	7	77	10.11
	B_{51}	1.95	2.15	2	13.20	26.00	72	7	38.5	7.89
	B_{52}	1.95	2.15	2	13.20	26.50	72	7	38.5	7.89
	B_{61}	1.95	2.15	2	13.20	27.00	82	7	38.5	7.59
	B_{62}	1.95	2.15	2	13.20	26.20	82	7	38.5	7.59
	S_{11}	2.44	2.5	4	10.00	127.20	30	7	154	28.71
	S_{12}	2.44	2.5	4	10.00	128.00	30	7	154	28.71
	S_{21}	2.44	2.5	4	13.20	140.00	28	7	154	29.40
	S_{22}	2.44	2.5	4	13.20	140.50	28	7	154	29.40

Note: (*) determined using the MSJC-13 unit-strength method;

The shape of the concrete block was prismatic, with external sizes of length, width and height, equal to 390±1 mm, 140±1 mm, and 190±2 mm respectively, with a gross area, and net area of 54600 mm² and 32800 mm², respectively [Fig. 4.3(b)].

Despite the curved form in the section of the hollow concrete block, for simplicity's sake the mathematical models in the calculations for the complete section assume a hollow rectangular cross section [Fig. 4.3(c)].

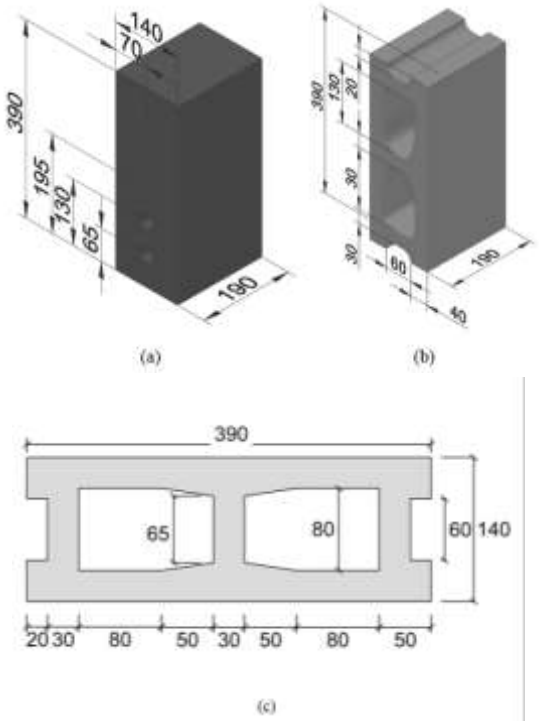

Figure 4. 3. Block geometry (a) Restraining block section (b) Block section (c) Cross section assumed (Dimensions: mm)

The beams were cured for a minimum of 28 days before prestressing. To prevent premature failure, prestressing was carried out on the floor the day of the test, and the stressing head is fitted with a load cell at the end of the stressing.

4.4.2 Material properties

4.4.2.1 Hollow concrete blocks

A sample of 115 hollow concrete blocks were tested to generate the complete stress-strain curves under uniaxial compression [Fig. 4.4], detailed information can be found at Garcia et al. (2013).

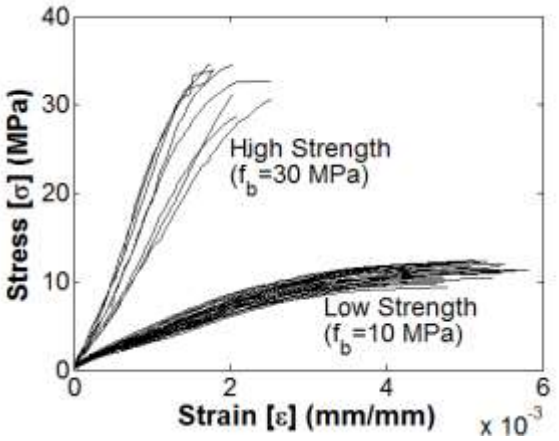

Figure 4. 4. Stress-strain curve in tested hollow concrete blocks (Garcia et al., 2013).

For this research, the strength correlation between individual blocks and masonry proposed by the TMS-2013 unit-strength method was adopted, where the mortar was classified according to their tested compressive strengths. The nominal strength obtained using this approach was used to predict tendon stress increase in the tested beams.

4.4.2.2 Mortar and concrete

Mortar mixed in a 1:2 cement to fine sand proportion by weight was used in the experimental program. Water content was adjusted by the bricklayer to give a workable mix. After 28 days of curing, the average compression strength was 32.4 MPa. The restraining blocks were made out of concrete in a 1:2:2 (cement: sand: coarse aggregate) proportion, giving an average compression strength of 35.6 MPa.

4.4.2.3 Prestressing steel

High-strength steel threaded bars of 15 mm, 19 mm and 25 mm diameter were used for prestressing in all test beams. Threaded bars of 19 mm and 25 mm diameter were made by using high-strength steel G75, with average value of initial modulus of elasticity, yield point (at 1% of strain), and maximum strength of 200 GPa, 517 MPa, and 690 MPa, respectively. Threaded bars of 15 mm diameter were made by using high-strength steel Y1050H, with average values of initial modulus of elasticity, yield point (at 1% of strain) and maximum strength of 205 GPa, 835 MPa, and 1030 MPa, respectively.

4.4.3 Test setup and instrumentation

Two simple supports were placed at the ends of tested beams, giving effective spans of 2400 mm or 3200 mm, approximately. A hydraulic jack was used to apply the monotonic load distributed at two [Fig. 4.5(a)], or four [Fig. 4.5(b)] loading points by a steel girder, supported on rollers to create an approximate uniformly distributed load. The variation in the method of applying the external load was principally due to the appearance of local failures under two loading points in the first tested beams. Subsequently, to avoid these local failures, four loading points were used for the following tested beams with very good results.

A load cell positioned above the jacking point in the testing rig has been employed to measure the applied load. The distance between loading points remained constant throughout the tests. For measuring beam deformations at midspan and quarterspan, linear variable differential transformers (LVDTs) were used. Also, other additional LVDTs were located next to the ends of specimens to measure the maximum rotation of the beams. Tendon stress increase was measured constantly through a load cell, located at the end of the beam. All specimens were tested under monotonically slowly increasing loads until beam failure. The ultimate load or failure was reached when the beam became incapable of taking any further load. Once peak load was reached, the test was terminated even though maximum deformation had not been achieved. A digital data acquisition was used to record in discrete intervals all measurement information in each tested beam.

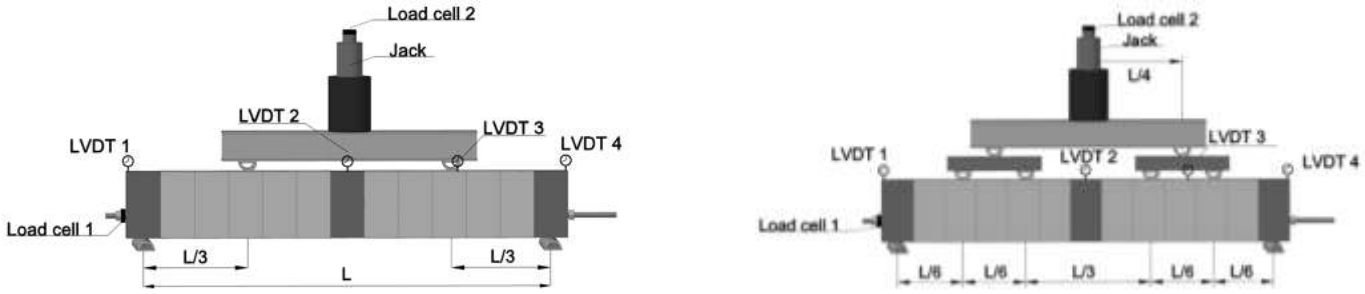

(a) Two point loading

(b) Four point loading.

Figure 4. 5. Test setup.

4.5 Experimental results

The force-deflection relationship was linear up to the point at which decompression occurred (i.e. first block separation load), after which inelastic behavior began. At this state, tensile cracks in the mortar beds increased, and the blocks began to separate, reducing the stiffness of the beam. All beams failed primarily by compression of the block, in the region where concrete crushing took place, close to the maximum constant

bending moment zone. A large percentage of the deformation was recovered upon unloading the beams. In all cases, the masonry reached its strain limit at ultimate state before the threaded bar yield.

4.5.1 Failure mode

All beams failed primarily in bending, after crushing of the mortar joints followed by chipping of the adjoining concrete block in the compression zone, near to the top of the beam within the maximum moment region [Fig. 4.6].

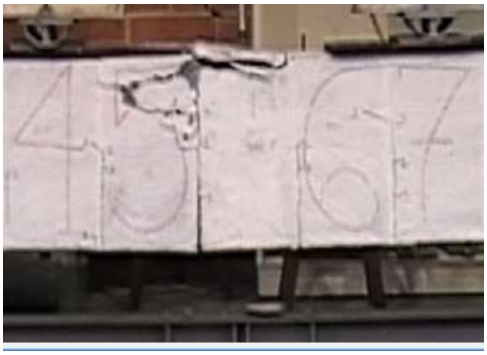

a) Beam B-10

b) Beam B-21

Figure 4. 6. Typical failure mode.

4.5.2 Load-deflection response

Two limit states in hollow concrete block beams were observed, at decompression block and failure, an approximately bilinear performance load-deflection and load-tendon force curves was observed in all beams [Fig. 4.7]. The boundary between the elastic and inelastic areas was influenced by decompression of the prestress as block separation occurs under tensile stress at the bottom beam. This mechanism initiates cracking and reduces the stiffness of the beam.

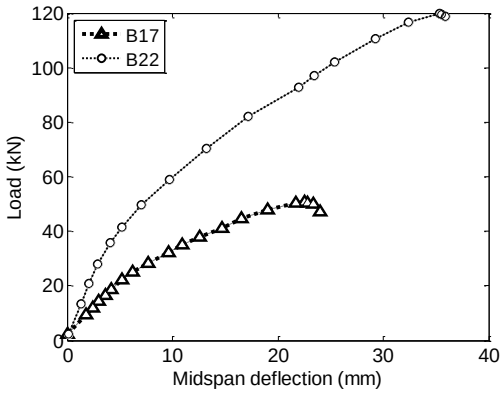

a) Load-deflection

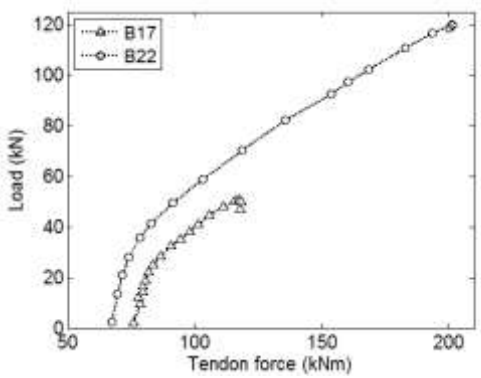

b) Load-Tendon Force

Figure 4. 7. Beam behavior curves for different masonry strength, a) Load-deflection b) Load-Tendon Force

Table 4.5 summarizes the results obtained for mid-span deflections (δ_{mid}), critical loads (P_u) and tension close to failure for all specimens (T_u).

Table 4. 5. Summary of test results

Tested Beam	P_u (kN)	δ_{mid} (mm)	T_u (kN)	M_u (kN)	ΔT_u (kN)	Tested Beam	P_u (kN)	δ_{mid} (mm)	T_u (kN)	M_u (kN)	ΔT_u (kN)
B-01	76.1	11.81	112.9	22.93	37.85	B_{11}	32.5	68	100.1	-	45.04
B-02	76.21	14.7	99.98	22.86	59.59	B_{12}	31.5	64	96.25	-	40.25
B-03	75.95	11.88	104.2	23.16	41.97	B_{21}	37.5	59.3	106.26	-	49.56
B-04	68	13.83	81.56	20.74	51.6	B_{22}	33.5	75.9	103.95	-	47.45
B-05	62.42	22.42	115	23.93	60.95	B_{31}	58.5	59.8	103.95	-	39.95
B-06	64.47	16.54	113.5	25.41	35.97	B_{32}	61	56.8	106.26	-	41.76
B-07	52.89	17.66	115.8	20.8	32.1	B_{41}	63	59.8	107.03	-	43.23
B-08	95.69	29.5	164	37.88	85.22	B_{42}	61.5	71.6	106.26	-	43.86
B-09	196.1	15.19	221.3	58.83	75.7	B_{51}	37.5	20.1	51.21	-	25.21
B-10	148.4	20.62	176.8	43.72	85.26	B_{52}	35.5	30	50.05	-	23.55
B-11	147.9	18.19	172.8	45.11	79.41	B_{61}	40	34	51.98	-	24.98
B-12	131.6	15.85	147.5	39.48	82.07	B_{62}	41	30	50.82	-	24.62
B-13	190.1	23.51	196.7	56.91	125	S_{11}	28	60.5	196.35	-	69.15
B-14	188.8	28.37	191.5	56.64	144.2	S_{12}	29	60	196.35	-	68.35
B-15	199	29.43	206.4	60.52	159.75	S_{21}	33.5	63	198.66	-	58.66
B-16	68.87	24.02	126.1	27.12	63.62	S_{22}	32.5	60	203.28	-	62.78
B-17	50.66	22.55	117.4	19.82	41.69						
B-18	48.49	17.97	104.5	19.12	34.51						
B-19	59.01	20.98	93.19	23.42	50.56						
B-20	64.63	23.79	115.7	25.89	69.97						
B-21	132.2	35.8	224.6	51.81	128.68						
B-22	119.8	35.47	201.4	47.17	134.08						
B-23	128.5	33.7	182.9	51.4	140.51						

4.5.3 Post-tensioned masonry codes accuracy

The British Standards Institution published the first code requirements for the design of post-tensioned masonry in 1985 (Schulz and Scolforo, 1991), and many of those expressions were taken from masonry and concrete codes used at that time. Currently, different countries have developed their own masonry codes for the design of post-tensioned masonry structures, which provide different expressions to calculate the unbounded tendon stress increase. The majority of these formulations come from an adapted methodology based on the concrete strain distribution method. Subsequently, these expressions have been modified in accordance to the tests results, but without having been checked in post-tensioned concrete masonry beams. A database of beam tests was compared against these code equations, as well as against the proposed methodology, to verify their precision. Tables 4.6a) and 4.6b) summarizes the results obtained in the calculation of ultimate tendon stress in accordance with the proposed methodology and the different proposals suggested by the main worldwide post-tensioned masonry codes.

Table 4. 6a) Summary of tendon force at ultimate for proposed methodology and code results (units: kN)

		Proposed	MSJC 2013	BS 5628	AS 3700	CSA	NZS
Beam	Tu (Exp)	Tu (Theo)	Tu (Theo)	Tu (Theo)	Tu (Theo)	Tu (Theo)	Tu (Theo)
B-01	112,900	118,570	142,940	89,550	100,070	162,620	113,440
B-02	99,980	98,550	131,270	62,660	70,040	152,230	78,610
B-03	104,200	111,100	138,320	79,560	88,800	158,420	100,740
B-04	81,560	101,090	146,400	59,480	66,390	171,340	68,800
B-05	115,000	105,830	136,410	68,350	72,270	158,950	77,090
B-06	113,500	108,840	130,720	85,070	88,110	148,160	93,470
B-07	115,800	114,030	135,020	91,110	94,370	152,230	99,970
B-08	164,000	126,920	144,930	88,310	90,650	165,820	96,420
B-09	221,300	204,730	224,040	142,580	152,730	254,590	166,050
B-10	176,800	185,520	208,920	113,690	121,920	241,040	131,950
B-11	172,800	185,740	207,870	114,590	122,630	239,610	133,750
B-12	147,500	170,000	195,540	90,890	97,360	228,580	105,750
B-13	196,700	189,570	225,660	102,130	109,420	264,300	112,940
B-14	191,500	175,010	214,020	81,250	87,040	253,640	88,640
B-15	206,400	174,040	212,570	80,170	85,810	252,080	87,840
B-16	126,100	116,760	148,960	80,720	88,210	171,610	101,400
B-17	117,400	116,320	136,950	87,350	95,490	155,590	114,040
B-18	104,500	112,760	134,440	82,530	90,180	153,270	108,240
B-19	93,190	104,080	140,590	64,150	70,050	164,000	81,300
B-20	115,700	128,740	163,650	69,370	74,380	192,620	85,350
B-21	224,600	181,980	195,590	112,730	119,000	224,770	136,350
B-22	201,400	164,600	179,820	87,190	92,020	210,140	107,650
B-23	182,900	162,180	188,420	68,950	72,710	225,010	83,240
B11	94,348	88,170	82,010	58,260	58,540	91,110	67,820
B12	91,834	89,030	82,890	59,190	59,480	91,980	68,760
B21	105,662	98,650	84,470	59,990	60,230	93,830	70,950
B22	100,633	98,470	84,280	59,790	60,030	93,640	70,750
B31	103,985	113,800	104,530	68,830	69,100	118,040	82,430
B32	105,662	114,270	105,000	69,330	69,600	118,500	82,930
B41	106,919	112,980	103,520	68,540	68,810	116,770	81,600
B42	105,662	111,670	102,200	67,150	67,420	115,460	80,200
B51	50,107	51,730	49,810	28,940	29,160	57,580	32,880
B52	49,688	52,180	50,260	29,430	29,650	58,020	33,380
B61	51,783	53,270	51,780	30,060	30,290	59,860	34,050
B62	48,012	52,560	51,060	29,270	29,490	59,150	33,250
S11	194,562	179,110	152,850	130,120	130,510	161,940	149,740
S12	194,562	179,850	153,620	130,920	131,310	162,700	150,540
S21	196,238	205,590	165,750	142,930	143,270	174,830	165,100
S22	201,267	206,050	166,230	143,430	143,770	175,310	165,600

Table 4. 7b) Summary of relation between Theoretical and Experimental results for tendon force at ultimate (units: kN)

	Proposed	MSJC 2013	BS 5628	AS 3700	CSA	NZS
Beam	Theo/Exp	Theo/Exp	Theo/Exp	Theo/Exp	Theo/Exp	Theo/Exp
B-01	1.05	1.27	0.79	0.89	1.44	1.00
B-02	0.99	1.31	0.63	0.70	1.52	0.79
B-03	1.07	1.33	0.76	0.85	1.52	0.97
B-04	1.24	1.79	0.73	0.81	2.10	0.84
B-05	0.92	1.19	0.59	0.63	1.38	0.67
B-06	0.96	1.15	0.75	0.78	1.31	0.82
B-07	0.98	1.17	0.79	0.81	1.31	0.86

	Proposed	MSJC 2013	BS 5628	AS 3700	CSA	NZS
Beam	**Theo/Exp**	**Theo/Exp**	**Theo/Exp**	**Theo/Exp**	**Theo/Exp**	**Theo/Exp**
B-08	0.77	0.88	0.54	0.55	1.01	0.59
B-09	0.93	1.01	0.64	0.69	1.15	0.75
B-10	1.05	1.18	0.64	0.69	1.36	0.75
B-11	1.07	1.20	0.66	0.71	1.39	0.77
B-12	1.15	1.33	0.62	0.66	1.55	0.72
B-13	0.96	1.15	0.52	0.56	1.34	0.57
B-14	0.91	1.12	0.42	0.45	1.32	0.46
B-15	0.84	1.03	0.39	0.42	1.22	0.43
B-16	0.93	1.18	0.64	0.70	1.36	0.80
B-17	0.99	1.17	0.74	0.81	1.33	0.97
B-18	1.08	1.29	0.79	0.86	1.47	1.04
B-19	1.12	1.51	0.69	0.75	1.76	0.87
B-20	1.11	1.41	0.60	0.64	1.66	0.74
B-21	0.81	0.87	0.50	0.53	1.00	0.61
B-22	0.82	0.89	0.43	0.46	1.04	0.53
B-23	0.89	1.03	0.38	0.40	1.23	0.46
B11	0.93	0.87	0.62	0.62	0.97	0.72
B12	0.97	0.90	0.64	0.65	1.00	0.75
B21	0.93	0.80	0.57	0.57	0.89	0.67
B22	0.98	0.84	0.59	0.60	0.93	0.70
B31	1.09	1.01	0.66	0.66	1.14	0.79
B32	1.08	0.99	0.66	0.66	1.12	0.78
B41	1.06	0.97	0.64	0.64	1.09	0.76
B42	1.06	0.97	0.64	0.64	1.09	0.76
B51	1.03	0.99	0.58	0.58	1.15	0.66
B52	1.05	1.01	0.59	0.60	1.17	0.67
B61	1.03	1.00	0.58	0.58	1.16	0.66
B62	1.09	1.06	0.61	0.61	1.23	0.69
S11	0.92	0.79	0.67	0.67	0.83	0.77
S12	0.92	0.79	0.67	0.67	0.84	0.77
S21	1.05	0.84	0.73	0.73	0.89	0.84
S22	1.02	0.83	0.71	0.71	0.87	0.82
Mean	**1.00**	**1.08**	**0.63**	**0.66**	**1.23**	**0.74**
SD	**0.10**	**0.22**	**0.10**	**0.12**	**0.27**	**0.14**
CV	**0.10**	**0.20**	**0.17**	**0.18**	**0.22**	**0.19**

Additionally, for a better understanding and interpretation of the results presented in the Table 4.5, results are reported in Fig. 4.8, where the solid line represents a perfect (i.e. 1:1) correlation.

As Fig. 4.8 shows, the code expressions predict tendon stress at the ultimate state with variable accuracy. The proposed equation was evaluated using the MSJC-2013 parameters for the equivalent stress block (α= 0.80, β= 0.80) and maximum useable compression strain in the masonry (ε_{mu}= 0.0025). Among the existing code equations, MSJC-2013 provided better results. The accuracy of most code equations is questionable, as prior research has shown (Bean, 2003; Wight et al., 2006; Wight and Ingham, 2008; and Bean and Schultz, 2010).

On the other hand, the new equations proposed in this study provide good results. Figure 4.5 shows that the CSA-2004 expression overestimates the tendon stress in most cases, while BS5628-2005 and NZS4230-2004 equations underestimate the tendon force in all cases. Both the MSJC-2013 and the proposed adapted equation, have not a clear tendency to overestimate or underestimate the tension values of tendon at ultimate.

The proposed equation provides good correlation, which shows that the methodology based on the deformed beam can be successfully used to determine the tendon stress increment in post-tensioned

masonry beams. The proposed expression (Eq. 4.31) offers better versatility due to the larger number of design parameters that use, and improved precision over a wider variety of post-tensioning levels, masonry strength, and tendon eccentricity.

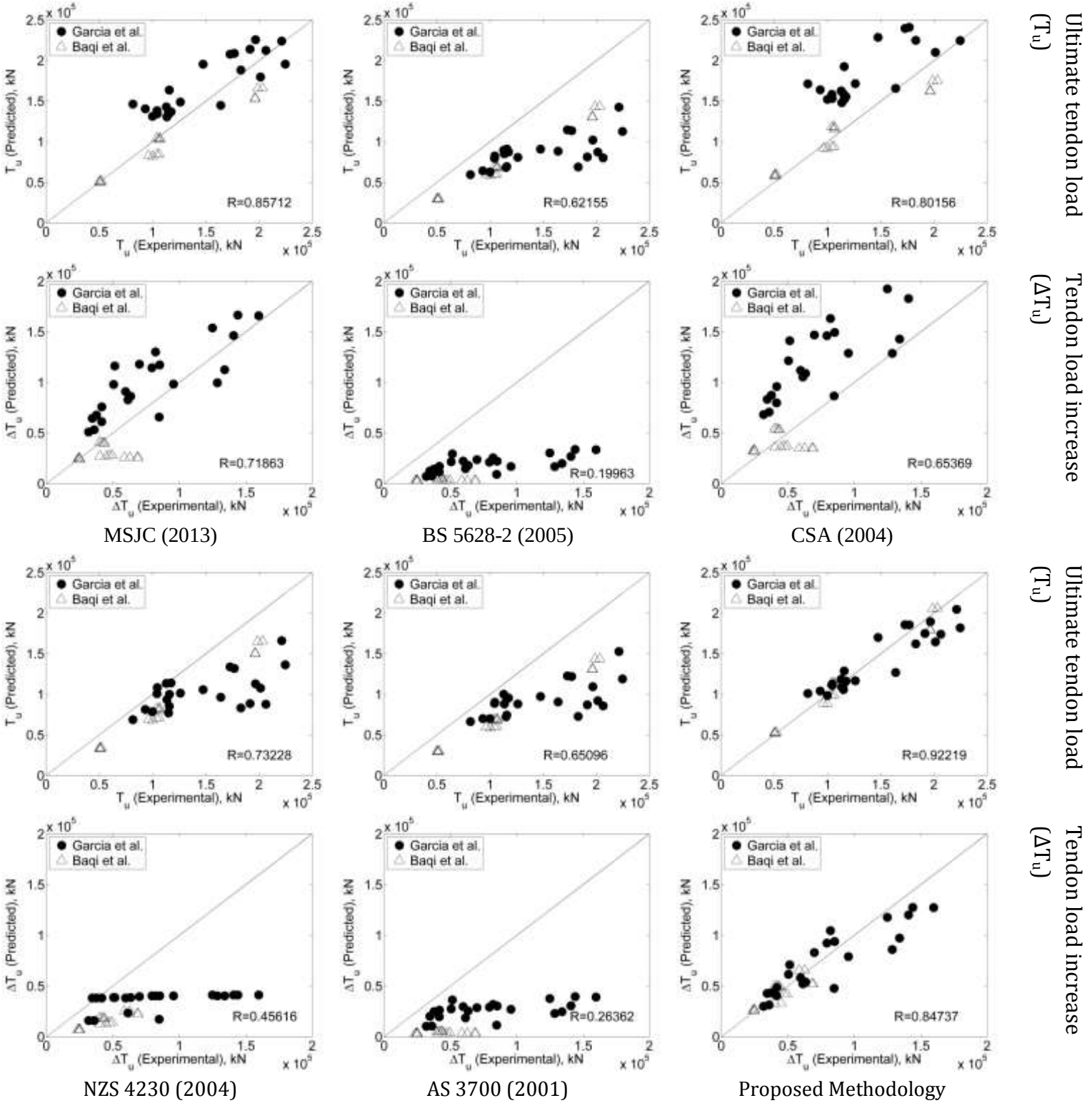

Figure 4. 8. Ultimate tension and tendon force increase expressions versus experimental results

4.6 Discussion and conclusions

Several experimental and analytical studies have been developed over the past four decades to predict tendon stress increase at ultimate in post-tensioned concrete flexural members. The estimation of tendon stress increase at failure is a prerequisite to compute the flexural loading capacity of an unbonded structural element. A number of expressions with different degrees of complexity, based on different approaches, physical models and experimental tests, have been suggested. Physical models based on strain distribution, strain reduction and beam deflection were analyzed in this paper as a rational formula for post-tensioned masonry beams with unbonded tendons was sought. A rational formula was derived and validated with experimental results of full-scale tests of post-tensioned concrete and clay masonry beams.

Various design formulas available in post-tensioned masonry codes worldwide (United States, Australia, Great Britain, Canada and New Zealand) were checked. The accuracy of these formulas to predict stress at ultimate was evaluated using data from the experimental tests conducted as part of this investigation, as well as with data collected from the literature on post-tensioned masonry beams with unbonded tendons. The majority of available code equations are empirical and their use may be limited to a certain set of beam characteristics.

The proposed analytical expression is based on fundamental solid mechanics that meets equilibrium, deformation compatibility and realistic stress-strain behavior. It can be applied to both elastic and inelastic states, and provides a simple and excellent resource to predict the behavior of prestressed masonry in simply supported beams. Thus, this formula enables the design of the structural system due to a broad range of parameters that govern structural behavior without having to resort to any empirical approximations. The analytical model demonstrates close correlation between predicted and experimentally measured ultimate tendon stress. Moreover, the proposed equation generally exhibited more accuracy than other currently used formulas in post-tensioned masonry codes throughout the world. Among code equations, MSJC-2013 gave close results as well (R=0.87019 and R=0.72904 for T_u and ΔT_u, respectively) followed by CSA-2014 (R=0.83562 and R=0.67669 for T_u and ΔT_u, respectively). The remaining code equations offered poor predictions of the unbonded tendon stresses in post-tensioned masonry beams at ultimate.

The proposed rational expression offers better flexibility due to its simplicity and better accuracy than studied code equations with the experimental data. Moreover the analytical procedure by which the proposed formula was derived can be applied to a large number of structural typologies, in general, including post-tensioned masonry elements in flexure. However, further research and analysis with experimental and theoretical studies is required to verify its applicability and extend it to other structural elements.

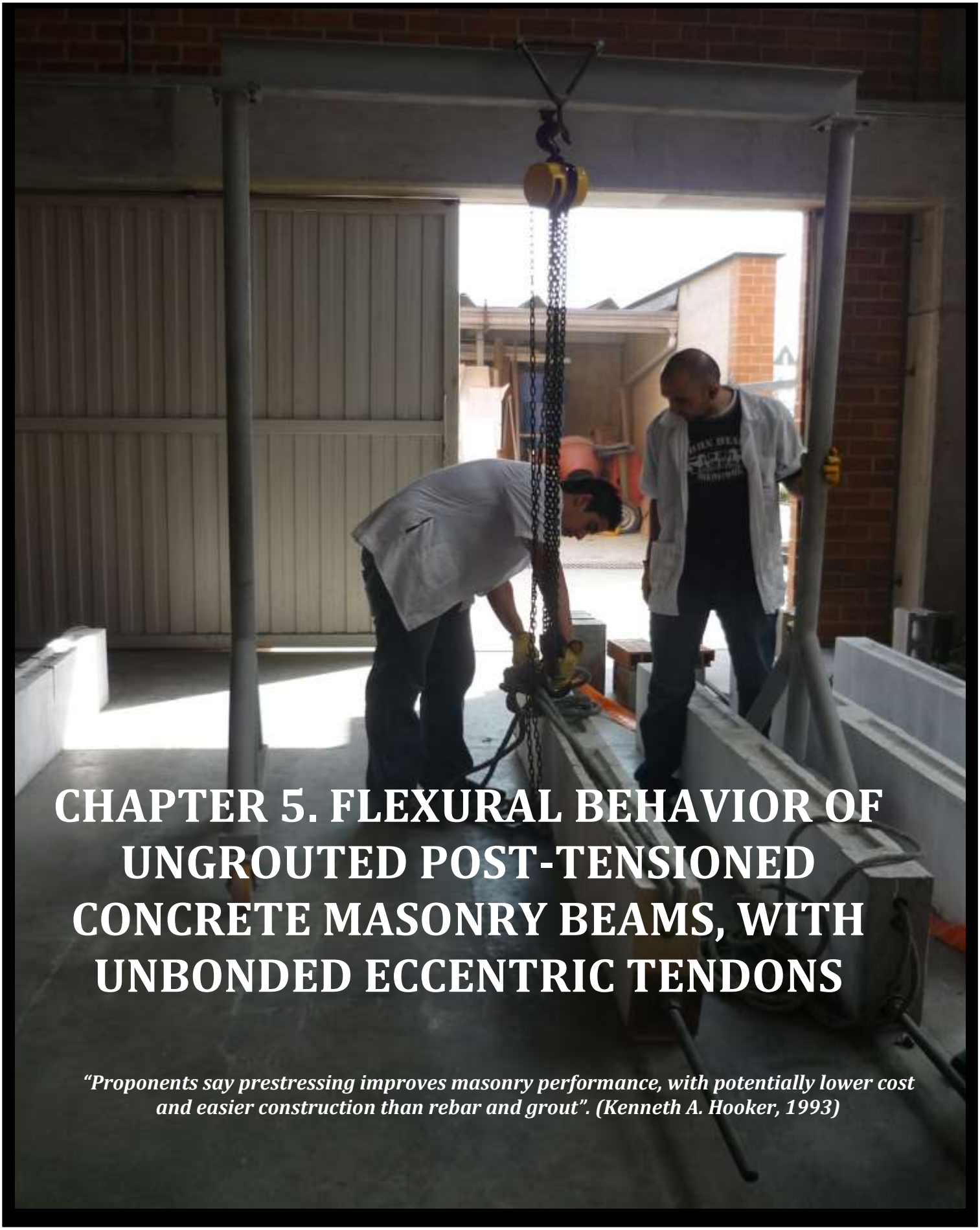

CHAPTER 5. FLEXURAL BEHAVIOR OF UNGROUTED POST-TENSIONED CONCRETE MASONRY BEAMS, WITH UNBONDED ECCENTRIC TENDONS

"Proponents say prestressing improves masonry performance, with potentially lower cost and easier construction than rebar and grout". (Kenneth A. Hooker, 1993)

Abstract

Construction techniques such as post-tensioning and precast, generate better efficiency for the building industry in various aspects including labor, time, and building costs. This study focuses on evaluating the flexural behavior of ungrouted post-tensioned concrete masonry beams that have been subjected to monotonic and cyclic loading until failure, and the influence of the main design parameters in the structural performance of ungrouted prestressed beams, including: masonry strength, tendon eccentricity, initial prestress and beam length. The test results reveal: nonlinear load-deflection behavior that can be estimated using a nearly bi-linear correlation, an approximately linear relationship between tendon stress increase and midspan deflection, and masonry strength as the most important parameter affecting flexural behavior. Monotonic and cyclic tests under similar beams exhibit equivalent envelope load-deflection behavior, and the deviator block in ungrouted beams allows levels of strength and deflection similar to grouted post-tensioned beams.

Keywords: Post-tensioning; Masonry; Beams; Ungrouted; Unbonded; Eccentric bar, Flexural behavior.

5.1 Introduction

Masonry has been recognized through countless human civilizations as a low maintenance material that offers excellent aesthetic, thermal and acoustic properties for building construction. Although it has low tensile strength, techniques such as post-tensioning can improve their tensile strength, thus it provides a good alternative to be used in flexural elements. The construction industry faces increasing demands to industrialize the fabrication and erection processes, reduce material consumption and improve efficiency (Pedreschi, 2013). Prefabrication and post-tensioning are techniques that increase productivity in the construction of buildings and infrastructure, allowing further cost reduction and optimized construction time.

Investigation of the flexural behavior of post-tensioned masonry beams has been undertaken during the last five decades focusing on grouted brick masonry members. Thomas (1963) investigated the feasibility of construction of suspended floors featuring prestressed brickwork beams. Other researchers continued with investigation of the flexural behavior and principal design parameters for prestressed solid bricks beams (Pedreschi, 2004). Common observations across these studies include: increased cracking load with prestressing [Ng and Cerny (1985), Garwood (1988), and Neis et al. (1989)], increased shear strength with prestressing [Sinha (1994), Walker (1987) and Baqi et al. (1999)] and benefits offered by restrained tendons regarding increased moment and deflection capacities at ultimate state [Roumani and Phipps (1983 1985 and 1986), Phipps and Montague (1987), Williams and Phipps (1982), Roumani and Phipps (1985 and 1988), Montague and Phipps (1984) and Al-Gahtani and Fairbairn (1995) and Urrego and Bonett (2011)].

Ungrouted and unbonded post-tensioned masonry has been widely questioned in terms of its deflection and strength capacity by several independent researchers and masonry codes. However, with the inclusion of a deviator block, which serves as a tendon guide at strategic points in the beam, ungrouted and unbonded masonry elements can develop similar or higher deflection and strength capacity than grouted and bonded masonry post-tensioned beams.

This study reports on the main findings obtained from a significant number of full-scale tests on ungrouted post-tensioned masonry beams with eccentrically prestressed bars. During these tests, parameters such as beam deflection, force in the prestressed bar, and applied load were monitored continuously, making it possible to correlate the incidence of the principal variables related to masonry design. From the obtained results, evidence shows that the use of the deviator block in ungrouted masonry beams allows levels of deflection similar to those achieved in previous investigations for grouted masonry beams [Sinha (1994), Walker (1987) and Baqi et al. (1999)], which provides a good starting point to consider the use of this structural element on structures that require a certain level of ductility.

5.2 Research significance

The aim of this study was to present the results obtained in a series of laboratory tests for members made using ungrouted hollow concrete masonry units with eccentric bars, and to report their flexural behavior and the effect of the main design parameters in both elastic and inelastic states. Likewise, the results show all the benefits when the deviator block is used, increasing levels of deflection and strength capacity at ultimate flexural state. These results will

also be used to evaluate the accuracy of worldwide code expressions to determine ultimate flexural capacity, and to provide a database of experimental findings that can be used to support the development of new theories for the prediction of the ultimate limit state of this structural system.

5.3 Experimental program

This study summarizes the test results of 14 full-scale ungrouted prestressed concrete masonry beams with unbonded eccentric bars guided by a deviator block at midspan beam, subjected to vertical loading until failure. The main design parameters were varied to investigate their effect on flexural behavior. The research involves the following variables: 1) tendon eccentricity (80 mm and 125 mm), 2) initial tendon stress ($0.22f'_m$, $0.33f'_m$ and $0.44f'_m$), 3) masonry strength (12 MPa and 21.09 MPa), 4) loading type (monotonic and cyclic), and 5) beam length (2.4 m and 3.2 m).

5.3.1 Beam construction

Full-scale ungrouted concrete masonry beam specimens were built in the structural laboratory of the University of Medellin (Colombia) using a single course, with the units placed in a soldier configuration. All tested beams were built with a deviator block at midspan, as well as placing two anchor blocks similar to the deviator block at the ends of the beam (Fig. 5.1).

The concrete blocks were joined together by means of 10±3 mm thick mortar joints and were laid on the floor. Mortar was placed initially while the masonry units were held in horizontal orientation and subsequently rotated carefully to a vertical orientation then joined with the other unit. For this reason mortar consistency was a little drier than conventional mixtures in order to avoid mortar slip. At one end of the beam a reinforced concrete element was placed, and later had specific perforations at the desired bar location. These elements served as anchoring blocks to distribute stress to the masonry during prestressing. This same type of concrete element was placed at the beam mid-span to serve as a deviator block and ensure a constant tendon eccentricity during the loading process. One day after construction, the beams were post-tensioned with a small prestress force to prevent premature damage, and they were allowed to cure with periodic water spraying for at least 28 days before testing.

Figure 5. 1. Beams construction

The prestressing bars were placed below the neutral axis of the beam during the construction process. Given the increase in shear strength enabled by the prestress force, and in order to simplify the constructive process, no shear reinforcement was used in the beams. Furthermore, no grouting was used to fill the cavities of the concrete block, thus the beam construction method was an "ungrouted".

5.3.2 Material properties

A detailed experimental program was conducted to determine the properties of the constituent materials used in the construction of post-tensioned masonry beams. All materials used in the investigation were tested according to the relevant American Society for Testing and Materials -ASTM Standards- (ASTM C140, ASTM C90, ASTM C1314, ASTM C780 and ASTM C1157). All of the equipment employed to test the materials and post-tensioned beams were certified for accuracy using suitable laboratory procedures.

5.3.2.1 Concrete block and masonry

Two-cell, extruded hollow concrete blocks, with two different strengths, and manufactured by a vibro-

compacted process were used throughout this study and are denoted as either high-strength or low-strength blocks, with average strength of 21.09 MPa and 12 MPa respectively. The units have average length, width and height, equal to 390±1 mm, 140±1 mm, and 190±2 mm, respectively [Fig. 5.2(a)], and the corresponding gross and average net areas are 54600 and 32800 mm^2, respectively. The perforations formed a greater proportion of the cross-section that did the solid elements, and the former represents nearly equal to 60% of the gross area of the section. By reason of the non-rectangular shape of some elements in the block cross section, a rectangular cross section was assumed to calculate cross-section properties [Fig. 5.2(b)].

Prisms comprising of two stacked units and one mortar joint, and with thickness, height and length equal to 140mm, 390mm and 590mm, respectively, as well as a height-to-thickness slenderness ratio of 4.21 were used to determine the compressive strength of the masonry. The mortar used in the construction of the prisms and beams was Portland cement to fine sand mix with weight proportions equal to 1:2 by weight, and the water content was adjusted by the bricklayer to give a workable mix (the typical water/cement ratio as approximately equal to 0.7). Standards ASTM C1314, ASTM C90 and ASTM C780 were used to determine the compressive strength of the masonry prism, masonry unit and mortar cylinders, respectively.

Table 5.1 summarizes the average value and the covariance of compressive strengths of hollow concrete blocks (f'_b) and mortar (f'_j) obtained from 90 tested hollow blocks and 24 cylinders specimens respectively, carried out under monotonically uniaxial compression to failure (Garcia et al., 2013). The proposed correlation by the MSJC-2013 between unit strength and masonry strength method was adopted according to the compressive strength results obtained in the laboratory for concrete blocks and mortar.

Table 5. 1. Compressive strength of masonry materials

	Property	f'_b (MPa)	f'_j (MPa)	f'_m (MPa)
Low Strength	Average value	12.00	28.09	12.00
	Number test	68	12	TMS Correlation
	COV	8.7%	13.8%	-
High Strength	Average value	32.00	29.41	21.09
	Number test	12	12	MSJC-2013 Correlation
	COV	8.9%	14.4%	-

5.3.2.2 Anchorage and deviator blocks

The concrete used to cast the deviator and anchorage blocks [Fig. 5.2(c)] was made using a 1:2:2 (cement: sand: coarse aggregate) concrete mix with a water/cement ratio of 0.6 and with an average compressive strength of 35.6MPa (COV= 2.08%), according to ASTM C1157. To avoid a local failure in the anchorage zone, the deviator blocks were reinforced with 1% mild steel and two 10 mm diameter confinement stirrups.

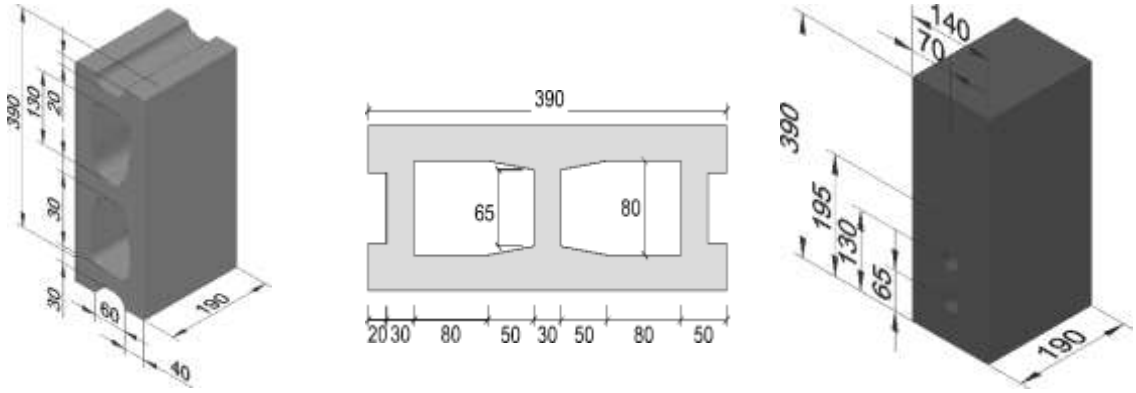

a) b) c)

Figure 5. 2. Concrete Blocks. a) Hollow block b) Simplified cross section c) Deviator and anchorage blocks (units: mm)

5.3.2.3 Prestressing steel

A threaded bar made of steel ASTM A615 Grade 75, with 25 mm diameter, and a nominal cross-sectional area of 506.7 mm^2, was used for post-tensioned all test beams. The average value of the initial modulus of elasticity, yield stress and the ultimate strength, were determined as 200 GPa, 517 MPa, and 690 MPa, respectively. Despite this, prestressed steel was not the most appropriate material to be used in prestressed masonry, it was the only one commercially available. Long-term losses due to creep, shrinkage and steel relaxation were negligible, because tests were conducted just after prestressing the beam. Losses were recorded before the beam was tested.

5.3.4 Specimen details

Fourteen full-scale beams under unidirectional monotonic (9 beams) and cyclic (5 beams) four-point loading were tested in a self-restraining test rig with the specimens on simple supports at their ends, and an effective span length of approximately 2.4 m or 3.2 m. (span-to-depth ratio between 7.5 and 11.5 respectively). The hollow concrete beams were post-tensioned with one 25 mm diameter threaded bar placed in a straight line through the hollow blocks and the deviator block perforations, which ensured a constant eccentricity along the beam, because the deviator blocks limited bar movement. The beams were post-tensioned the day of the test using a hollow plunger jack, and a manually operated hydraulic pump. Three different levels of post-tensioning were studied (approximately $0.22f'_m$, $0.33f'_m$ and $0.44f'_m$) corresponding to 35%, 48% and 60% of the threaded bar yield stress respectively. Post-tensioning levels were calculated based on the maximum compression strength at the bottom fiber using the material properties of the concrete block. Long term measurement of prestress losses (i.e due to creep, shrinkage, and steel relaxation) were not needed in this study because the prestressing was done immediately before testing. Mild steel anchor plates with 150 mm side dimensions and 10 mm thickness were bedded above the deviator block to prevent stress concentrations. The average dead load on the beam from self-weight was approximately 0.84 kN/m for the high strength block and 0.74 kN/m for the low strength block. Beams dimensions, properties and posttensioning data are listed in Table 5.2. The number of tested beams is not consecutive, because the entire experimental program included 24 beams, of which 14 were selected for this study, that correspond to those beams which have a flexural failure mechanism which were the object of analysis in this paper, the other 10 beams had a shear failure.

Table 5.2. Test beam details

Beam	f'_m (MPa)	T_i (kN)	L_l (m)	L (m)	e_{mid} (mm)	L/d	Load type
B-1	9.36	75.05 (44%)	2.41	2.62	80	8.76	Monotonic
B-2	9.36	40.39 (22%)	2.40	2.60	80	8.73	Monotonic
B-3	9.36	62.23 (33%)	2.44	2.61	80	8.87	Monotonic
B-10	26.61	91.54 (44%)	2.36	2.59	80	8.57	Monotonic
B-11	26.61	93.39 (44%)	2.44	2.63	80	8.87	Cyclic
B-13	26.61	71.70 (33%)	2.40	2.58	125	7.48	Monotonic
B-14	26.61	47.30 (22%)	2.40	2.61	125	7.50	Monotonic
B-15	26.61	46.65 (22%)	2.43	2.62	125	7.60	Cyclic
B-17	9.36	75.71 (44%)	3.13	3.34	80	11.38	Monotonic
B-18	9.36	69.99 (44%)	3.15	3.34	80	11.47	Cyclic
B-21	26.61	95.92 (44%)	3.14	3.35	80	11.40	Monotonic
B-22	26.61	67.32 (33%)	3.15	3.34	80	11.45	Monotonic
B-23	26.61	42.39 (22%)	3.20	3.36	125	10.00	Cyclic
B-24	26.61	72.03 (33%)	2.38	2.58	125	7.44	Cyclic

(xx%) indicates the percentage of initial prestress respect to the degree of masonry strength

5.3.5 Test configuration and instrumentation

The beams were tested under a symmetric four-point loading arrangement over the span to create a nearly uniform distributed load (Fig. 5.3). The single hydraulic jack which was connected to the hydraulic pump transferred the load to the beam using a system of steel distribution beams, of which the spacing remained constant. The average weight for the steel beams and loading system was approximately 1.0 kN. Nine (9) beam specimens were tested under slowly increasing monotonic loads in equal increments until the ultimate load was reached at failure. For the remaining five (5) beams, loading cycles with increasing displacement amplitude 1mm, 2mm, 4mm, 6mm, 8mm, 10mm and 12mm were executed, and each cycle was repeated three times.

Total applied load was measured using a 250 kN load cell with an accuracy of at least 2kN, positioned above the jack in the test rig (load cell 2). Tendon stresses, including the effective prestress after losses due to anchorage seating, were monitored using an electronic load cell located at the end of the threaded prestressing bar (load cell 2). Vertical deflections were measured using four Linear Voltage Differential Transformers (LVDTs) at midspan(LVDT 2) and quarterspan (LVDT 3), as well as both ends of the beams (LVDT 's 1 and 4), with a least count of 0.001 mm (Fig. 5.3). At each load increment, load cell, deflection and tendon stress measurements were taken and recorded using a digital data acquisition system. At three different load stages (30%, 50% and 70% of ultimate load based on theoretical predictions) the load was held constant and the crack patterns were marked on the face of the beams, especially in the constant moment zone, to monitor flexural cracking and to observe the possible variation in neutral axis depth along the beam. The ultimate load was reached when the beam became incapable of taking any further load.

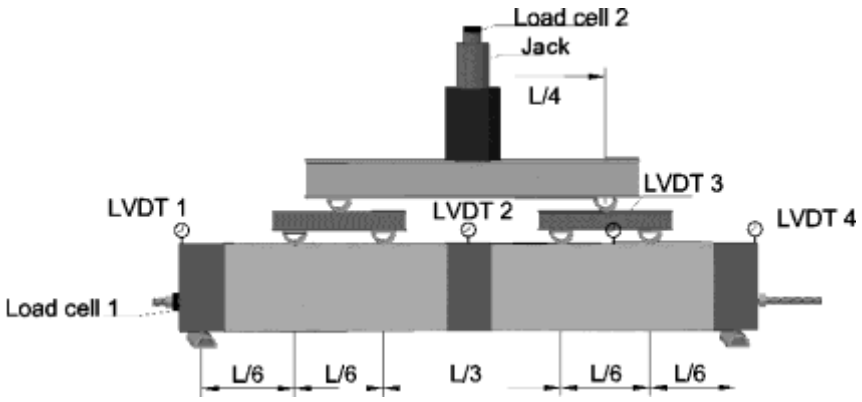

Figure 5. 3. Test setup and instrumentation

5.4 Experimental results

All beams failed in flexure associated with crushing of the compression zone, and after the load was removed, the tested beams showed a considerable recovery in both deflection and cracking. In all cases, the masonry reached the nominal strain limit at ultimate before the prestressing bars reached their yield strength or shear failure occurred. Thus, the prestressing steel in all of the tested beams remained in the linear elastic range. Table 5.3 summarizes the principal results obtained from the test specimens.

Table 5.3. Summary of test results

Beam	P_u (kN)	$\delta_{mid,u}$ (mm)	M_u (kN*m)	T_u (kN)	$\delta_{mid,u}/L$ (mm/m)	$K_{elastic}$ (kN/mm)
B-1	76.1	11.81	23.63	112.9	4.90	12.97
B-2	76.21	14.7	23.56	99.98	6.13	11.91
B-3	75.95	11.88	23.86	104.2	4.87	14.96
B-10	148.4	20.62	44.92	176.8	8.75	16.70
B-11	147.9	18.19	46.31	172.8	7.45	17.02
B-13	190.1	23.51	58.11	196.7	9.82	14.64
B-14	188.8	28.37	57.84	191.5	11.82	10.34
B-15	199	29.43	61.72	206.4	12.10	9.56
B-17	50.66	22.55	20.52	117.4	7.20	4.06
B-18	48.49	17.97	19.82	104.5	5.70	3.42
B-21	132.2	35.8	53.01	224.6	11.42	9.02
B-22	119.8	35.47	48.37	201.4	11.26	9.59
B-23	128.5	33.7	52.6	182.9	10.53	6.61
B-24	211.1	25.91	64	206.4	10.89	12.11

5.4.1 Load deflection response

Load-deflection behavior in ungrouted beams is very similar to that of typical grouted masonry beams as reported in previous research (Fincher 1969; Pedreschi, 1983 and Uduehi, 1989). An initial, almost linear stage was followed by a nonlinear stage with a gradual reduction in stiffness until reaching values at ultimate, that were close to 45% of the initial stiffness in all of the specimens. Similarly, all tested beams show significant displacement capacity with deflection-span ratios at failure of 1/130 to 1/205 for high strength masonry and 1/85 to 1/115 for low strength masonry. Generally, a typical load–deflection response of post-tensioned masonry beams presented four-stages behavior, which could be characterized by a linear elastic stage (I), cracked stage (II), tendon yield stage (III), and post-peak load stage (IV) [Fig 5.4].

- **Linear elastic stage (I):** The first linear zone concerns the elastic behavior observed upon initial loading and continuing to first cracking occurring in all tested beams, with an almost linear elastic relationship between applied load and mid-span deflection (see Fig. 5.4). For this stage, tendon stress increase is negligible.
- **Cracked stage (II):** This stage starts from when block separation begins to take place, and more space opens up between blocks as load increases. The cracking load depends to a large extent on the magnitude of initial prestress, and for tested beams this took place between 12% and 34% of the maximum load. Although in literature, the boundary between stage (I) and stage (II) commonly is called the cracking state, for ungrouted masonry beams cracking means that block separation takes place through decompression. A nonlinear stage that reduces the stiffness of the beam, tendon stress increase and hence a sudden increase in midspan deflection is observed. The cracking load is found assuming a linear elastic behavior in the section and the magnitude of the bottom fiber strain due to prestress and applied load is equal to zero. It is

assumed that tensile strength between the mortar and concrete block is insignificant.

- **Tendon yield stage (III):** This stage is achieved when tendon stress exceeds yield strength in prestressing steel, stiffness is reduced significantly and there is a large displacement with moderate load increase. This stage is complete when beam reaches peak load and is unable to support any further load. None of the tested prototypes presented yield stress in tendon bars, and thus stage (III) is not observed in the studied beams.
- **Post-peak load stage (IV):** Once maximum load in the beam is reached, the load decreases gradually simultaneously at deflection increments until beam failure. This stage corresponds to the downward part of the curve. Upon unloading the beam, a large percentage of deformation was recovered, and some cracks closed completely. In the tested beams, the recovery of beam deflection was higher than 65% with an average of 72.9%.

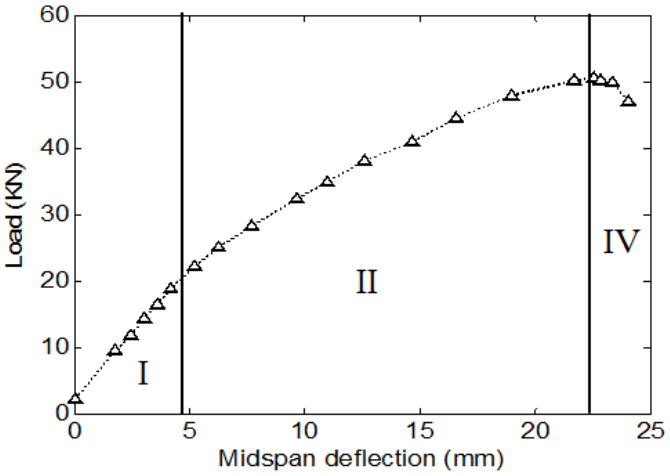

Figure 5.4. Typical load–deflection response (B-17)

Given the significant quantity of the variables analyzed in this study, a normalization of the load-deflection curve was necessary in order to interpret the results better. The normalization related to the load axis was made using an equivalence between the main variables involved in the external moment applied to the beam ($PL/8$) and the approximated internal moment capacity of the section ($\alpha\beta f'_m bd^2$). Similarly, the normalization related to midspan deflection axis was made using an equivalence between midspan deflection (δ) and the approximation of the deflection calculated by the moment-curvature method ($1/9\ \emptyset L^2 \approx 4\varepsilon_{mu}/9\ L^2/d$). Figure 5.5 shows the normalization of the load-deflection of all the tested beams, in this normalization the influence of bar eccentricity in the normalized load-deflection curve can be immediately identified.

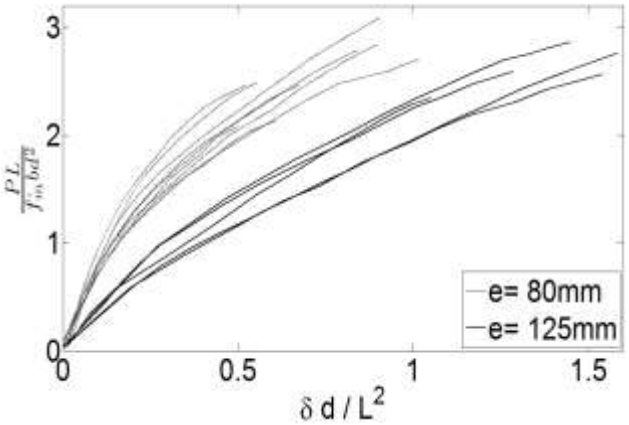

Figure 5. 5. Normalized load–deflection beams

The effect of the tendon eccentricity varies the flexural behavior significantly in post-tensioned masonry elements. In all conducted tests, an increase of tendon eccentricity enhanced the flexural capacity of the tested beams. This increase in the flexural behavior may be explained by the largest moment capacity in the cross-section provided by the greater lever arm that produces a larger eccentricity.

5.4.2 Cracking patterns

The distribution of the cracks in each beam was monitored periodically for different load levels up to 75% of the estimated ultimate load. Experimental results show a similar crack pattern in all tested beams. Before the laboratory test started, beams showed a low precamber that caused some slight negative curvature in all the specimens due to the tendon eccentricity [(Fig 5.6(a)]. With further increasing in the load, precamber decreases rapidly and the beam section turns horizontally with no cracks. When the cracking load is reached, a first vertical crack appears in the vertical bed joint between the blocks at the bottom beam over constant moment zones, most frequently near to midspan [(Fig 5.6(b)]. Block separation continued to rise gradually and cracks propagated vertically as the global load demand increased, and new cracks started to initiate, but without apparent damage on the concrete block structure [(Fig 5.6(c)]. Although load reaches levels close to 75% of ultimate load, vertical cracks continued to increase proportional to the load increment and the structural integrity of blocks remained, without apparent damage or cracks that

affect the integrity of the hollow concrete blocks [(Fig 5.6(d)]. After 75% of the ultimate load, a group of diagonal cracks started to develop diagonally cracks that affected the structural integrity of the concrete block appearing on top of the ungrouted masonry beam. This pattern of cracks raise significantly with moderate load increase, and propagated toward the adjacent load point until the ultimate load is reached [(Fig 5.6(e)]. In post-peak load, flexural capacity of masonry beams decrease with additional deflection. Finally, the load is removed, and a notable recovery in deflection and closing cracks was observed [(Fig 5.6(f)]. In shear span of the beam (shear different from zero), the damage level was minimal without cracking patterns observed.

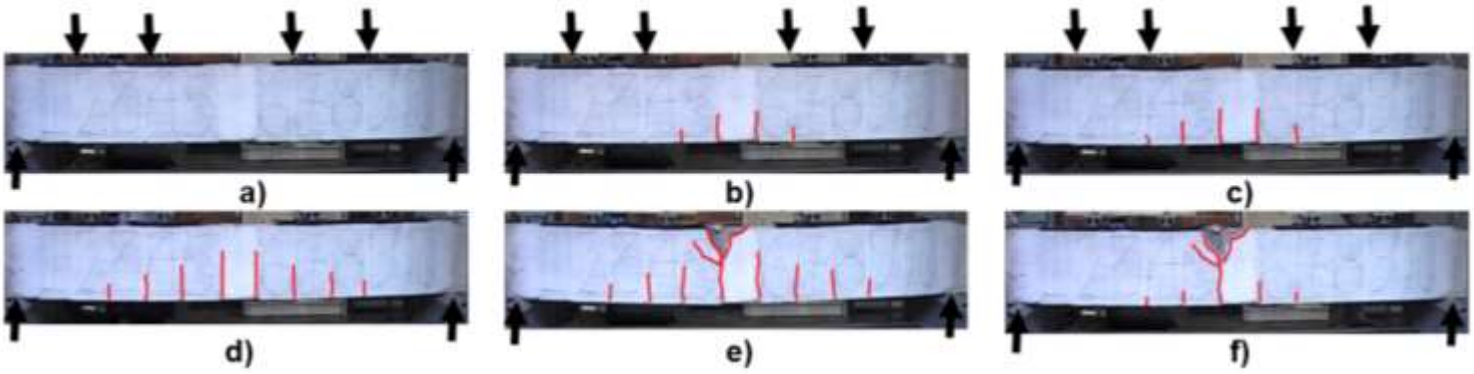

Figure 5.6. Cracking patterns B-13 a) $0P_u$, b) $0.25P_u$, c) $0.5P_u$, d) $0.75P_u$, e) P_u, and f) Unload

For ungrouted masonry beams with a higher level of initial prestress the number of vertical cracks were reduced, as a result of increased cracking load. Similarly, block separation in beams with low strength masonry was higher than beams with high strength masonry, due to the largest load capacity of the beam cross-section.

5.4.3 Failure mode

All beams failed primarily in bending after crushing of the mortar joints followed by chipping of the adjoining concrete block in the compression zone near to the top of the beam within the maximum moment region (Figure 5.7).

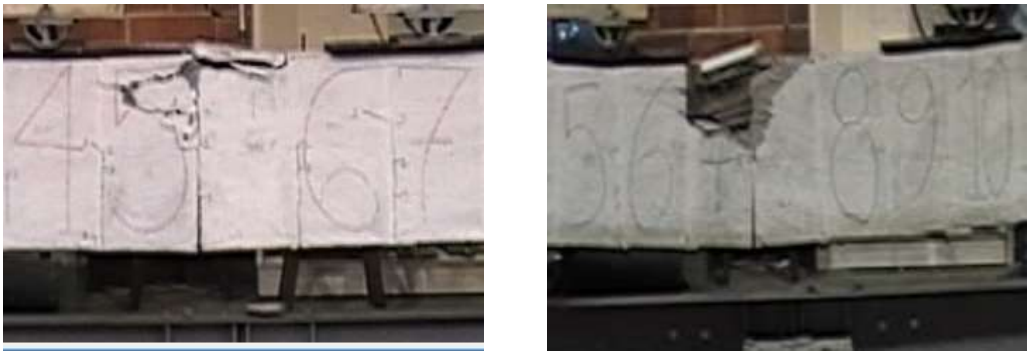

a) b)

Figure 5.7. Typical failure mode a) Beam B-10, b) Beam B-21

Subsequent to first cracking appearing, an increment in external load caused the vertical crack propagate upward rapidly, producing a change in the neutral axis of the section. With the progressive cracking increase, a rapid rise of compressive strains in the top masonry fibers produced crushing in the concrete masonry. The concrete block and mortar joints reached the compressive ultimate strain and crushed in flexural failure prior to yielding of the post-tensioned threaded bar or shear failure. Damage is concentrated only over a small portion of the constant moment zone in the beam. In the remaining beam length, the damage was minimal and the integrity of blocks located in this area remained almost intact, only slightly vertical cracks

between mortar joints caused by the block separation were presented. In most cases, failure occurred in blocks adjacent to the deviator block at the midspan of the beam.

5.4.4 Effect of design variable factors

Although the overall incidence of the main design factor are included in the worldwide code expressions, many of them come from empirical studies in grouted post-tensioned elements. The results obtained in this research can be used to analyze the effect of main design parameters in flexural behavior of ungrouted post-tensioned masonry.

5.4.5 Masonry strength effect

Compressive strength is one of the most important parameters in the design of masonry structures, a variation in masonry strength is sufficient to modify the ultimate moment, ultimate midspan deflection and failure type. Experimental results show that masonry strength had a significant effect on the structural behavior of post-tensioned masonry members in flexure (Fig. 5.8). The use of high-strength masonry provides an additional flexural capacity at ultimate state, complemented by an additional displacement capability and a higher cracking load than low-strength masonry.

As might be expected, an increase in masonry strength leads to better performance of ungrouted post-tensioned masonry beams. An increase of 167% in masonry strength on beams B17 and B21 with other similar design parameters provides an increase of 158% (20.52 kN*m to 53.01 kN*m) in ultimate flexural capacity, and 59% (22.55 mm to 35.8 mm) in midspan deflection at maximum load. For beams B1 and B11 the increase is 96% (23.63 kN*m to 43.61 kN*m), and 54% (11.81 mm to 18.19 mm) for the ultimate moment capacity and midspan deflection, respectively. According to these results, it is possible to conclude that the ultimate flexural capacity and ultimate midspan deflection are not a linear function of the masonry strength.

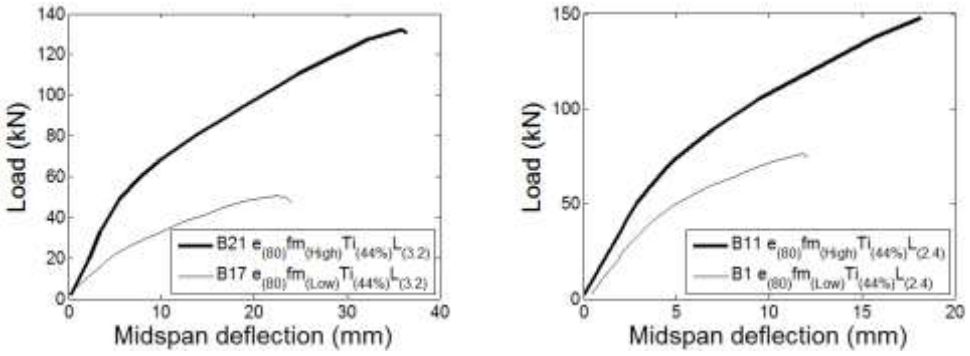

a) b)

Figure 5.8. Effect of masonry strength a) B-17 vs B-21 b) B-1 vs B-11

Throughout the whole load-deflection curve, beams with higher masonry strength show a higher level of flexural capacity than lower masonry strength beams, with an average 140 % more elastic stiffness.

5.4.6 Initial tendon prestress effect

Tests results show that a variation in initial prestressing force presented a slight change in the initial stiffness on the load-deflection curve, but there is no significant variation in the ultimate flexural capacity. In spite of initial tendon prestress tested beams had variations between 22% and 44% of masonry strength, the biggest increment in ultimate flexural capacity was always lower than 3%. Equally, an increase of tendon stress reduces up to 24% of the ultimate midspan deflection. Another important effect that could have been observed in tested beams, was the incidence of the initial prestress in the magnitude of the decompression limit, higher decompression limits values are obtained with greater levels of initial prestress. Beams with significant difference in their initial tendon prestress, may share their initial linear elastic stage, and the nonlinear behavior in the load-deflection curve shows a parallel trend, being the nonlinear stiffness for both beams very similar (Fig. 5.9). Increasing the post-tensioning force results in a large cracking moment, delaying the development of

nonlinear behavior, higher post-tension reduces displacement capacity.

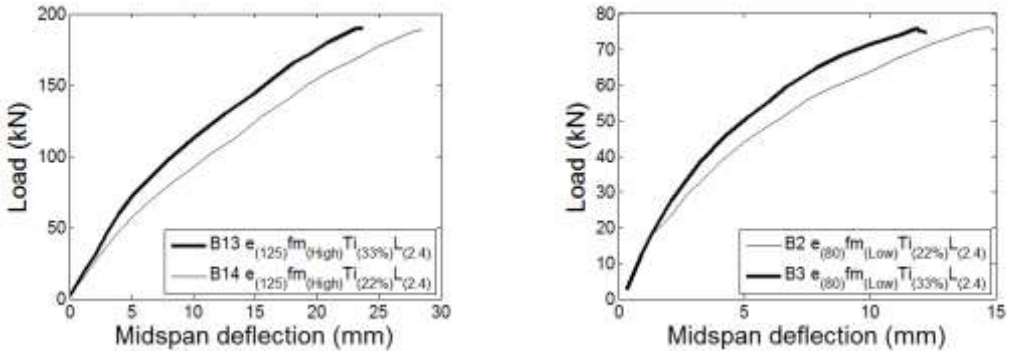

a) b)

Figure 5. 9. Effect of initial tendon prestress a) B-13 vs B-14 b) B-21 vs B-22

5.5 Cyclic behavior

One of the fundamental aims of the performance-based design is the control of structural damage during a powerful earthquake. Structural damage can be expressed as a combination of different dynamic parameters obtained through a cyclic load test. Recent research on prestressing masonry has shown their good structural performance to be useful in seismic areas (Rosenboom and Kowalsky 2004, Wight et al. 2007).

Figure 5.10 shows that after each cyclic load the residual deflection is very small, which proves the self-centering mechanism in post-tensioned masonry elements is a useful feature for service loads. This behavior is also linked to low energy dissipation. For each cycle corresponding to the same load level, degradation of the strength was not observed. Due to block separation, the secant stiffness of tested beams decreases when increasing displacement amplitudes, the values of secant stiffness reduced to almost 83% of the initial values when beams reached a midspan displacement of 12 mm, and 47% at ultimate state.

5.5.1 Cyclic versus monotonic behavior

In order to enable a comparison between monotonic and cyclic behavior, six pair of beams were tested using the same design parameters, but differentiated by type of applied load. Fig. 5.10 shows the correlation between two similar beams when a different load procedure is applied.

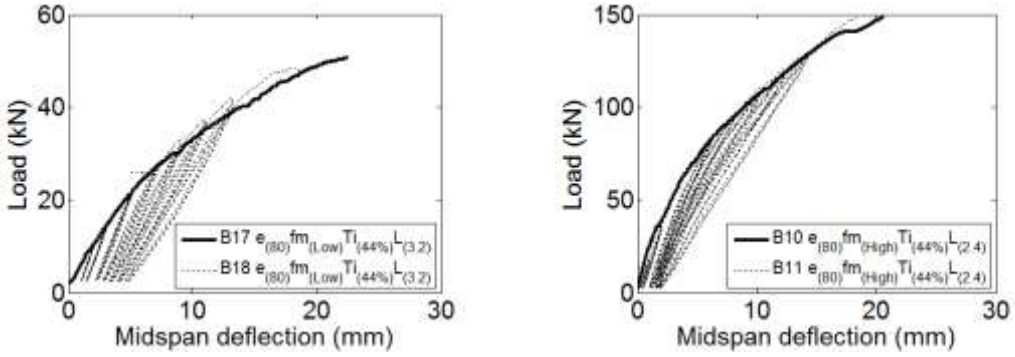

a) b)

Figure 5. 10. Cyclic versus monotonic a) Low strength masonry b) High strength masonry

Results show that, both in monotonic and cyclic beams tests, exhibit a similar load-deflection behavior. The difference observed between ultimate load and maximum displacement, between monotonic and cyclic tests, was insignificant, this may be due to the inherent scatter of mechanical properties of the

materials and small modifications in the execution of the beams tested (Fig. 5.10). In general, the monotonic beam curve behaves like an envelope curve of the cyclic beam curve.

5.5.2 Tendon stress increase

In the linear elastic range of beams, it is clear that the relationship between the main design variables should be almost linear. Once the elastic stage has been completed, load-midspan deflection curve starts to become nonlinear.

Moreover, experimental observations in the tested beams show a linear relationship in tendon stress increase versus midspan deflection curve valid throughout the entire loading phase, even inelastic stage. Fig. 5.11 shows that the linear correlation between both elastic and inelastic range is highly tenable, independent of load type.

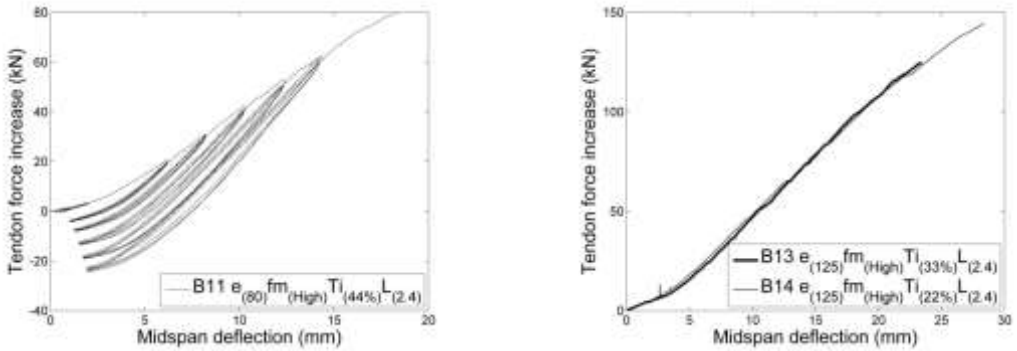

a) b)

Figure 5.11. Tendon stress increase a) Cyclic load B-11 b) Monotonic load B-13 and B14

The load-deflection curve shows a bilinear behavior, the first linear stage corresponds to the linear elastic behavior of the beam until the block separation occurs, next, a second linear behavior is observed in all the tested beams, related to inelastic behavior even in loads levels close to ultimate load taking place. In the cyclic test curve can be observed a significant difference between the slope in load and unload conditions, due to the accumulation of local plastic deformations in the beam for each load cycle. For monotonic beams B-13 and B-14, which differed only in their initial prestress force, they show a similar trend in the tendon force increment curve [(Fig 5.11(b)], however the tendon force at ultimate state is very similar for both beams. It can be noted that the beam with a lower initial prestress tends to generate a greater increase in tendon force until failure.

This linear relationship between midspan deflection and tendon stress increases, even for the inelastic stage, allows a simplification of expression in the design process to predict flexural behavior of ungrouted post-tensioned masonry beams.

5.5.3 Stiffness degradation

Despite the low levels of cracking and damage in the integrity of hollow concrete blocks for all the tested beams, it was noted that secant stiffness in cyclic tested beams decreases rapidly with the subsequent midspan deflection increase in each cycle (Figure 5.12). For midspan displacement of 10 mm a secant stiffness between 35% and 60% of initial stiffness is expected. The stiffness degradation is primarily attributed to the deterioration and permanent deformation of the masonry elements, which follows each load cycle.

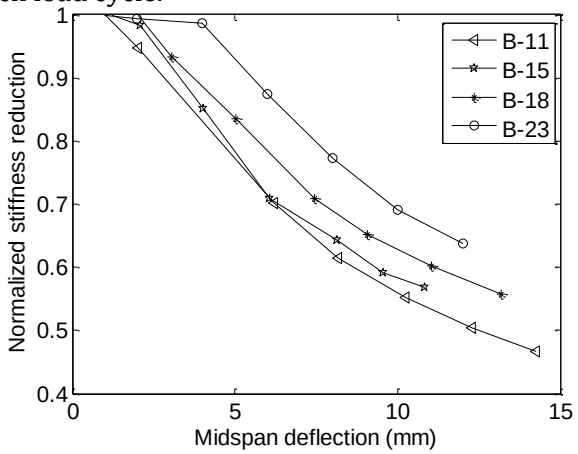

Figure 5. 12. Normalized stiffness reduction

5.6 Codes predictions

Worldwide prestressed masonry codes typically provide design expressions to calculate flexural capacity at ultimate state, and most of them apply strain compatibility between the tendon and the surrounding masonry to estimate flexural behavior in post-tensioned masonry with empirical correlations for ungrouted elements. The accuracy of the code equations is questionable, as prior researchers have shown (Bean, 2003; Wight et al., 2006; Bean and Schultz, 2010). Table 5.4 provides several design formulas to estimate the ultimate flexural capacity available in worldwide post-tensioned masonry codes that were checked in this investigation to verify their accuracy. It is important to note that all of these expressions have been developed for grouted prestressed members loaded out-of-plane, even some of them are not allowed to use ungrouted prestressed masonry beams. However, it is intended to observe the potential application of these equations for the prediction of the ultimate capacity of ungrouted prestressed masonry beams. For consistency, some symbols in the following equations have been changed from the original formula to provide standard notation and avoid confusion.

Table 5.4. Worldwide code expressions

Code	Equations	β_1	β_2	ε_{mu}
British (BS5628-2, 2005)	$f_{pu} = f_{pe} + 700\left(\frac{d}{L}\right)\left[1 - 1.4\frac{f_{ps,u}A_{ps}}{f'_m bd}\right]$ (MPa)	0.50	1.00	0.0035
Australian (AS 3700, 2011)	$f_{pu} = f_{pe} + 700\left(\frac{d}{l_p}\right)\left[1 - 0.7\frac{f_{pu}A_{ps}}{f'_m bd}\right]$ (MPa)	1.10	0.85	0.0035
USA (MSJC, 2013)	$f_{pu} = f_{pe} + 0.03\left(\frac{E_{ps}d}{L}\right)\left(1 - 1.56\frac{f_{ps,u}A_{ps}}{f'_m bd}\right)$	0.80	0.80	0.0025
New Zealand (NZS 4230, 2004)	$f_{pu} = f_{pe} + 70 + \frac{f'_m bd}{NA_{ps}}$ (MPa)	0.85	0.85	0.0030
Canadian (CSA, 2014)	$f_{pu} = f_{pe} + \frac{E_{ps}}{25L}\sum_{n_p}(d - c)$	0.85	0.80	0.0030

To estimate the moment at ultimate state, an equivalent rectangular Withney stress distribution was adopted. For hollow sections, the mathematical operations to calculate ultimate moment of the section can be difficult and time consuming, for this reason the computation has been tried with different effective widths, b_{eff}, in order to simplify the design procedures and work with an equivalent rectangular cross section. For the proposed effective width, two different alternatives were proposed, the first option consists of an effective width calculated as the ratio of the net area of the section, A_n, to the overall depth, h, of the section ($b_{eff} = A_n / h$), the second option consists of the effective width calculated as the sum of the vertical partitions, t_{ef}, of the hollow concrete blocks ($b_{eff} = 2\ t_{ef}$). These options were then analyzed and compared with the calculation of a complete hollow section, were can be observed that the approximation corresponding to $b_{eff} = A_n/h$ was very close to results for the complete section. That is why it was decided to use this approximation to calculate the theoretical ultimate moment capacity of the section for the different masonry code expressions.

For internal force equilibrium at ultimate state, Equation (5.1) must be satisfied:

$$A_{ps}f_{ps} = \beta_1 f'_m a b_{eff} = \beta_1\beta_2 f'_m b_{eff} c \qquad (5.1)$$

Once equilibrium of forces is achieved, the ultimate design moment of the section is given by Equation (5.2):

$$M_u = \beta_1\beta_2 f'_m b_{eff} c\left(d - \frac{a}{2}\right) = A_{ps}f_{ps}\left(d - \frac{a}{2}\right) \qquad (5.2)$$

Table 5.5 summarizes a comparison between the predictions using the equations given in the main worldwide code expressions versus the results from the conducted experimental tests.

Table 5.5. Summary of code calculations versus experimental results for ultimate moment.

	Experimental	$M_{u,T}$ Theoretical $(kN*m)$					$\frac{M_{u,T}\ Theoretical}{M_{u,T}\ Experimental}$				
Test Beam	$M_{u,T}$	**MSJC 2013**	**BS5628 2005**	**AS3700 2011**	**CSA 2014**	**NZS 2004**	**MSJC 2013**	**BS5628 2005**	**AS3700 2011**	**CSA 2014**	**NZS 2004**
B-1	23.62	26.07	16.78	23.79	29.32	24.40	1.10	0.71	1.01	1.24	1.03
B-2	23.55	24.65	13.55	17.51	28.04	18.74	1.05	0.58	0.74	1.19	0.80
B-3	23.85	25.58	15.77	21.67	28.84	22.55	1.07	0.66	0.91	1.21	0.95
B-10	44.93	40.76	24.42	30.33	46.68	31.74	0.91	0.54	0.67	1.04	0.71
B-11	46.30	40.81	24.61	30.64	46.69	32.09	0.88	0.53	0.66	1.01	0.69
B-13	58.11	51.55	27.23	32.27	60.31	33.14	0.89	0.47	0.56	1.04	0.57
B-14	57.84	49.26	22.70	25.66	58.67	26.70	0.85	0.39	0.44	1.01	0.46
B-15	61.71	49.10	22.50	25.38	58.54	26.48	0.80	0.36	0.41	0.95	0.43
B-17	20.50	25.53	16.60	22.98	28.54	24.49	1.25	0.81	1.12	1.39	1.19
B-18	19.83	25.25	16.13	21.96	28.27	23.67	1.27	0.81	1.11	1.43	1.19
B-21	53.02	39.34	24.41	29.80	45.13	32.59	0.74	0.46	0.56	0.85	0.61
B-22	48.35	37.09	20.36	23.34	43.32	26.84	0.77	0.42	0.48	0.90	0.56
B-23	52.60	45.38	19.99	21.80	54.84	25.19	0.86	0.38	0.41	1.04	0.48
B-24	63.99	51.69	27.50	32.69	60.41	33.53	0.81	0.43	0.51	0.94	0.52
						Mean	**1.01**	**0.57**	**0.72**	**1.17**	**0.76**
						COV	**0.21**	**0.26**	**0.33**	**0.21**	**0.33**
						R^2	**0.9121**	**0.7804**	**0.4938**	**0.8981**	**0.5453**

The results show that the United States and Canadian codes provide a better prediction with respect to the experimental results, but without a clear trend between conservative and non-conservative in the prediction. The remaining codes provide results that differ significantly from experimental results, but their predictions show a clear conservative tendency.

5.7 Conclusions

After a detailed experimental study of flexural behavior conducted on full-scale beams, the results obtained indicate that ungrouted post-tensioned masonry beams with unbonded elements are able to develop an appropriate flexural capacity in terms of strength and deflection, due to the use of the deviator block or restrained block in the midspan beam. During cyclic testing, a low energy dissipation capacity was observed, however, this structural system shows a high degree of recovery in deflection after unloading, associated with a "self-centering" mechanism. Likewise, damage is concentrated at midspan over a small portion of the beam lower than 25% of the beam length.

This building technique is a promising construction option with great potential to be used on structures that require a certain level of ductility. Based on experimental results and analytical models in this study, the following is concluded:

- Before cracking, the stress in the unbonded tendons increased only slightly with the applied load, while block separation occurred, subsequent, tendon stress increased significantly.
- The load-midspan deflection curve can be simplified approximately to a bi-linear relation, with a first linear elastic region until the first cracking appears, followed by an approximately linear inelastic region with an important stiffness degradation, exhibited by a high deformation capacity and an overload capacity prior to failure.
- Masonry strength is the most relevant variable in the structural behavior of the ungrouted post-tensioned masonry beams, where an increase in masonry strength provides an additional ultimate flexural and displacement capacity.
- Changes in tendon eccentricity and initial tendon stress developing in this study, showed a slight incidence on the structural behavior of ungrouted post-tensioned masonry beams in flexure.
- Based on the observations made in this study, MSJC-2013 and CSA-2014 codes provided better correlation with the experimental data.

CHAPTER 6. STRUCTURAL TESTING OF UNGROUTED POST-TENSIONED CANTILEVER WALLS UNDER CYCLIC TRANSVERSE LOAD

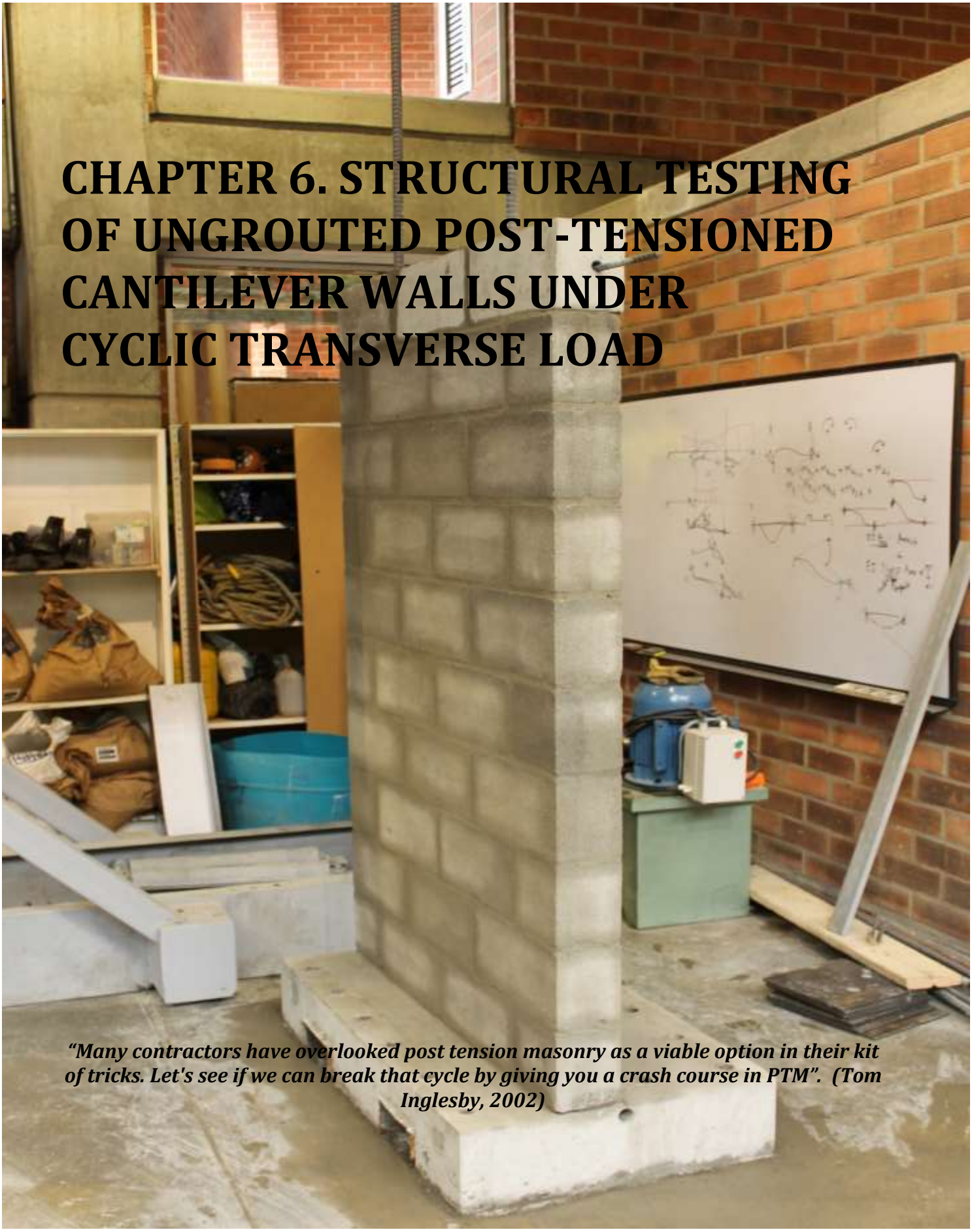

"Many contractors have overlooked post tension masonry as a viable option in their kit of tricks. Let's see if we can break that cycle by giving you a crash course in PTM". (Tom Inglesby, 2002)

Abstract

Post-tensioning techniques substantially improve the structural behavior in masonry under tensile strength making post-tensioning masonry a construction technique with similar or better mechanical properties than reinforced concrete. Cantilever walls are very useful in a variety of structural applications, one of the most common is the construction of retaining walls, and although investigations have been made into post-tensioned masonry cantilever walls, most of them focused on grouted elements and in-plane loads. Grout increases the cost of prestress masonry, increased labor and time construction, and it is for this reason that this research studies the mechanical behavior of prestressed ungrouted cantilever masonry walls. This study investigated the influence of initial prestress and masonry strength in the out of plane mechanical behavior of ungrouted cantilever prestressed masonry walls, as well as the accuracy of different worldwide prestressed masonry codes expressions to calculate the ultimate flexural load capacity. The results show the ability of this structural system to withstand large lateral displacements with a limited and concentrated damage zone. The impact of initial prestress at ultimate state is less evident than the effect of masonry strength, likewise, the results of code expressions to predict flexural capacity show differences with the experimental data.

Keywords: Post-tensioning; Masonry; Cantilever wall; Ungrouted; Unbonded, Out of Plane.

6.1 Introduction

The developed research in post-tensioned masonry over the past three decades has shown the structural advantages of this building practice. Post-tensioning provides a significant strength increase of the masonry wall. Ungrouted prestressed masonry has great potential to be used in different types of structural elements. Since ancient times, wall construction has been one of the most natural applications of masonry. One of the first development and application of prestressed masonry walls began in Australia during the mid-1960s (Schultz and Scolforo, 1991), but it was not until the early 1970s that the first scientific research and testing on full-scale specimens were carried out and reported in the United Kingdom (Lissel, 2001), in order to understand the out-of-plane behavior in post-tensioned masonry walls. Most of them were low aspect ratios walls (i.e., less than 10), with efficient geometric cross sections, the most common geometric section in tested and constructed walls was the diaphragm wall or cavity wall (wall with a hollow cross section formed from different masonry unit arrangements), followed by the T-shaped wall, where the initial prestress, primarily influenced the elastic behavior (Schultz and Scolforo, 1991). English Engineer Curtin, has been considered as a pioneer of the study of out-of-plane behavior in post-tensioned masonry walls, with his remarkable research and developments on this issue.

Few studies in cantilever post-tensioned masonry walls have been conducted, most of them in diaphragm brickwork grouted walls, but each of them revealed all the benefits of the post-tensioned masonry for these boundary conditions (Curtin and Phipps, 1982; Hobbs and Daou, 1988; Fisher et al. 1989; Garrity and Garwood, 1990; Curtin and Howard, 1991; Shafii, 1994; and Shafii and Hobbs, 1996). Among the main research findings include: increased cracking load, flexural stiffness, ultimate capacity, reduced serviceability deflections, and after unload cracks closed completely. To further understand the behavior in ungrouted post-tensioned concrete masonry cantilever walls, an experimental program was conducted at the University of Medellin to observe the cyclic response of six 2.0 m height ungrouted post-tensioned concrete masonry cantilever walls subject to out-of-plane lateral loading. The purpose of the research was to check the viability of this structural system for further implementation as an earth retaining wall. It was also studied the effects of initial tendon stress and masonry strength on the lateral load behavior of the cantilever masonry wall, and the accuracy of the main worldwide codes to predict flexural behavior of post-tensioned cantilever masonry walls at ultimate.

6.2 Experimental setup

A set of full-scale specimens was tested in order to study the structural behavior of ungrouted and unbonded post-tensioned masonry cantilever walls. Despite the large amount of parameters that govern the mechanical behavior of post-tensioned masonry, the decision to study only the effect of initial tendon stress, and masonry strength was taken by a limited number of tested samples and the importance of these

variables in the mechanical behavior of this structural system.

6.2.1 Materials properties

Standard hollow concrete block units with nominal dimensions 190 mm high, 140 mm wide, and 390 mm long were used to construct all the walls, with approximately 10 mm thick mortar. A hydraulic cement mortar with a mix weight ratio of 1:2 (cement:sand) was employed. After the construction, all the walls were cured with water sprayed on them for at least 28 days prior to testing. A solid threaded bar of 25 mm diameter of steel Grade 75 was used, with a cross-sectional area of 506.7 mm^2 and a modulus of elasticity of 200GPa, yield stress of 517MPa (at 1% of strain) and ultimate strength of 690 MPa in accordance with ASTM A615.

The walls were built on a stiff and strong reinforced concrete base of dimensions 1200 x 700 x 200 mm (length, width and height respectively), reinforced with 8 #8 (25.4 mm diameter) longitudinal corrugate mild steel bars, and 15 #3 (9.5 mm diameter) closed shear stirrups along the length of the beam. This foundation contains a 200 mm holes grid for the post-tensioning bars to pass through. For concrete base construction, a hydraulic concrete with a mix weight ratio of 1:2:2 (cement:sand:gravel) and water/cement ratio of 0.6 was employed. The reinforced concrete base was fixed to the testing rig with high strength bolts and nuts around its perimeter. Test rig consisted of a strong steel plate supported by a rigid steel reaction frame. Table 6.1 provides a summary of masonry, concrete and mortar properties. Concrete, mortar and masonry compressive strength was determined in accordance with ASTM C109/C109M (ASTM 2002), ASTM C270 (ASTM 2003) and ASTM C62 (ASTM 2004), respectively.

Table 6.1. Masonry, specimen properties.

	Low Strength Masonry							
Property	**Unit f'_b (MPa)**	**Mortar f_j (MPa)**	**Masonry f'_m (MPa) ***	**Height(h) (mm)**	**Width (t) (mm)**	**Length(b) (mm)**	**Area(A) (cm^2)**	**Weight(W) (kg)**
Value	12.6	28.09	12	189.5	141	389	316.23	12.58
Number of test	64	16	-	64	64	64	64	64
COV	8.7%	13.8%	-	1.0%	1.1%	0.5%	4.2%	1.9%
	High Strength Masonry							
Value	30	29.41	21.06	188.5	139.67	388.5	310.12	14.14
Number of test	16	16	-	16	16	16	16	16
COV	8.9%	14.4%	-	1.0%	1.0%	0.4%	2.6%	1.0%

*** MSJC-2013 Correlation**

6.2.2 Details of specimens

An experimental program was developed to evaluate the structural behavior of post-tensioned concrete masonry cantilever walls under out-of-plane load, this was done using different levels of post-tensioning and two masonry strengths. The experimental program covered the test of six 2.0 m tall large scale ungrouted and unbounded cantilever walls, with standard commercially available single-wythe hollow concrete block units 190x1200 mm of cross section. Running bond with mortar was placed for the construction of all walls using a common bond pattern. The walls were built at the Laboratory of Structural Engineering at the University of Medellin-Colombia.

Three different magnitudes of initial tendon prestress ($15\%f'_m$, $25\%f'_m$ and $35\%f'_m$) (maximum compression stres at the wall section by tendon prestress) and two masonry strengths (12.00 MPa and 21.06 MPa, low and high strength respectively) were used. Precast reinforced concrete solid blocks developed in the University of Medellin were placed at the top of the wall on the last course of blocks. Both vertical and horizontal holes were incorporated through these solid blocks to allow the post-tensioned bars to pass through. In this last course of precast solid blocks, a horizontal prestress force was applied to obtain a similar effect to a capping reinforced concrete beam that serves to uniformly transfer the post-tensioning force to the masonry.

The horizontal post-tensioning in the upper solid course of the wall, played a fundamental role in successfully transferring vertical post-tensioning in the wall, a low or zero horizontal post-tensioning in the upper solid blocks would have caused local failures at the upper anchorage regions.

Two eccentrically unbonded and unrestrained (free to move within wall) threaded steel bars, with a constant eccentricity of 200 mm from the wall center, were used as internal prestressing bars without lateral restrain. They were inserted after construction of the wall, symmetrically positioned through the wall cavities on both sides of wall. Square steel bearing plates (150 mm in size) were placed on the upper end of each bar to avoid any localized failure. The lower end of the bar was positioned to the strong reaction plate in the steel frame by means of a high strength nut. There was no bond between tendon and masonry over its whole length. The tendons were post-tensioned using a 300 kN hydraulic jack with a similar load, sequentially with load increases of 25% in alternation until the initial prestress has been reached on each bar. The jack was removed after post-tensioning and tightening the nuts. The walls were able to withstand prestress force without apparent damage. Some adjustments in post-tensioning force were made to compensate for the elastic shortening in the wall.

No other reinforcement was used in the wall. Test walls were given the notation W-N, where N denotes the test number. Table 6.2 shows the test matrix that provides properties and details of all tested walls.

Table 6.2. Tested walls properties

Wall Number	Load Type	Block strength	Initial force south tendon (kN)	Initial force north tendon (kN)	Initial tendon prestress (kN)	Height (m)
W-1	Cyclic	Low	43.07	41.56	84.63 (15%)	1.8
W-2	Cyclic	Low	64.18	65.97	130.15 (25%)	2.0
W-3	Monotonic	Low	67.99	63.92	131.91 (25%)	2.0
W-4	Cyclic	Low	42.89	46.92	89.81 (15%)	2.0
W-5	Cyclic	Low	104.72	107.08	211.8 (35%)	2.0
W-6	Cyclic	High	102.49	104.15	206.64 (15%)	2.0
W-7	Monotonic	High	200.42	194.93	395.35 (25%)	2.0

6.2.3 Load history and instrumentation

All the walls were tested against a rigid steel reaction frame in the upright cantilever position, with free upper edge and fixed bottom supports. Lateral cyclic or monotonic loading in the out-of-plane direction was provided by a singular horizontal actuator on one side of the wall, about one third up from the top of the reinforced concrete base. This apportioned single force through a vertical whiffle tree consisting of a set of simply-supported steel girder beams. That force simulated an approximate triangular uniformly distributed pseudo-static earth pressure load by applying eight equidistant point loads, emulating an equivalent earth pressure load. Additionally, in each point load a square steel plate (250mm) with neoprene pads was placed to distribute the concentrated load. A displacement controlled one-directional cyclic out of plane stepped load/unload history was applied in the laboratory by gradually increasing and decreasing monotonic displacement. Each cycle was repeated twice consecutively with sequential increments double in displacement up to a maximum of 124 mm (6.2% drift), subsequently the wall lost their lateral capacity and failed. The applied load history is shown in Fig. 6.1. Even though, the applied load system differs from a triangular uniformly distributed load, the shape of their moment diagram is very similar (Fig. 6.2), and the load patterns share the same strength values in the critical section of the wall than triangular distributed load.

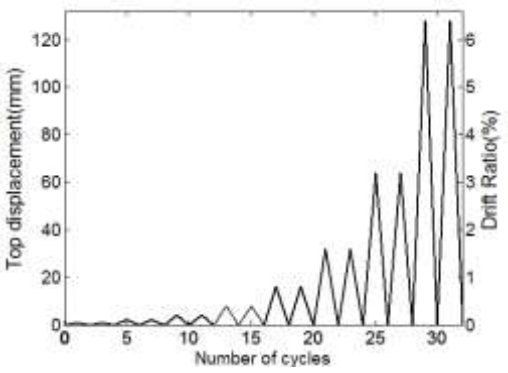

Figure 6. 1. Applied load history.

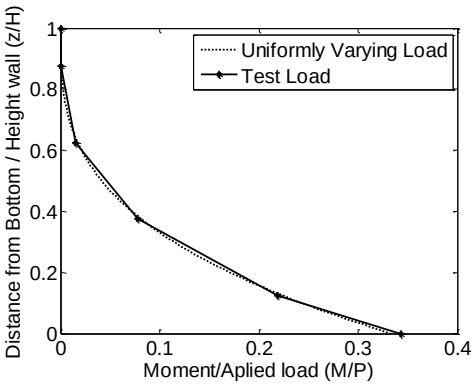

Figure 6. 2 Applied moment diagram

The global wall response was measured using three load cells, seventeen linear potentiometric displacement transducers and four linear variable differential transformers (LVDTs), thus allowing a complete record of the principal deformations and forces during the entire loading process [Figure 6.3(a)]. Two load cells installed at the top of each wall at end bar to measure and record the force variation in tendon stress, and an extra one used to monitor the load applied on the actuator [Figure 6.3(b)]. Likewise horizontal displacement transducers to monitor wall displacement (F20 to F21), lateral movement and wall rotation in the bottom wall (F12 and F9), as well as to determine whether any wall twisting has occurred. Vertical displacement (F2 to F6, F11, and F13 to F19) was used to determine the strain profile and neutral axis for different cross-sectional areas at the bottom of the wall.

The tendon eccentricity advantages in this kind of wall (retaining wall), which are only loaded in one direction, can be seen in an optimal section design. When the cracking load is reached at the bottom of the wall, tension stress begins to appear at the tension face, and the compression face still has a great load capacity compared to a similar concentric tendon wall.

a) Lateral view

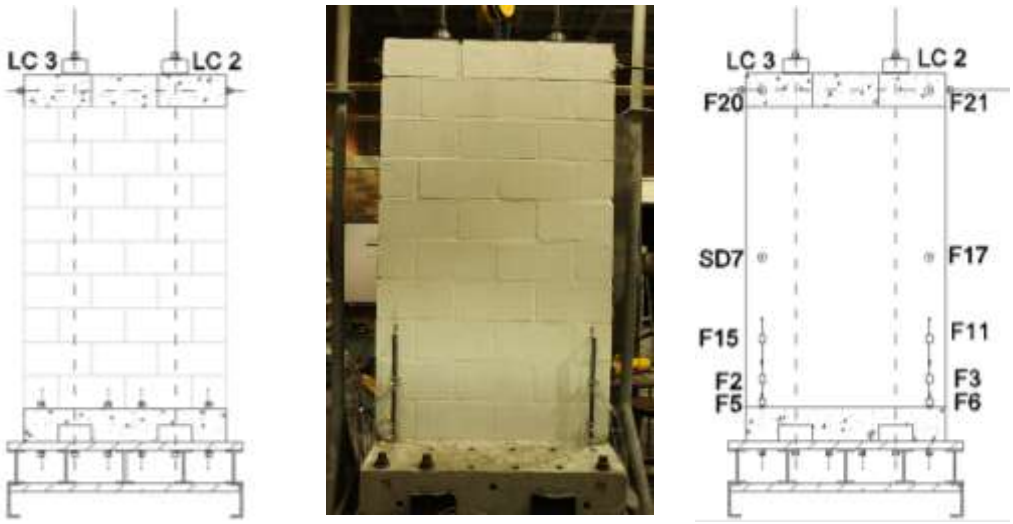

b) Frontal view

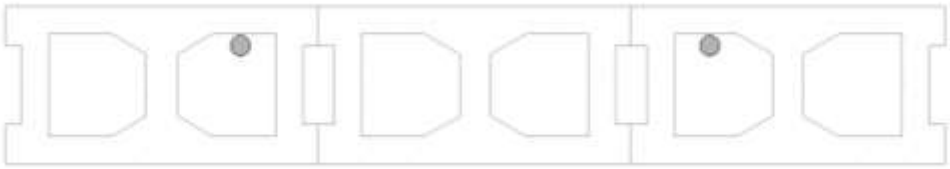

c) Top view

Figure 6. 3 Test specimen and instrumentation

6.3 Test results

In the carried out tests, cantilever post-tensioned masonry walls proved their good structural behavior in out-of-plane strength, they showed their ability to withstand large lateral displacements without major damage. The summarized results of the wall behavior is shown in Table 6.3, where P_u corresponds to the ultimate wall load, T_u is the ultimate tendon load, the maximum displacement at the top of the wall at failure $\delta_{max,u}$ and ΔT_u maximum tendon load increment at ultimate state.

Table 6.3. Test results

	Ultimate					**Tendon Force Increase**		
Wall Number	Load P_u (kN)	Maximum Displacement $\delta_{max,\,u}$ (mm)	Final Force North Tendon (kN)	Final Force South Tendon (kN)	Final Tendon Force T_u (kN)	Force increase South Tendon (kN)	Force increase North Tendon (kN)	Final Tendon Force Increase ΔT_u (kN)
W-1	35.89	107.6	153.92	150.84	304.77	107.77	112.36	220.14
W-2	30.93	128.8	140.51	158.86	299.37	94.68	74.54	169.22
W-3	29.49	100.6	137.34	139.81	277.15	71.82	73.42	145.24
W-4	31.97	148.6	143.39	152.70	296.09	109.81	96.47	206.28
W-5	37.33	125.6	205.85	192.85	398.70	88.13	98.77	186.90
W-6	37.64	122.6	210.5	207.93	418.43	105.44	106.35	211.79
W-7	49.67	121.9	295.24	315.56	610.80	115.14	100.31	215.45

6.3.1 Load-displacement curves

In Figure 6.4 for tested walls 4 and 5, a nearly bi-linear approximation to load-deflection behavior with a small energy dissipation was observed. The initial wall response was linearly elastic up until the initial cracking load was reached, without accumulation of damage, and after unloading, displacement was almost completely restored. A nonlinear behavior, with important stiffness reduction until peak load was reached was observed, subsequently the applied load decreased up to failure. The limit between elastic and inelastic regions is not a true yield limit, because in all tested walls for this load capacity the threaded bar remains in elastic state. This limit corresponds to a geometric nonlinear region product of the decompression of the hollow concrete block by the "rocking" response, shown by the appearance of tensile forces at the bottom of the wall. Post-tensioned masonry cantilever walls show a reasonable ductility and overloading capacity before failure when first cracking appears. A stable cyclic behavior until rupture was observed in all the walls. Before the walls lose their load capacity, a large drift ratio of 5% to 7% was observed, without it compromising the structural integrity of the wall. It was considered a failure of the wall when the load dropped by 25% and deflection increased significantly.

The amount of initial prestress controlled the cracking load in all the tested walls. The flexural capacity increase depends mainly on the masonry strength and in second instance on the initial prestressing load. Based on the observed cyclic load-displacement loops, a clear pinched loops trend in all cyclic testing can be seen, this structural behavior implying a limited energy dissipation. Sliding displacement between the wall and concrete base was insignificant in comparison with the lateral deflection for all the tested walls, measurements indicate that wall sliding did not exceed 1mm during test. An adequate friction between the wall and foundation was created by the initial prestress force.

Maximum drift measurements in tested walls were between 6% and 7.5%, generated by flexural deflection and the rotation of the rocking behavior. Similar range was reported by Ismail et al. (2011) and Ismail and Ingham (2012) in previous experimental studies for posttensioned masonry walls (4.4% and 11.9%).

During a large part of the test, walls did not present any crack or evidence of failure, even at higher levels of displacement (drift ratio higher than 5%) and loads exceeding 85% of ultimate flexural capacity. Damage is concentrated at the bottom of the wall (extended along a 200 mm section approximately from foundation).

In low strength masonry wall, tendons did not reach yielding, in contrast to high strength masonry wall where tendons reached their elastic limit and yielded, but the effect of this yielding was not visible in the load-deflection curve. A complete record of walls 4 and 5 over all load-displacement cycles are plotted in Figure 6.4.

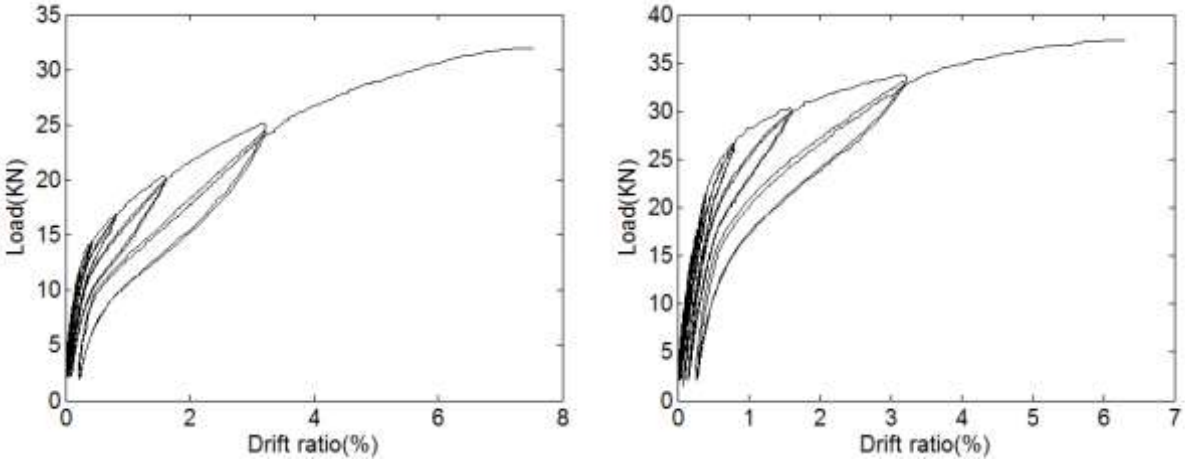

Wall 4 Wall 5

Figure 6.4. Load-Displacement curve.

The envelope load-displacement response of all tested walls is shown in Figure 6.5; the effect of masonry strength on load capacity is clearly evident, even though displacement capacity is very similar for the different masonry strengths. Although there are differences between the tested walls, the average initial wall secant stiffness was very similar despite the differences that exist in wall and masonry properties.

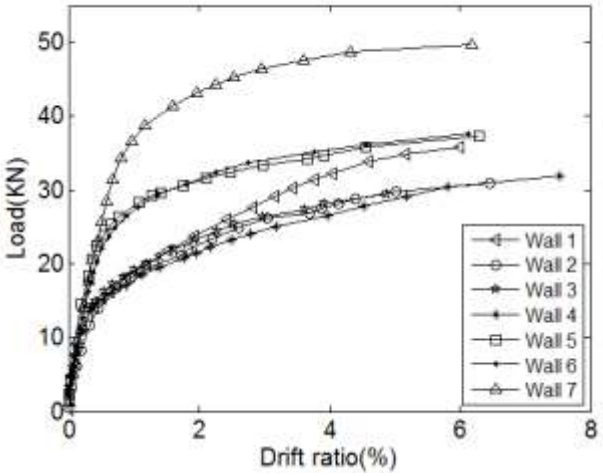

Figure 6.5. Envelope Load-Displacement curves

6.3.2 Failure modes

Bending was the dominant failure mode in all tested walls under flexural loads, characterized by the formation of one plastic hinge at the bottom of the wall in the flexural compression zone with a general crushing of the compression zone, and a focused masonry and mortar crushing in the toe regions. This was the typical failure mode observed in all the tested walls. The opening at the bottom of the wall changed the cantilever wall into a hinged mechanism. Block separation due to decompression produces large cracks at the bottom of the wall without affecting the integrity of the wall. The first cracks inside the walls were observed on most of the tested walls with a upper drift ratio of 5% at the bottom of the wall, the size of these first cracks were extremely small and a great deal of them could not be observed with the naked eye. The failure pattern consisted of a crushing concentration at the toe regions and an uplift at the heel side. Damage was limited and concentrated to a small focal portion at the bottom of the wall (200 mm), where masonry crushed locally in the area of the greatest bending moment. The zone on the bottom of the wall generates the largest amount of cracking, and the rest of the specimen had negligible damage. Figure 6.6 shows a typical flexural behavior observed in all the tested walls.

a) Lateral view b) Frontal view

Figure 6.6. Typical failure mode

When the external forces in the wall begin to generate tensile stresses at the bottom of the wall, the limitation of unbonded post-tensioned masonry to counter tension stresses produces the decompression of the cross section at the heel region. This decompression causes the rotation of the whole wall around the toe region of one rigid body hinging about one point, and the appearance of an opening horizontal crack along the wall base in the mortar joint acting as a hinge (Figure 6.7). The compression regions is decreased as the lateral displacement increases, shifting the neutral axis towards the toe regions of the wall and leading to an increase in the tendon force when the wall is deformed laterally. This phenomenon was visible in all the tested walls and is known by the name of "rocking". The "rocking" behavior was observed in all

tested walls in the toe regions, and a self-centering behavior even after large wall displacements occurred. After unloading, the wall returned near to the original vertical alignment, almost to its original location, without considerable residual displacement or damage. This phenomenon is most common in flexural failure of unbonded post-tensioned walls that have a sufficient initial prestress force to resist sliding at the base of the wall and an adequate shear resistance to avoid shear failure. The "rocking" mechanism is the leading cause of how unbonded post-tensioned masonry walls provide low energy dissipation (Rosenboom and Kowalsky, 2004).

a) b)

Figure 6. 7. Rocking mechanism a) Lateral view b) Back view

6.3.3 Bars tension measurements

The tendon force history for walls 4 and 5 in both threaded bars are plotted in Figure 6.8. For walls with low strength masonry all bars remained in the elastic state through the entire test, unlike walls with high strength masonry, whose threaded bar exceeded their elastic limit before wall failure. By the symmetry of the structural system, both bars in the wall present a similar behavior throughout the entire test (Fig. 6.8). Increases in tendon force at the beginning of the test were insignificant until the decompression at the base wall appeared, subsequently, tendon force is significantly increased when external load is rising. This increase was due primarily to the rocking in the wall that leads a deflection between the two anchorages of tendon bars at the bottom and top of the wall. Initial prestress has a significant impact on decompression load as can be seen from Figures 6.4 and 6.8, when initial tendon prestress is duplicated between wall 4 and wall 5, the load required to produce the decompression at the bottom of the wall is also double.

A considerable loss in bar tension was observed (between 13% and 37%) as the walls were unloaded and returned to their vertical positions, this was due to the elastic shortening and crushing of the masonry. In this way, the wall itself shortened, causing the threaded bar to loosen. With an increase in the lateral displacement, for each following loading cycle, a higher loss in tension bar is produced (up to 20% after each loading cycle). The influence of the elastic shortening and crushing of masonry shows in the unload tendon force curve, where the decreasing portion of the curve shows a different slope than the increasing portion, it also shows an additional energy dissipation within threaded bars.

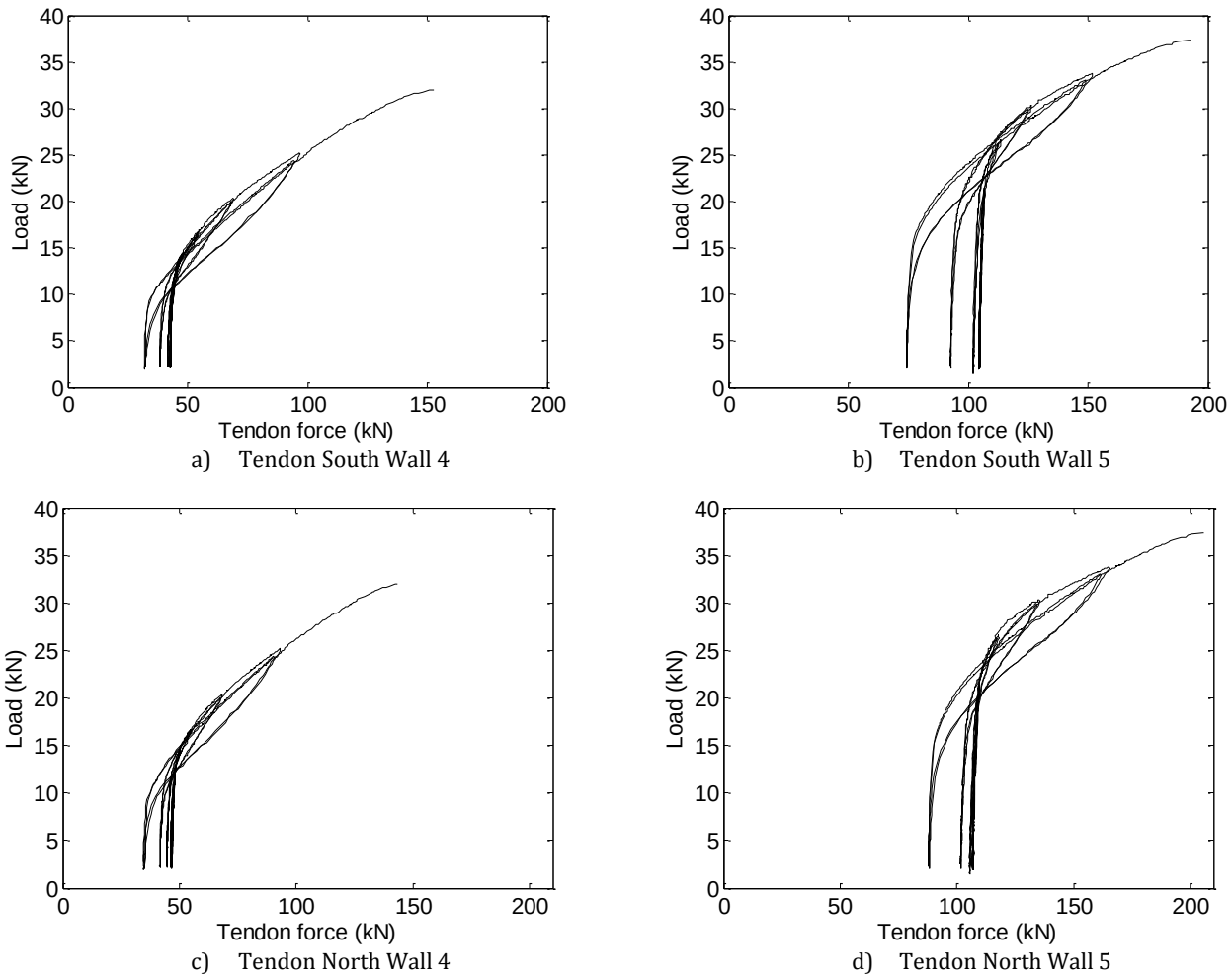

Figure 6. 8. Load-Tendon Force curve (Low strength masonry)

Figure 6.9 shows the tendon force increment versus displacement curve, in which a nearly bi-linear approximation can be observed. Similar observations have been made in several different experimental investigations: Bean and Schultz (2011), Wight and Ingham (2008), Bean et al. (2007), Mojsilovic and Marti (2000), Marzahn (1998), Campbell and Chouinard (1991), Harajili and Kanj (1991), Yaginuma (1995), Lazzarini et al. (2010) and Du and Liu (2003). The first short linear portion is approximately horizontal and corresponds to the linear-elastic behavior of the structural system. Subsequently, the second and more long linear portion of the curve, corresponds to inelastic region of load-displacement curve after decompression at the bottom of the wall. In spite of their inelastic behavior, a nearly linear trend is observed in tendon force increment vs displacement curve, even if yield limit in threaded bars is exceeded for wall 7 [Fig. 6.9(b)]. The effect of the elastic shortening and crushing of masonry was also noted in the tendon force increment curve, because the cyclic test loading curve shows a different behavior to the unloading curve, but after reloading, the curve returns to its original state equivalent to a monotonic test.

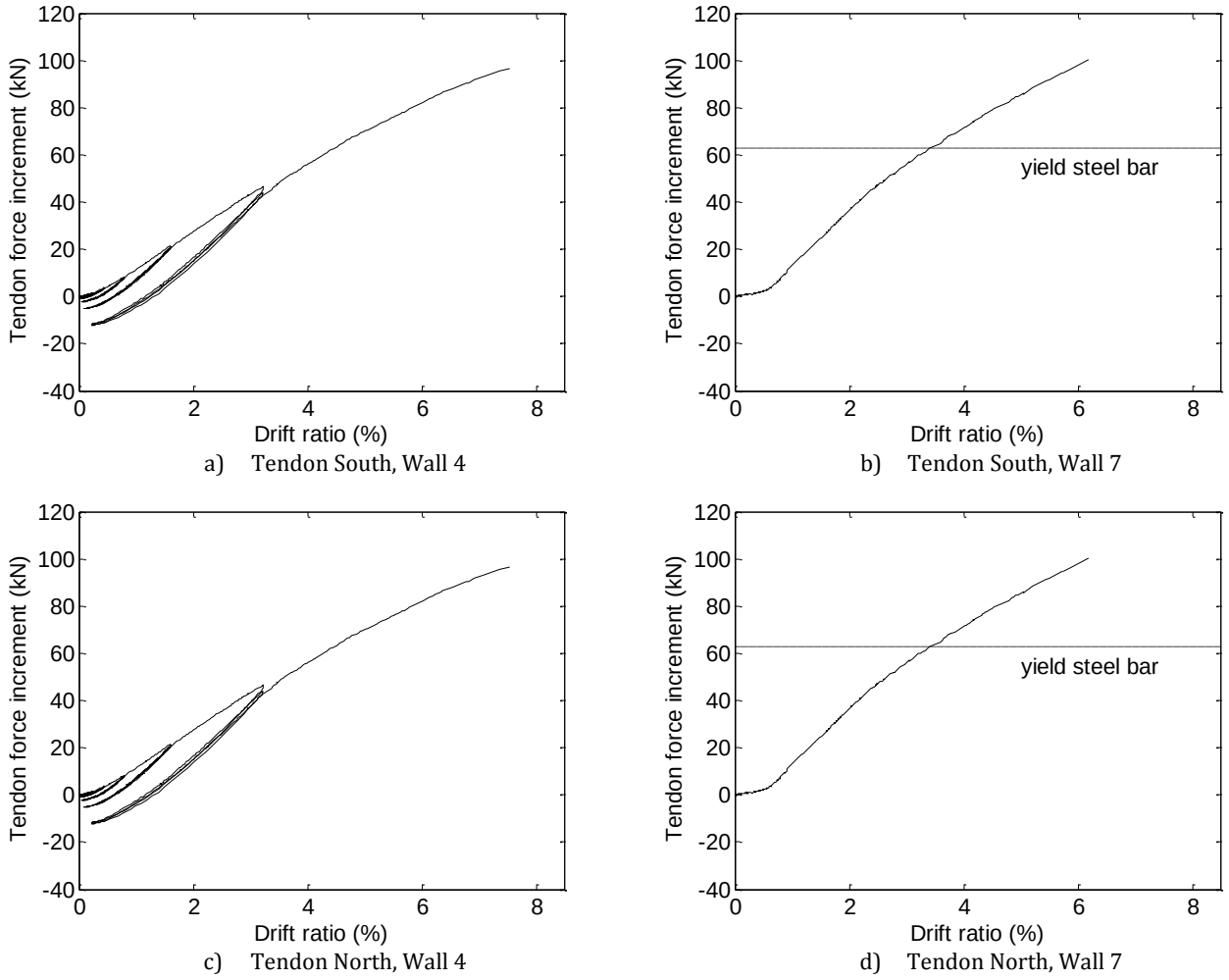

Figure 6. 9. Tendon force increment.

6.3.4 Patterns of displacements measurements

The wall deflection is due to the combined effect of wall rocking, flexural behavior, base sliding, and shear effect, but "rocking" is the principal factor that determines the lateral displacement in the wall because once rocking appears the flexural deflection by curvature remained almost constant (Rosenboom and Kowalsky, 2004). As a result of "rocking", when the wall is deflected it behaves as a rigid body, and the variation of displacement within wall height can be assumed as linear [Figure 6.10(a)].

This effect can be noted in experimental results [Figure 6.10(b)], where the displacement profile for each load cycle is almost linear. The only exception is the deflection near to the ultimate state seen as a slight deviation in the linearity of the displacement profile of the wall, due to a rise in of flexural deflection.

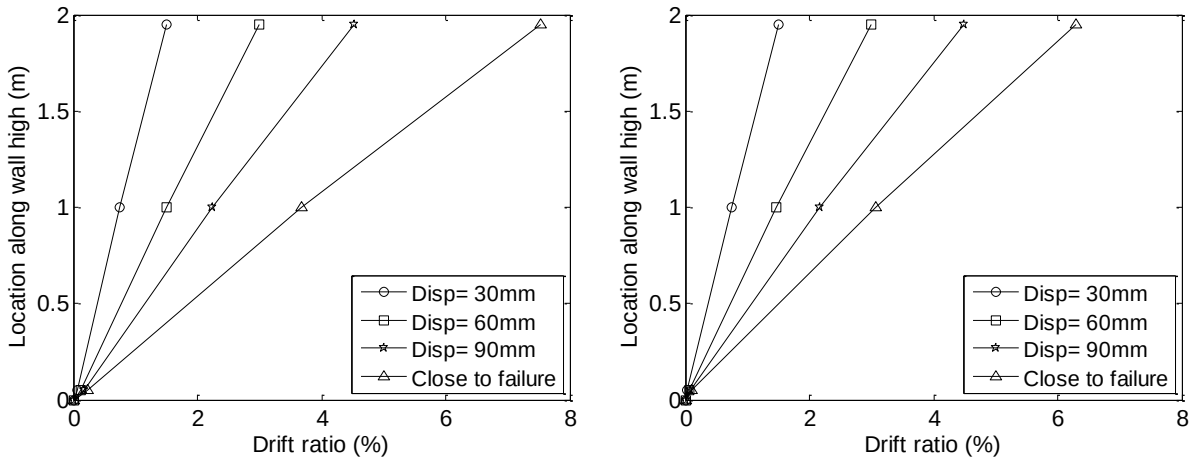

Wall 4 Wall 5

a)

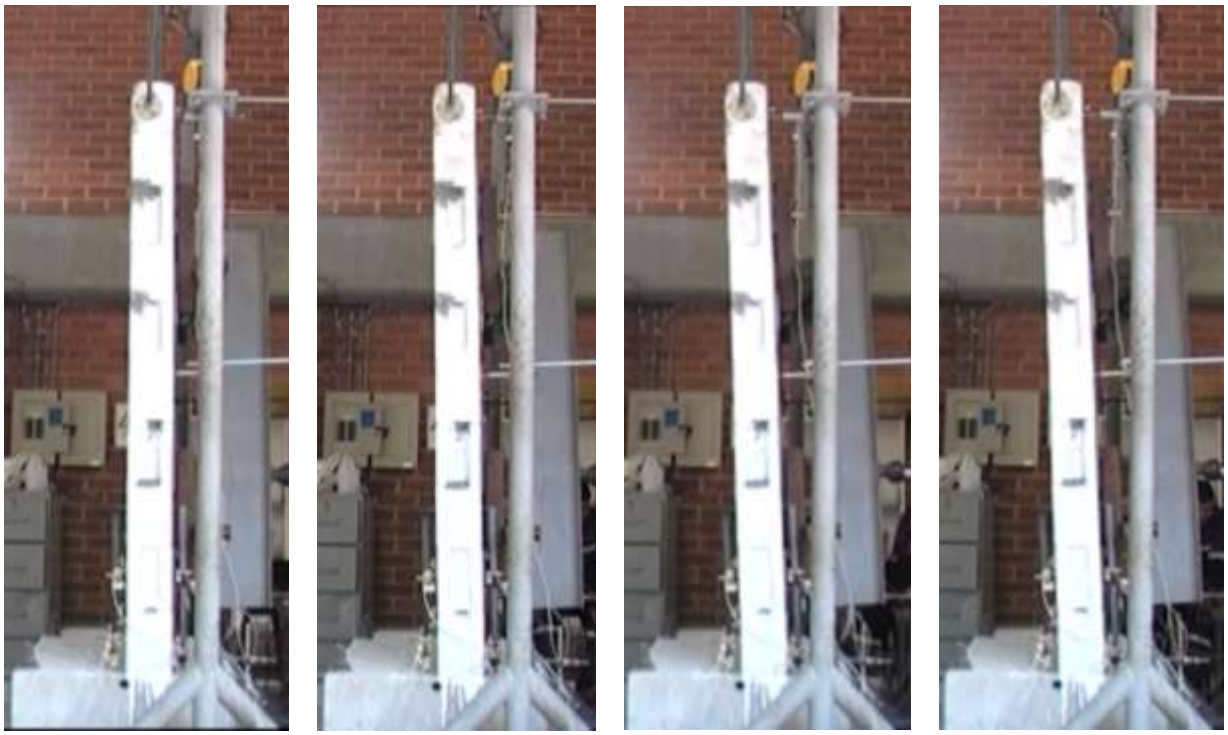

a) δ_{max}=30 mm (1.5% drift)
b) δ_{max}=60 mm (3.0% drift)
c) δ_{max}=90 mm (4.5% drift)
d) Failure (6.0%-7.5%drift)

b)

Figure 6. 10. Displacement profiles wall 4 a) Measurement profiles b) Experimental profiles

6.4 Discussion

6.4.1 Cyclic and monotonic test

In order to review the differences between the structural behavior of monotonic and cyclic testing of ungrouted out-plane post-tensioned masonry, two cantilever walls with similar physical properties were built. Both walls were tested under different load histories, monotonic (wall 3) and cyclic (wall 2), to verify any structural behavior difference that occurred with the change in the load history. Figure 6.11 shows the comparison between cyclic and monotonic behavior, with a dotted line showing the load-deflection curve of a cyclic load wall, and the continuous line representing the behavior of a similar wall tested under monotonic load. The structural behavior of cyclic and monotonic load is very similar, the monotonic wall represents the envelope of the cyclic test, both of which have the same initial stiffness, elastic limit and inelastic behavior. Despite the similarity in their load-deflection curve and structural behavior, the discrepancies for maximum load and ultimate deflection (approximately 7% and 33%, respectively) may be attributed to the deviation in masonry strength from the reported material properties values (Table 6.1).

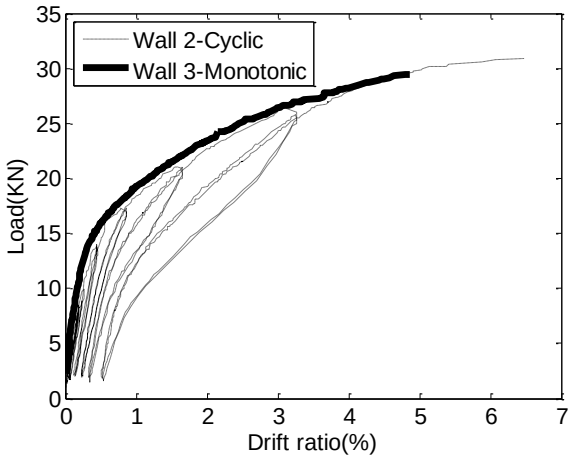

Figure 6. 11. Monotonic versus Cyclic curve.

It has been observed experimentally that the structural development of ungrouted post-tensioned cantilever masonry walls did not lead a significant degradation of their mechanical behavior when an out of plane cyclic load is applied, if compared to a similar wall under out of plane monotonic load.

6.4.2 Effect of masonry strength

Masonry strength is the main parameter that controls the structural behavior of post-tensioned masonry, its magnitude primarily determines the mechanical behavior of any type of structural element built with this system. Compared to the wall W2, a 76% increase of the masonry strength in wall W7 increased the ultimate load by 61% (Fig 6.12). There were no significant changes in the initial elastic stiffness (2.8677 kN/mm for W-2 and 2.3064 kN/mm for W-7) and the ultimate deflection (128.8 mm for W-2 and 121.9 for W-7).

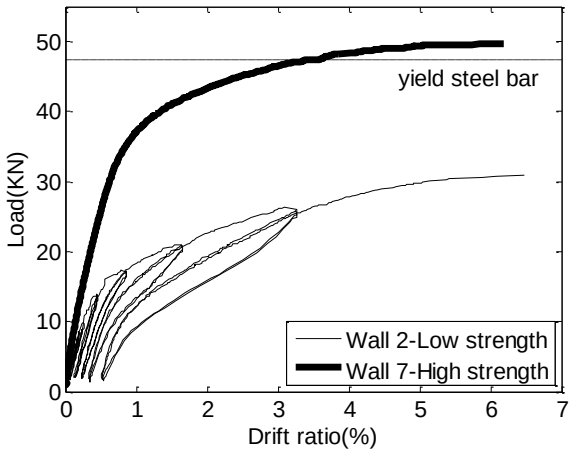

Figure 6. 12. Low strength versus High strength curve.

6.4.3 Effect of initial prestress

The magnitude of initial prestress has been classified in this study as one of the main design parameters involved in the structural behavior of ungrouted prestressed masonry cantilever walls. For practical application, initial prestress can be influenced over time by creep, shrinkage and elastic shortening in the masonry, and steel relaxation. These factors must be taken into account to make a good choice in selecting the optimal initial prestress. Initial prestress has a direct impact on the decompression force. In the tests carried out, the effect of a change in levels of initial prestress was studied, with the aim of examining their incidence in the structural behavior of prestressed masonry. Generally, laboratory tests showed that an increase of initial prestress generates a gradual decrease of the maximum displacement at ultimate state, and an increase of their ultimate capacity. Despite having a broad range of initial prestress, Figure 6.13 shows that initial tendon prestress for values of $15\%f'_m$ and $25\%f'_m$ did not have a significant

influence on the structural behavior of ungrouted post-tensioned masonry walls, but a considerable difference in load capacity can be observed for value $35\%f'_m$.

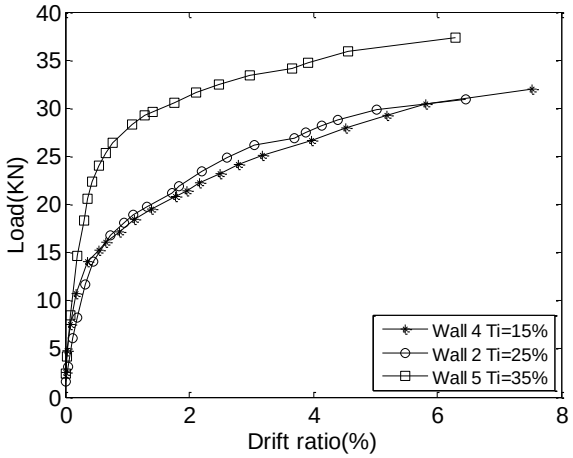

Figure 6. 13. Incidence of initial prestress

The magnitude of the initial prestress had no significant effect on the elastic stiffness for the different tested walls, as can be seen from Figure 6.13. It can also be seen that for some values of initial prestress ($15\%f'_m$ and $25\%f'_m$), the structural behavior of ungrouted post-tensioned cantilever walls is very similar, indicating that when the initial prestress is below a certain value, ungrouted post-tensioned masonry cantilever walls produce a similar structural behavior. Thus, it has been observed experimentally that for a particular value range of initial prestress, the structural behavior of ungrouted post-tensioned masonry wall was very similar despite differing in the magnitude of initial prestress, as it has been seen in other studies (Laursen and Ingham, 2004). Their observation suggests the need for future research to identify the range of values of initial prestress that represent differences in their structural behavior.

6.4.4 Initial stiffness and secant stiffness reduction

The secant stiffness was calculated as the relation between the force and displacement for each peak load cycle taken of the enveloped load-deflection curve. This parameter was normalized by elastic stiffness which is defined by taking an average value of the three cycles in the first phase as the ratio between the force and the maximum horizontal top displacement. Table 6.4 shows the initial elastic stiffness for all tested walls.

Table 6.4. Initial elastic stiffness and stiffness at ultimate

Wall Number	T_u (kN)	δ_{max} (mm)	$K_{elastic}$ (kN/mm)	$K_{inelastic}$ (T_u/δ_{max}) (kN/mm)
W-1	35.89	107.6	6.4564	0.3335
W-2	30.93	128.8	2.8677	0.2401
W-3	29.49	100.6	2.0358	0.2932
W-4	31.97	148.6	5.5136	0.2151
W-5	37.33	125.6	5.8887	0.2972
W-6	37.64	122.6	5.3841	0.3070
W-7	49.67	121.9	2.3064	0.4075

Despite the low levels of damage for large displacement levels, it was noted that the wall secant stiffness ratio decreases rapidly with the subsequent drift increase in each cycle (Figure 6.14). For a drift ratio of 0.5% (10 mm), a secant stiffness between 60% to 80% of initial stiffness is expected, similar to that observed by Ismail and Ingham (2012). The stiffness reduction is primarily attributed to the degradation and permanent deformation of the masonry, which follows each load cycle.

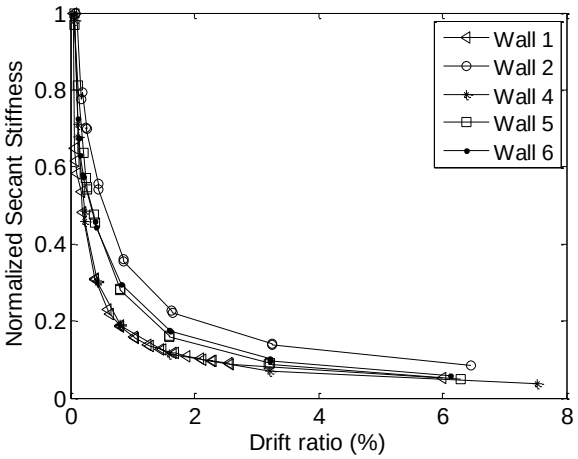

Figure 6. 14. Normalized stiffness reduction.

6.4.5 Residual post-tensioning force ratio

Tendon force decreased slightly during each loading cycle, a result of inelastic shortening in masonry wall. As can be seen in Figure 6.15 the loss of the prestress force when the load is removed occurs rapidly for lateral deflections that exceeds a drift ratio of 0.5% (10 mm) in all walls. It may be observed in Figure 6.15 that for high strength masonry, a greater residual post-tensioning force ratio at large displacement compared to low strength masonry occurs. Likewise,

there is not a distinct trend between the initial prestress ratio and the residual post-tensioned force ratio for the same masonry strength, given that, factors determining residual post-tensioning, such as, elastic shortening, crushing and cracking of masonry depend entirely on the mechanical properties of masonry.

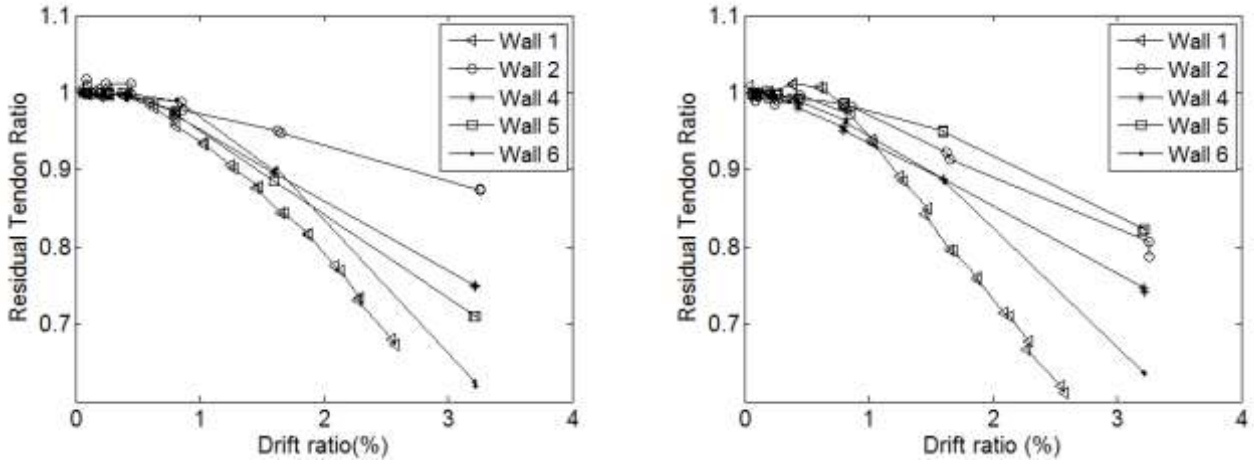

Tendon South Tendon North

Figure 6. 15. Residual tendon prestress ratio

6.4.6 Residual displacement

In order to study residual displacement of ungrouted cantilever post-tensioned masonry walls, residual displacement was calculated by measuring the lateral top displacement of wall relative to the original position of the wall. Figure 6.16 shows residual displacement generated at each load cycle after unloading the wall, which is already relatively low due to the "self-centering" behavior. For each displacement increment, an approximately linear increase in residual displacement is observed, and an average of residual drift ratio of 0.25% (5mm) was observed in most of the tested walls for a drift ratio of 3.2% (64mm). Only in walls 2 and 6, higher residual displacements are observed, above a drift ratio of 0.5% (10mm), which is associated with a preliminary vertical crack caused by the low level of horizontal prestress in the upper solid course of the wall.

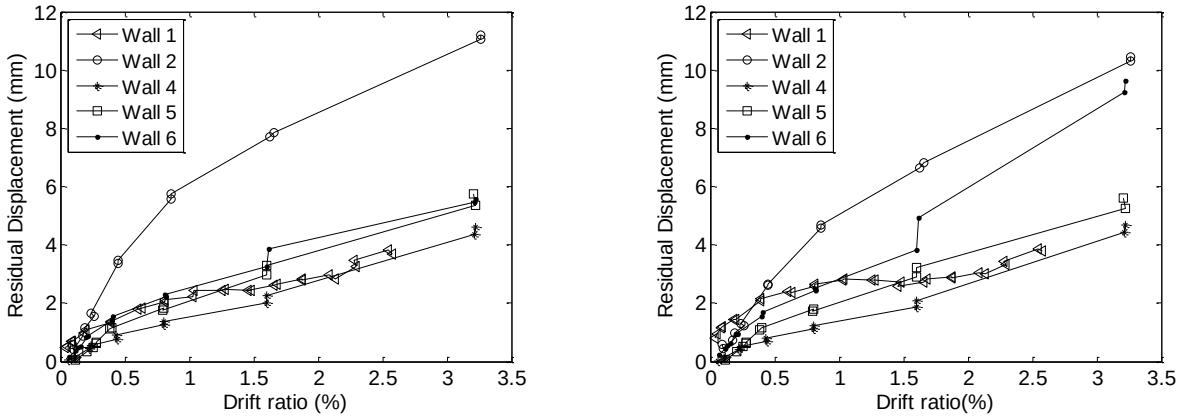

South Potentiometer North Potentiometer

Figure 6. 16. Residual displacement

6.5 Codes results

The main worldwide post-tensioned masonry codes were used to predict the behavior of the walls and compare them with measured experimental results in order to validate the accuracy of the proposed design equations that provide each code. Calculations were

developed assuming negligible tensile strength in hollow blocks, mortar and the bond between them. The British Standards Institution published the first code requirements for the design of post-tensioned masonry in 1985 (Schulz and Scolforo, 1991), and many of those expressions were taken from masonry and concrete codes used at that time. The majority of codes propose a methodology where the mechanical behavior is governed by a rocking mechanism and an equivalent plastic hinge length is assumed. At ultimate state, the stress distribution in the compression face of the wall becomes nonlinear, in accordance with codes recommendations. Whitney's rectangular compression stress distribution is assumed typically, and each code recommends different values of the empirical stress block parameters to produce their design which is obtained from test data and statistical correlations.

Code expressions are based mostly on tendon elongation due to a single hinge or crack opening at mid-height in simple support walls. The purpose of this study is also to analyze the applicability of the code expression to predict flexural behavior in cantilever walls, although, a similarity in flexural behavior between the cantilever wall and the half simple support wall is predicted.

Even though all codes use the same expression to calculate ultimate design moment, the formula employed to calculate ultimate tendon stress (f_{pu}) by each code is different, Table 6.5 provides a summary of the various expressions to estimate ultimate tendon stress used by some worldwide post-tensioned masonry codes. For consistency, some symbols in the following equations have been changed from the original formula to provide standard notation and avoid confusion.

Table 6.5. Worldwide code expressions to calculate ultimate tendon stress

Code	Equations	β_1	β_2
British (BS5628-2, 2005)	$f_{pu} = f_{pe} + 700\left(\frac{d}{L}\right)\left[1 - 1.4\frac{f_{ps,u}A_{ps}}{f'_m bd}\right]$ (MPa)	0.50	1.00
Australian (AS 3700, 2011)	$f_{pu} = f_{pe} + 700\left(\frac{d}{l_p}\right)\left[1 - 0.7\frac{f_{pu}A_{ps}}{f'_m bd}\right]$ (MPa)	1.10	0.85
USA (MSJC, 2013)	$f_{pu} = f_{pe} + 0.03\left(\frac{E_{ps}d}{L}\right)\left(1 - 1.56\frac{f_{ps,u}A_{ps}}{f'_m bd}\right)$	0.80	0.80
Canadian (CSA, 2014)	$f_{pu} = f_{pe} + \frac{E_{ps}}{25L}\sum_{n_p}(d - c)$	0.85	0.80

Equations in Table 6.5 are the main input for the prediction of the flexural behavior of post-tensioned masonry elements at ultimate state, the result of this calculation is a determining factor in estimating the ultimate flexural capacity correctly. Table 6.6 and 6.7 summarize the results obtained in the calculation of ultimate tendon stress and ultimate moment capacity in accordance with the different proposals suggested by the main worldwide post-tensioned masonry codes.

Table 6. 6. Summary of code calculations for ultimate tendon stress versus experimental results

Wall Number	Tu Experimental (kN)	Tu Theoretical (kN)				Theoretical/Experimental			
		MSJC 2013	BS 5628	AS 3700	CSA	MSJC 2013	BS 5628	AS 3700	CSA
W-1	304.77	264.40	112.22	115.76	300.27	0.87	0.37	0.38	0.99
W-2	299.37	277.07	152.44	156.78	308.26	0.93	0.51	0.52	1.03
W-3	277.15	277.72	154.10	158.48	308.85	1.00	0.56	0.57	1.11
W-4	296.09	255.41	114.50	117.76	294.80	0.86	0.39	0.40	1.00
W-5	398.70	307.40	220.05	235.76	335.49	0.77	0.55	0.59	0.84
W-6	418.43	418.07	233.38	235.76	497.21	1.00	0.56	0.56	1.19
W-7	610.80	582.34	417.99	422.26	661.40	0.95	0.68	0.69	1.08
					Mean	**0.91**	**0.52**	**0.53**	**1.03**
					S.D	**0.08**	**0.11**	**0.11**	**0.11**
					COV (%)	**9.17**	**21.15**	**20.72**	**10.71**

For internal force equilibrium at ultimate state, Equation 6.1 must be satisfied:

$$A_{ps}f_{ps} = \beta_1 f'_m ab = \beta_1\beta_2 f'_m bc \quad (6.1)$$

Once the equilibrium of forces in the cross-section is established, the common approach to predict the ultimate design moment of resistance for grouted solid section in all codes, is then given by Equation 6.2. In order to simplify the design operations for hollow sections to calculate ultimate moment, the computation of the ultimate moment is based on an effective beam width (b_{eff}), to work with an equivalent rectangular cross section. The effective width was calculated as the ratio of the net area of the section, A_n, to the overall depth, h, of the section ($b_{eff} = A_n/h$). This approximation was very close to the results for the complete section.

$$M_u = \beta_1\beta_2 f'_m b_{eff} c\left(d - \frac{a}{2}\right) = A_{ps}f_{pu}\left(d - \frac{a}{2}\right) \quad (6.2)$$

For ungrouted hollow sections present in all tests carried out in this study, the equilibrium of forces, the point of application of the resultant forces and its magnitude was set in accordance with the laws of mechanics of materials, and ultimate design moment is calculated in an equivalent way as Eq. 6.2. For this expression, each code calculation used their equivalent stress block parameters (β_1 and β_2) mentioned in Table 6.5.

Table 6. 7. Summary of code calculations for ultimate moment versus experimental results

Wall Number	Mu (kN*m) Experimental	Theoretical Mu (kN*m)				Theoretical/Experimental			
		TMS 2013	BS 5628	AS 3700	CSA	TMS 2013	BS 5628	AS 3700	CSA
W-1	21.53	19.91	8.98	9.88	22.27	0.92	0.42	0.46	1.03
W-2	20.62	20.66	11.65	13.12	22.69	1.00	0.57	0.64	1.10
W-3	19.66	20.69	11.76	1325	22.72	1.05	0.60	0.67	1.16
W-4	21.31	19.36	9.14	10.04	21.97	0.91	0.43	0.47	1.03
W-5	24.89	22.17	14.78	18.97	23.92	0.89	0.59	0.76	0.96
W-6	25.09	34.21	19.30	20.43	40.20	1.36	0.77	0.81	1.60
W-7	33.11	45.77	32.15	35.47	51.47	1.38	0.97	1.07	1.55
					Mean	**1.07**	**0.62**	**0.70**	**1.21**
					S.D	**0.21**	**0.19**	**0.21**	**0.26**
					COV (%)	**19.66**	**31.37**	**30.39**	**21.73**

Results are summarized in Table 6.7, TMS 2013 and CSA codes provide a good approximation for walls with low strength masonry, and predictions for walls with high strength masonry are overestimated in the experimental results. The remaining codes, BS5628 and AS3700 provide results that differ significantly from the experimental results for both high and low strength masonry, but their predictions show a clear conservative tendency.

6.6 Discussion and conclusions

A main conclusion of the experimental exploration of full-scale testing in ungrouted post-tensioned concrete masonry cantilever walls, was the ability of this structural system to withstand large lateral displacements with limited damage showing their potential to be used in the construction of out of plane walls. Additionally, the following conclusions can be abstracted from this study:

- The wall "rocking" was the most common type of structural behavior observed in all tested walls, accompanied by flexural dominant failure, with a self-centering behavior, and after unloading, the wall returning near to the original position.
- The load-deflection curve in all the tested walls showed a nearly bi-linear approximation with reasonable ductility and pinched loops that are associated with small energy dissipation.
- With higher displacement cycles, in excess of 85% of ultimate load capacity, no crack evidence could be detected with the naked eye. This is accompanied with a low damage level, and its repair requires, labor and materials costs are lower.
- A good linear approximation can been see on the tendon force increment vs displacement curve, in particular for the inelastic state, even threaded bars yield.
- Cyclic and monotonic test have a similar mechanical behavior until failure as evidence in their load-deflection envelope curve.
- The most crucial parameter affecting the ultimate capacity load of post-tensioned cantilever masonry subject to out of plane loads was the masonry strength. However, the change in masonry strength did not have a significant effect on ultimate deflection. Initial prestress had only a significant impact on the ultimate load capacity for an initial prestress value of $35\%f'_m$, the mechanical behavior of cantilever walls for initial prestress values of $15\%f'_m$ and $35\%f'_m$ were very similar and did not differ significantly.
- The self-centering behavior in prestressed cantilever masonry walls contributed to reduce residual displacement caused after unloading the wall, compared to similar reinforced concrete or masonry walls.
- MSJC 2013 and CSA 2014 codes accurately predicted, with a good approximation, the ultimate moment capacity for walls with low strength masonry, although neither codes predicted the flexural capacity for high strength masonry walls accurately.

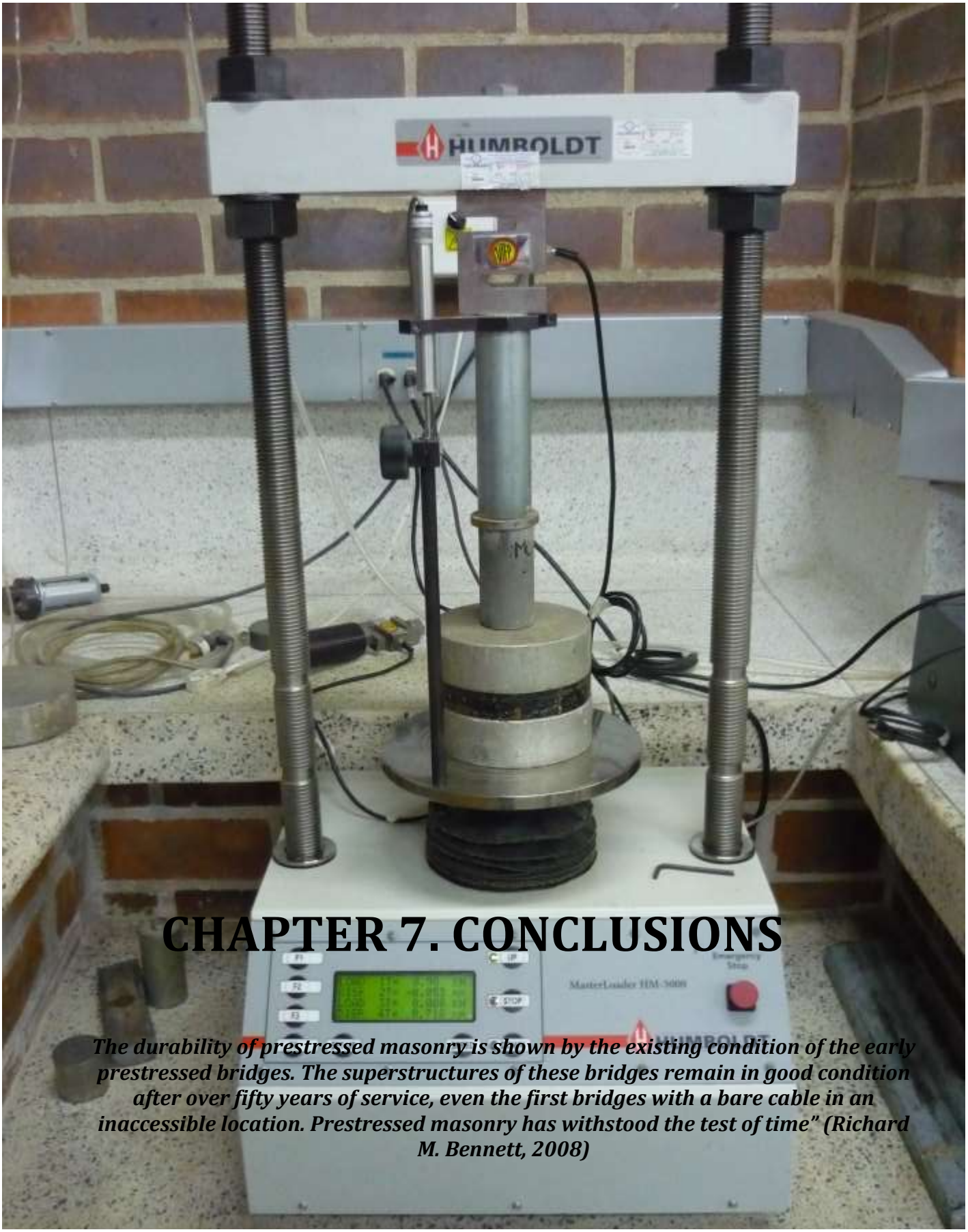

CHAPTER 7. CONCLUSIONS

The durability of prestressed masonry is shown by the existing condition of the early prestressed bridges. The superstructures of these bridges remain in good condition after over fifty years of service, even the first bridges with a bare cable in an inaccessible location. Prestressed masonry has withstood the test of time" (Richard M. Bennett, 2008)

After concluding the experimental and analytical stage of this doctoral thesis, several of the initial questions posed at the beginning of this investigation phase have been answered. There have been several contributions to the knowledge of post-tensioned masonry, as well as the generation of new challenges in the research of this area. Each one of the chapters makes their respective contribution to the solution of a specific problem, each of these solutions remained focused on obtaining an application of prestressing masonry to be implemented in the construction of a full-scale retaining wall prototype.

Ungrouted post-tensioned masonry retaining walls would be a viable alternative both technically and economically and offer the following benefits: safe construction, high strength, easy and fast construction, low maintenance, low construction costs, pleasing aesthetics, and reduced waste, among others. Additionally, a summary of the main conclusions throughout this study are reported below:

- The main findings of previous research in the last four decades about post-tensioned masonry included: increase in cracking and ultimate load, reduced costs, tendon restrain or tendon guide increased the ultimate capacity, has a reasonable ductility, reduced serviceability deflections, after unloading displacement is almost completely restored, improved shear strength, simple to repair, and changed the failure mode for the better.
- Experimental results in the uniaxial compression test of hollow concrete blocks show that the best correlation between the modulus of elasticity and compression strength on the masonry unit is better reflected in the expression $E_b = 450f'_b$. Even so, the tendency observed in the experimental results is not linear as proposed by several masonry codes, but rather slightly curved. The failure mode of hollow concrete blocks was characterized by a diagonal crack, produced by a combination of the low slenderness of the block and the lateral confinement generated by steel load plates. The shape of the stress-strain curve of a hollow concrete block is dependent on the magnitude of maximum compression strength. Stress-strain curve displayed a relatively elastic linear behavior up to about 30% of its maximum strength and a good agreement between the obtained results and the expression proposed by Popovics (1973) for conventional concrete.
- A new analytical expression based on fundamental solid mechanics theory, that meets the equilibrium, deformation compatibility and realistic stress-strain behavior in both elastic and inelastic states, provides a simple and excellent resource to predict the tendon stress increase of prestressed ungrouted masonry beams under bending loads. The remaining code equations offered less accuracy than the proposed expression in unbonded post-tensioned masonry beams at ultimate. The proposed rational expression offers better flexibility due to its simplicity and their better accuracy than studied code equation with the experimental data.
- The inclusion of a deviator block, which serve as a tendon guide at strategic points in the post-tensioned masonry beam, increasing levels of deflection and strength capacity at ultimate flexural state, making the ungrouted and unbonded masonry elements can develop similar structural than grouted and bonded beams.
- For the flexural tests on ungrouted masonry elements, load-midspan deflection curve can be simplified approximately to a bi-linear relation, an approximately first linear elastic region until block separation occurs, followed by an inelastic region with an important stiffness degradation. Ungrouted masonry element exhibited a high deformation and overload capacity prior to bending failure, with concentrated damage only over a small portion of the maximum constant moment zone, and its repair requires lower time, labor and materials costs.
- The wall “rocking” was the most common type of structural behavior observed in all tested ungrouted masonry cantilever walls, with self-centering behavior, i.e after unloading the wall returning near to the original position. As a result of “rocking”, when the wall is deflected it behaves as a rigid body, and the variation of displacement within wall height can be assumed to be linear.
- Secant stiffness of ungrouted post-tensioned masonry tested elements decreases significantly when increasing displacement amplitudes, attributed primarily to the deterioration and permanent deformation of the masonry elements, which follows each load cycle. During cyclic testing, a low energy dissipation capacity was observed. Cyclic and monotonic test for similar ungrouted posttensioned masonry elements have a related envelope mechanical behavior. Residual displacement generated at each load cycle after

unloading tested elements, which are already relatively low due to the "self-centering" mechanism. For each displacement increment, an approximately linear increase in residual displacement was observed.

- Given the constant monitoring of tendon stress during all experimental tests, it was found that unbonded tendons increased only slightly with the applied load before cracking, on the other hand, when block separation occurred, tendon stress increased significantly. Likewise, a good linear approximation can been see on the tendon force increment vs maximum displacement curve, in particular for the inelastic state, even the threaded bars yield.
- Based on the observations made in this study for ungrouted posttensioned masonry elements tested under flexural loads, expressions provides by MSJC-2013 and CSA-2014 codes give a better correlation with the experimental data in flexural capacity at ultimate state.
- Ungrouted post-tensioned masonry building technique, is a promising construction option with great potential to be used on structures that require a certain level of ductility.

CHAPTER 8. FUTURE RESEARCH

"Innovation is a response to a need. If there is no need for innovation it will not happen". (West HWH, 1998)

8.1 Introduction

This section aims to point out some future lines of research derived from this doctoral thesis work, this study serves as a starting point for other researchers, and for practitioners in the field of prestressed masonry.

As is always the case in any research project, it helps to generate new knowledge in a specific area of research, but simultaneously, create new unknowns, explore new ideas, discover new knowledge gaps, and open new research horizons.

8.2 Materials and elements

- From the experimental results of tested beams and walls, it was observed that masonry strength is one of the most important parameters in the mechanical behavior of ungrouted prestressed masonry. Experimental results in this study indicate that the compression masonry strength has an important impact on mechanical behavior of ungrouted post-tensioned masonry subjected to bending stresses. For this reason, there is a need for a new methodology to determine an adequate value of compression masonry strength to be used in the flexural design of ungrouted post-tensioned elements. According to the materials used in its construction (masonry unit and mortar), and considering the geometric properties (shape of the cross section and slenderness), the new methodology will be very useful in optimizing design processes, and better understand the real performance of masonry elements subjected to compressive stresses which are variable through their cross section. Therefore, future research intends to further develop a broader experimental stage and define a new methodology to adjust the coefficient of slenderness proposed for worldwide prestressed masonry codes applicable to ungrouted masonry.
- It requires designing a new masonry shape unit that will maximize the benefits of post-tensioned masonry elements under bending loads. Despite the amount of different shapes of masonry units covered in the market, each of them focuses on meeting a diverse set of architectural and structural needs related to traditional masonry. Prestressed masonry differs from traditional masonry in their mechanical behavior, the long-term structural needs of prestressed masonry requires future research that allows it to obtain a practical new typology of masonry unit, whose shape improves the structural performance of the different elements of ungrouted prestressed masonry subjected primarily to bending stress.
- Mortar, traditionally has been the cementitious material used in the construction of masonry walls, its mechanical properties, durability, workability, and low cost, has enabled mortar to be the leading basic source material for masonry wall building. Unfortunately, the time required in the process of setting and hardening in the mortar decreases labor productivity significantly, which increases the project delivery time and project costs. In order for the ungrouted post-tensioned masonry to fulfill its function as a prefabricated system, a new contact element to replace the mortar like adhesive between masonry units needs to be found. This new material should provide good stress transfer and require shorter setting and curing times. This new material, unlike conventional mortar, does not need to be a cementitious material, since the post-tensioned force applied to masonry guarantees a secure bond between the masonry units.
- Applied loads on anchoring blocks may produce high stresses while prestressed force is applied, for this reason, anchor blocks must be reinforced to withstand the stresses to which it is subjected. Anchor blocks are an essential part of the ungrouted prestressed masonry, and the optimum design of these elements help to improve the functional performance of this structural element. A study that would allow identification of the most appropriate shape and optimal reinforcement of anchor blocks would be useful in the implementation and future marketing of ungrouted post-tensioned masonry. All requirements of this anchor block must be compatible with mass production, like any other pre-cast material, in such a way as to allow its industrialization.
- Create wide experimental tests based on controlled strain in order to establish the values of compressive strain of masonry associated with maximum strength and the ultimate capacity.

8.3 Analyses and design methods

- Numerical models that currently exist are used to mathematically represent the mechanical behavior of grouted prestressed masonry with very good results. These modelling tools are useful to investigate the structural behavior of prestressed masonry through the adoption of computational techniques and analytical tools, that significantly reduce the time and cost of the experimentation in a laboratory. By the constitutive laws that regulate these numerical models, the vast majority of them may not be

appropriate for the simulation of ungrouted post-tensioned masonry, primarily because the strain compatibility hypothesis is not properly fulfilled. This is why it is necessary to develop a new numerical model governed by new constitutive laws that faithfully represent the mechanical behavior of ungrouted post-tensioned masonry.

- In view of the absence of worldwide standards in ungrouted post-tensioned masonry, there is a need to develop a simplified design and analysis methodology for ungrouted prestressed elements subjected to a series of static and dynamic bending loads.
- As well as major parts of the American continent, Colombia and Chile do not have specific regulation for the analysis and design of post-tensioned masonry elements. It is for this reason that after observing the structural and constructive advantages of the post-tensioned masonry in this study, it is necessary to develop the first version with specific regulations for the Chapter Post-tensioned Masonry. This should be added into the Colombian and Chilean structural earthquake code regulations.

8.4 Behavior of the structural system

- Although, several studies confirm that prestress increases shear strength in concrete elements, to date, there is a limited number of research projects working on this issue for prestressed masonry, and most of them are focused on grouted elements. A full investigation into shear strength of ungrouted post-tensioned masonry will be very helpful in the future to complement this doctoral thesis project. It is also necessary to develop research to study the incidence of main design parameters in shear strength of post-tensioned masonry elements in bending, and identify which of these design factors control the structural behavior of a post-tensioned masonry element in which shear strength predominates.
- Prestress force is vital to the mechanical behavior of ungrouted post-tensioned masonry. Short-term losses depend on prestress techniques, and they can be controlled depending on the technique used, or re-tightening the structural element as many times as is necessary. Long-term prestress losses due to material properties, such as creep and shrinkage, depend primarily on environmental factors, the initial prestressing force, and material properties. Long-term losses are not easily controlled, and currently there is no specific information on long-term forces in ungrouted post-tensioned masonry. A careful analysis of the effects of long-term losses on ungrouted prestressed masonry is essential to guarantee the proper operation of ungrouted post-tensioned masonry over time.
- There is very little technical information available to support the study of the dynamic behavior of ungrouted post-tensioned masonry, likewise, expressions used to characterize dynamic behavior of structural elements have been developed for elements with grouted or homogeneous solid sections. It would be appropriate to focus on developing a new study of dynamic behavior of ungrouted post-tensioned masonry elements to establish the incidence of design parameters on dynamic behavior and the correlation and differences between dynamic behavior of grouted and ungrouted masonry elements.

8.5 Construction procedure

- Masonry diaphragm walls have been shown to be an excellent alternative for the building of high walls that are subject to large out of plane loads, and therefore require a greater slenderness ratio and section modulus than the traditional cavity wall or single section wall. New research to explore the further potential of this type of construction focuses on ungrouted masonry, it would be very useful to promote this type of section in structures with high demand on lateral loads.
- The use of soil anchorages increase the structural efficiency and stability of the retaining walls. The combined use of post-tensioned masonry and soil anchorage could significantly improve the lateral load strength of retaining walls and shallow foundations. For this reason, it would require further research to determine the benefits of soil anchorage on the internal and external stability of retained walls built with ungrouted post-tensioned masonry.

REFERENCES

ABNT NBR 15812-1. (2010). Associação Brasileira de Normas Técnicas: Alvenaria estrutural – Blocos cerâmicos. Parte 1: Projetos. Rio de Janeiro. Brazil.

ABNT NBR 15961-1. (2011). Associação Brasileira de Normas Técnicas: Alvenaria estrutural - Blocos de concreto - Parte 1: Projetos. Rio de Janeiro. Brazil.

ACI (American Concrete Institute). (2002). "Building code requirements for reinforced concrete." ACI 318-02, Farmington Hills, Mich.

ACI 530-05/ASCE 5-05/TMS 402-05 (2005) American Concrete Institute. Building Code Requirements for Masonry Structures. Detroit, United States of America.

Al-Gahtani N.Z., and Fairbairn D.R. (1995) "Prestressed brick/masonry slabs and retaining wall". The fourth Saudi Engineering Conference. Volume II.

Allen, L.N. (1986). "Post tensioned Brickwork at Rushden Fire Station". Engineers File Note No.1. 372 (21) F. The Brick Development Association, United Kingdom.

AS 3700-2011. (2011). Masonry Structures. Standards Australia International, Sydney, NSW, Australia.

ASCE. (2006). "Seismic rehabilitation of existing buildings." ASCE/SEI 41- 06, Reston, VA.

Asociación Colombiana de Ingeniería Sísmica. (2010). Normas Colombianas de Diseño y Construcción Sismo Resistente NSR-10. Bogotá, Colombia.

Au, F.T.K., and Du, J.S. (2004). "Prediction of ultimate stress in unbonded prestressed tendons." Mag. Concrete Res., Vol. 56, N°1, pp. 1–11.

Baker L.R. (1949). "Plastic theory of design for ordinary reinforced and prestressed concrete including moment redistribution in continuous members". Mag Concrete Res., Vol. 1, N°2, pp. 57–66.

Baker, L.R. (1981). "The flexural action of masonry structures under lateral load". PhD Thesis, Deakin University, Australia.

Baqi, A. and Bhandari, N.M. (2007). "Postcracking Behavior of Prestressed Masonry in Flexure". Journal of Structural Engineering, Vol. 133, No. 4.

Baqi, A., Bhandari, N.M., and Trikha, D.N. (1999). "Experimental study of prestressed masonry flexural elements". Journal of Structural Engineering, Vol. 125, N°3, pp. 245–254.

Barbosa, C.S., and Hanai, J.B. (2009). "Strength and deformability of hollow concrete blocks: correlation of block and cylindrical sample test results". Ibracon Structures and Materials Journal, Vol. 2, N°1, pp. 85-99.

Barbosa, C.S., and Hanai, J.B. (2006). "Resistência e deformabilidade de blocos vazados de concreto e suas correlações com as propriedades mecânicas do material constituinte" (in Portuguese). Cadernos de Engenharia de Estruturas, Vol. 8, N°34, pp. 45-74.

Bean, J.R. and Schultz, A.E. (2011). "Finite-Element Models for Slender, Posttensioned Masonry Walls Loaded Out-of-Plane." J. Struct. Eng. Vol. 137, N°12, pp. 1489-1498.

Bean, J.R. (2003). "Experimental Verification of the Resistance of Masonry Walls Under Transverse Loads." M.S. Thesis, University of Minnesota, 140 pp, Minneapolis, MN.

Bean, J.R. (2007). "Mechanics and Behavior of Slender, Post-tensioned Masonry Walls to Transverse Loading." Ph.D. Thesis, University of Minnesota, Minneapolis, MN.

Bean, J.R. and Schultz, A.E. (2003). "Flexural Capacity of Posttensioned Masonry Walls: Code Review and Recommended Procedure". Post-Tensioning Institute Journal, Vol 1, N°1, pp. 28-44, Farmington Hills, MI.

Bean, J.R. and Schultz, A.E. (2010) "Design Provisions for Post Tensioned Masonry Walls Loaded Out-of-Plane". The Masonry Society Journal, Vol. 28, N°2, pp. 9-26.

Bennett, R.M. (2008). "The First United States Prestressed Masonry Structures". The Masonry Society Journal, Vol. 26, N°2, pp. 67-72.

Biggs, D.T. (2001). "Planning projects to use prestressed masonry". Structures 2001, pp. 1-8.

Biggs, D.T. (2003). “Putting prestressed masonry to use.” Masonry Magazine, Vol. 42, N°10.

Bonett, R.L., and Urrego, H. (2008). “Post-tensioned concrete brick masonry without mortar joint”. The 14th World Conference on Earthquake Engineering, Beijing, China.

Bradshaw, R.E., Drinkwater, J.P., and Bell, S.E., (1982). “A Multi-Purpose Farm Building Incorporating Prestressed Brickwork Diaphragm Walling”. Proceedings of the British Ceramic Society, Load-Bearing Brickwork (7), Vol. 30, pp. 308-315.

BS 5628-2 (2005), “Code of Practice for the Use of Masonry. Part 2: Structural Use of Reinforced and Prestressed Masonry.” British Standards Institution, London, United Kingdom.

Campbell, T. I., and Chouinard, K. L. (1991). “Influence of nonprestressed reinforcement on the strength of unbonded partially concrete members.” ACI Struct. J., Vol. 88, N°5, pp. 546–551.

CEN, European Committee for Standardization. (1995). Eurocode 6: “Design of masonry structures. Part 1-1: General rules for reinforced and unreinforced masonry structures.” EN1996-1-1:1995, Brussels, Belgium.

CEN, European Committee for Standardization. (2005). Eurocode 6: “Design of masonry structures. Part 1-1: General rules for reinforced and unreinforced masonry structures.” EN1996-1-1:2005, Brussels, Belgium. 131p.

Crigler, J. (1991). “Home of the future built with post-tensioned masonry”. VSL News, VSL Eastern Springfield Virginia, Issue two, pp. 11

CSA S304.1-14. (2014). “Design of masonry structures”. Canadian Standards Association, Mississauga, Ontario, Canada.

Curtin, W.G. and Phipps, M.O. (1982). “Prestressed Masonry Diaphragm Walls". Proceedings of the Sixth International Brick Masonry Conference. Rome, ANDIL, pp. 971-980.

Curtin, W.G. (1986). “Post-tensioning opens brickwork frontiers”. Contract Journal. Vol 333, N° 558, pp. 26-27.

Curtin, W.G. (1990). “Prestressed and reinforced brickwork”. The Structural Engineer, Kerensky conference volume, Glasgow, United Kingdom.

Curtin, W.G. and Phipps, M. (1982). “Prestressed Masonry Diaphragm Walls”. Proceedings of 6th International Brick Masonry Conference, ed. Laterconsult, Rome, pp. 971-980.

Curtin, W.G., Shaw, G., Beck, J.K. and Bray, W.A. (1982). “Modern philosophy of structural brickwork design and change of outlook for the industry”. Proceedings of the 6th International Masonry Conference. ANDIL, Rome, pp. 939-948.

Curtin, W.G., Shaw, G., and Howard, J. (1991). "Structural Testing of a Post-Tensioned Brick Fin Wall," 9th International Brick/Block Masonry Conference, Proceedings, Berlin, Germany, pp. 333-341.

Dawe, J.L. and Aridru, G.G. (1993). "Prestressed Concrete Masonry Walls Subjected to Uniform Out-Of-Plane Loading". Canadian Journal of Civil Engineering, Vol. 20, N° 6, pp. 969-979.

Devalapura, R.K., Krause, G.L., Sweeney, S.C., Littler, D., Stabb, E. and Tadros, M.K. (1997). “Development of an Innovative Post-tensioning System for Prestressed Clay Brick Masonry Walls”. Construction Engineering Research Laboratories. US Army Corps of Engineers. United States of America.

Drake, C.R. (2004). “Out-of-plane behavior of slender post-tensioned masonry walls constructed using restrained tendons”. M.S. Thesis, University of Minnesota, 142 pp.

Drinkwater, J.P., and Bradshaw, R.E. (1982). “Reinforced and Prestressed Masonry in Agriculture”. Reinforced and Prestressed Masonry, Thomas Telford Ltd., London, England, pp. 89-96.

Drysdale, R.G., Hamid, A.A., and Baker, L.R. (1994). “Masonry Structures: Behavior and Design”. New Jersey: Prentice Hall.

Drysdale, R.G., Hamid, A.A., and Baker, L.R. (1999). "Masonry Structures: Behavior and Design". Prentice Hall, Inc.

Du, J.S. and Liu, X.L. (2003). "Research on the variations of unbonded prestressed tendon stresses based upon the structural deformation." China Civ. Eng. J., Vol. 36, N°8, pp. 12–19.

FEMA. (2006). "Techniques for the seismic rehabilitation of existing buildings." FEMA 547-06, Washington, DC.

Fisher, K., Haseltine, B.A., and Templeton, W. (1989). "Structural Testing of Brickwork Retaining Walls". Proceedings of the Fifth Canadian masonry Symposium, Vancouver, B.C., pp. 827-836.

Foster, D. (1970). "Design and Construction of Prestressed Brickwork Water Tank". Proceedings of the Second International Brick Masonry Conference, Stoke-on-Trent, England, pp. 287-294.

Foti, D. and Monaco, P. (2000) "Post-tensioned masonry: state of the art". Progress in Structural Engineering and Materials, Vol. 2, pp. 311-318.

Ganz, H.R. (1990). "Post-tensioned Masonry Structures". VSL International Ltd, Berne, Switzerland, 35 p.

Ganz, H.R. (1990b). "New post-tensioning system increases strength and height potential of masonry structures". VSL News, N° 1, pp. 4-5.

Ganz, H.R. (2003). "Post-tensioned Masonry Around the World". Concrete International, Vol. 25, N° 1, pp. 65-69.

García, J.M., Ledezma, C. and Bonett, R. (2013). "Analytical Model for Compression Behavior of Hollow Concrete Blocks" (in Spanish). Revista de la Construcción, Vol. 12, N°3, pp. 76-82.

Garrity, S.W. and Garwood, T.G. (1990). "The Construction and Testing of a Full-Scale Prestressed Clay Brickwork Diaphragm Wall Bridge Abutment," Proceedings of the British Masonry Society, N° 4, July, pp. 24-29.

Garwood, T.G. (1983). "The Construction and Test Performance of Four Prestressed Brickwork Beams". The 8th International Symposium on Loadbearing Brickwork, London.

Garwood, T.G. (1984). "The Flexural Behaviour of Fully Prestressed and Partially Prestressed 'Pier-Bond' Brickwork Beams". International Symposium on Reinforced and Prestressed Masonry, Edinburgh, pp. 411-426.

Garwood, T.G. (1988). "A Comparison of the Behavior of Reinforced, Prestressed and Partially Prestressed Brickwork Beams," Proceedings of the British Masonry Society, N° 2, pp. 76-81.

Ghallab, A. (2013). "Calculating ultimate tendon stress in externally prestressed continuous concrete beams using simplified formulas". Eng. Struct., 46 (2), 417–430.

Guiglia, M., Taliano, M. and Debernardi, P.G. (2012). "Calculation of the ultimate stress of unbonded tendons in prestressed concrete members considering the rotation capacity". Magazine of Concrete Research. Vol. 65, N° 1, pp. 14-26.

Haach, V.G., Vasconcelos, G., Lourenço, P.B. and Mohamad, G. (2010). "Influence of the mortar on the compressive behavior of concrete masonry prisms" (in Portuguese). Revista da Associação Portuguesa de Análise Experimental de Tensões, Vol. 18, pp. 79-84.

Halsall, R. (1986). "Post tensioned Brickwork at Rushden Fire Station". Engineers File Note No.1. 372 (21) F. The Brick Development Association, United Kingdom.

Hanlon, J.R.G. (1970). Concrete masonry in New Zealand: Prestressed concrete masonry. Concrete, The Concrete Society (England). Vol. 4, N°9, pp. 356-358.

Harajli, M.H. (1990). "Effect of span-depth ratio on ultimate steel stress in unbonded prestressed concrete members." ACI Struct. J., Vol. 87, N°3, pp. 305–312.

Harajli, M.H. (2006). "On the stress in unbonded tendons at ultimate: Critical assessment and proposed changes." ACI Struct. J., Vol. 103, N°6, pp. 803–812.

Harajli, M.H. and Kanj, M.Y. (1991). "Ultimate flexural strength of concrete members prestressed with

unbonded tendons." ACI Struct. J., Vol. 88, N°6, pp. 663–673.

Haseltine, B.A. (1982). "Codification of Reinforced and Prestressed Masonry Design and Construction," Reinforced and Prestressed Masonry, Proceedings, Thomas Telford Ltd., London, England, pp. 115-121.

Hassanli, R. (2015). "Behavior of unbonded post-tensioned masonry walls." Ph.D. thesis, School of Natural and Built Environment, Univ. of South Australia, SA, Australia.

Hassanli, R., ElGawady, M. and Mills, J. (2015). "Strength and Seismic Performance Factors of Posttensioned Masonry Walls". Journal of Structural Engineering, Vol. 141, N° 11.

He, Z. and Liu, Z. (2010). "Stresses in External and Internal Unbonded Tendons: Unified Methodology and Design Equations". Journal of Structural Engineering, Vol. 136, No. 9, pp. 1055-1065.

Hognestad, E. (1951). "Study of combined bending and axial load in reinforced concrete Members". Illinois, The Reinforce Concrete Research Council of the Engineering Foundation.

Ismail, N. and Ingham, J.M. (2012). "Cyclic Out-of-Plane Behavior of Slender Clay Brick Masonry Walls Seismically Strengthened Using Posttensioning". Journal of Structural Engineering, Vol. 138, No. 10, pp. 1255-1266.

Ismail, N., Laursen P., Schultz A. and Ingham, J.M. (2011). "Cyclic out of Plane Behaviour of Post Tensioned Clay Brick Masonry". The 11th North American Masonry Conference.

Jaafar, S., Thanoon, W., Amad, N., Abdulkadir, R. and Abang, A. (2006). "Strength correlation between individual block, prism and basic wall panel for load bearing interlocking mortarless hollow block masonry". Construction and Building Materials, Vol. 20, N°7, pp. 492–498.

Jansen, P., and Tilly, G. (1999). "Prestressing Understrength Walls and Parapets". Structural Faults and Repairs, 8th International Conference and Exhibition. London.

Kaushik, H.B., Rai, D.C. and Jain, S.K. (2007). "Stress-strain characteristics of clay brick masonry under uniaxial compression". Journal of Materials in Civil Engineering, Vol 19, N°9, pp. 728-739.

Korany, Y., Drysdale, R. and Chidiac, S. (2001). "Retrofit of unreinforced masonry buildings: The state-of-the-art." Proceedings of the 9th Canadian Masonry Symposium, Fredericton, New Brunswick, Canada.

Laursen, P.T. (2002). "Seismic Analysis and Design of Post-tensioned Concrete Masonry Walls." PhD. Thesis, University of Auckland. New Zealand.

Laursen, P.T. and Ingham, J.M. (1999). "Design of prestressed concrete masonry walls." Journal of the Structural Engineering Society of New Zealand, Vol. 12, N° 2, pp. 21-39.

Laursen, P.T. and Ingham, J.M. (2001). "Seismic resistance of prestressed concrete masonry shear walls", 2001 Structures Congress and Exposition, Washington, D.C.

Laursen, P.T. and Ingham, J.M. (2004). "Structural Testing of Large-Scale Posttensioned Concrete Masonry Walls". Journal of Structural Engineering, Vol. 130, N° 10, pp. 1497–1505.

Lazzarini D.L., Laursen, P.T. and McDaniel, C. (2010). "Out-of-plane seismic performance of unreinforced masonry walls retrofitted with unbonded post-tensioning tendons". Masonry Research. TMS E-Newsletter. The Masonry Society Publications, pp. 4-4.

Lissel, S.L. (2001). "Behaviour and Design of CFRP Post-Tensioned Masonry Diaphragm Walls". PhD Thesis, University of Calgary, Alberta, Canada.

Lissel, S.L., Shrive, N.G. and Gilliland, J. (2005). "Design of carbon fibre reinforced polymer post-tensioned masonry diaphragm retaining walls". Canadian Journal of Civil Engineering, Vol 32, N°3, pp. 579-594.

Lissel, S.L., Tilleman, D., Sayed-Ahmed, E.Y. and Shrive, N.G. (1999). "Testing of Diaphragm Walls Post-Tensioned with Carbon Fibre Reinforced Polymers (CFRP)," 8th North American Masonry Conference, Proceedings, Austin, USA, 12p.

MacGregor, R.J.G. (1989). "Strength and ductility of externally posttensioned segmental box girders." Ph.D. Thesis, University of Texas at Austin, Austin, Tex.

Marzahn G.A. (1998). "The Shear Strength of Dry-Stacked Masonry Walls". LACER N°3, pp. 247-262.

Masonry Standards Joint Committee. (2013). Building Code Requirements for Masonry Structures. ACI 530-13 / ASCE 5-13 / TMS 402-13, The Masonry Society, Boulder, CO, 2013.

Mattock, A.H., Yamazaki, J. and Kattula, B.T. (1971). "Comparative study of prestressed concrete beams, with and without bond." ACI Struct. J., Vol. 68, N°3, pp. 116–125.

Mohamad, A., Farid, B.J. and Al-Janabi, A.I.M. (1990). "Stress-Strain Relationship for concrete in compression made of local materials". Journal of King Saud University - Engineering Sciences, Vol. 2, pp. 183-194.

Mojsilovic, N. and Marti, P. (2000). "Load tests on post-tensioned masonry walls". TMS Journal. The Masonry Society Publications. July, pp. 65-70.

Montague, T.I. and Phipps, M.E. (1984). "The Behaviour of Post-tensioned Masonry in Flexure and Shear", International Symposium on Reinforced and Prestressed Masonry, Edinburgh.

MSJC 2002. (2002). "Building code requirements for masonry structures." ACI 530-02, ASCE 5-02, TMS 402-02.

MSJC 2005. (2005). "Building code requirements for masonry structures." ACI 530-05, ASCE 5-05, TMS 402-05.

MSJC 2013. (2013). "Building code requirements for masonry structures." ACI 530-13, ASCE 5-13, TMS 402-13.

Mutsuyoshi, H., Tsuchida, K., Matupayont, S. and Machida, A. (1995). "Flexural behavior and proposal of design equation for flexural strength of externally PC members." Proc., JSCE, 508(26), pp. 67–76.

Naaman, A.E. and Alkhairi, F.M. (1991). "Stress at ultimate in unbonded post-tensioning tendons: Part 2—Proposed methodology." ACI Struct. J., Vol. 88, N°6, pp. 683–692.

Nazir, N.A. and Hart, G.C. (2001). "Analytical Stress Strain Curves for Confined and Reinforced Concrete Masonry," TMS Journal, Vol. 19, N°1, pp. 9-20.

Neis, V.V., Chow, T., and Ritchie, L. (1989). "Behavior of Prestressed Masonry Beams Under Static Loading," 5th Canadian Masonry Symposium, Proceedings, Vancouver, Canada, pp. 177-186.

Ng, L.Y, and Cerny, L. (1985). "Post-Tensioned Concrete Masonry Beams". Proceedings of the Third North American Masonry Conference, Arlington, Texas, pp. 77.1-77.12.

NTC 4024. (2001). Prefabricados de concreto: Muestreo y ensayo de prefabricados de concreto no reforzados, vibro-compactados". Norma Técnica Colombiana. Bogotá, Colombia.

NTC 4026. (1997). Ingeniería Civil y Arquitectura. Unidades (Bloques y Ladrillos) de concreto, para mampostería estructural. Norma Técnica Colombiana. Bogotá, Colombia.

Nwofor, T.C. (2012). "Experimental determination of the mechanical properties of clay brick masonry". Canadian Journal on Environmental, Construction and Civil Engineering, Vol. 3, N°3, pp. 127-145.

NZS 3101 (1995). "Concrete Structures Standard". Standards New Zealand, Wellington, New Zealand.

NZS 4320 (2004). "Design of Reinforced Concrete Masonry Structures." Standards New Zealand, Wellington, New Zealand.

Ozkul, O., Nassif, H., Tanchan, P. and Harajli, M. (2008). "Rational Approach for Predicting Stress in Beams with Unbonded Tendons". ACI Struct. J., Vol. 105, N°3, pp. 338-347.

Pannell, F.N. (1969). "The Ultimate Moment of Resistance of Unbonded Prestressed Concrete Beams." Magazine of Concrete Research, Vol. 21, N°66, pp. 43-54, Thomas Telford Ltd, United Kingdom.

Parsekian, G.A., Souza, P.R.A., Franco, L.S. and Barros, M.M.B. (2007). "Cases of Prestressed Masonry in Brazil". Proceedings of the 10th North American Masonry Conference, Saint Louis, USA. The Masonry Society, Vol. 1, pp. 1-12.

Pedreschi, R. (2004) “Structural innovation in pre-stressed brickwork”. Construction and Building Materials, Vol. 18, N° 2, pp. 99–109.

Pedreschi, R. (2013). “A feasibility study of post-tensioned stone for cladding”. Construction and Building Materials, Vol. 43, pp. 225–232

Phipps, M. and Al-Safi, S. (2001). “Post-Tensioned Prestressed Masonry Columns”. Structures 2001, pp. 1-15.

Phipps, M.E. (1992). “The Codification of Prestressed Masonry Design.” Proceedings of the 6th Canadian Masonry Symposium, Saskatoon, Saskatchewan, Canada, pp. 561-571.

Phipps, M.E. and Montague, T.I. (1987). "The testing of plain and pre-stressed concrete blockwork beams and walls of geometric cross section," Masonry International, Vol. 1, N° 3, pp. 96-99.

Plowman, J.M., Sutherland, R.J.M. and Couzens, M.L. (1967). “The Testing of Reinforced Brickwork and Concrete Slabs Forming Box Beams”. The Structural Engineer, Vol. 45, N° 11, pp. 379-394.

Popovics, S. (1973). “A numerical approach to the complete stress-strain curve of concrete”. Cem. Concr. Res, Vol. 3, N°5, pp. 583-599.

Ramaswamy, G.S. (1953). “Prestressing and Assembly of Stone Blocks by Post-Tensioning”. Indian Concrete Journal, Vol. 27, N°12, pp. 450-451.

Robertson, K. and Scott, P. (2014). “Armory Park Elderly Housing Project”. Structure Magazine.

Roberts-Wollmanm, C.L. and Kreger, M.E. (2005). “Stresses in external tendons at ultimate.” ACI Struct. J., Vol. 102, N°2, pp. 206–213.

Robson, I.J., Hulse, R., Ambrose, R. and Morton, J. (1983). “Performance of Post-Tensioned Brickwork Beams Under Service and Ultimate Load Conditions”. Proceedings of 3rd Canadian Masonry Conference, Paper N° 14.

Rosenboom, O.A. and Kowalsky, M.J. (2003) “Investigation of alternative details for seismic design of post-tensioned clay masonry walls.” Proceedings of the 9th North American Masonry Conference, Clemson, South Carolina, pp. 475-486.

Rosenboom, O.A. and Kowalsky, M.J. (2004). “Reversed in-plane cyclic behavior of posttensioned clay brick masonry walls”. Journal of Structural Engineering. Vol. 130, N° 5, pp. 787-798.

Roumani, N., and Phipps, M.E. (1983). "The Shear Strength of Prestressed Brickwork Sections" 8th International Symposium on Loadbearing Brickwork, British Ceramic Society, London.

Roumani, N. and Phipps, M.E. (1985). “The Shear Strength of Prestressed Brickwork I and T Sections”, Proceedings of the 7th International Brick Masonry Conference, Melbourne, Australia, Vol. 2, pp. 1001-1014.

Roumani, N., and Phipps, M.E. (1986). "The Shear Strength of Prestressed Brickwork I Sections," Proceedings of the British Masonry Society, Vol. 1, pp. 110-113.

Roumani, N. and Phipps, M.E. (1988). “The Ultimate Shear Strength of Unbonded Prestressed Brickwork I and T Section Simply Supported Beams”. Proceedings of the British Masonry Society, N° 2, pp. 82-84.

Ryu, D, Wijeyewickrema, A.C. ElGawady, M.A. and Madurapperuma, M.A. (2014). “Effects of Tendon Spacing on In-Plane Behavior of Posttensioned Masonry Walls”. Journal of Structural Engineering, Vol. 140, N° 4.

Sargin, M., Ghosh, S.K., and Handa, V.K. (1971). “Effect of lateral reinforcement upon the strength and deformation properties of concrete”. Mag. Concrete Res, Vol. 23, N°75-76, pp. 99-110.

Schultz, A.E. and Scolforo, M. (1991). “An overview of prestressed masonry”. TMS Journal, The Masonry Society, Vol. 10, N° 1, pp. 6-21.

Shafii, F. (1994). “Shear Behaviour of Post-Tensioned Brickwork Cantilever Fin Walls”. PhD Thesis, University of Sheffield, United Kingdom.

Shafii, F. and Hobbs (1996). “Experimental Modelling for the Investigation of Shear in Post-tensioned Brickwork Cantilever Fin Walls”. Conference on

Computational Mechanics and Testing, Wessex University, United Kingdom.

Shaw, G. (1988). "Modern use of Reinforced and Prestressed Masonry". Proceedings of the 8th International Brick/Block Masonry Conference, Dublin, Ireland, Vol. 4, pp. 1551-1562.

Shaw, G., Curtin, W.G., Priestly, C.L. and Othick, G.J. (1988). "Prestressed channel section masonry walls". The Structural Engineer, 66, pp. 117-120.

Shrive, N.G. (1988). "Post-Tensioned Masonry-Status & Prospects". Annual Conference of the CSCE, Proceedings, Calgary, Canada, pp. 679-696.
SIA V177 (1995). Masonry (in German). Swiss Standard, Swiss Society of Engineers and Architects (SIA), Zurich, 52 p.

Sinha, B.P. (2002). "Development and potential of structural masonry". Seminário sobre Paredes de Alvenaria, P.B. Lourenço & H. Sousa, Porto, Brazil.

Sinha, B.P. (1994). "Comparative Performance of Reinforced and Prestressed Brickwork Pocket-Type Retaining Walls in Shear". The 10th International Brick/Block Masonry Conference, Proceedings, Calgary, Canada, pp. 423-430.

Sivaleepunth, C., Niwa, J., Diep, B.K., Tamura, S. and Hamada Y. (2006). "Prediction of tendon stress and flexural strength of externally prestressed concrete beams". Doboku Gakkai Ronbunshuu E [J JSCE]. Vol. 62, N° 1, pp. 260–73.

Smith, G.M. and Young, L.E. (1955). "Ultimate Theory. Ultimate theory in flexure by exponential function". Journal of the American Concrete Institute, Vol. 52, N°11, pp. 349–359.

Subasic, C.A. (2001). "A case for prestressed masonry." Masonry Construction, pp. 30-36.

Torres, J. (2001). "Estabilidad Estructural de Elementos Postensados y su Aplicación en Vivienda de Interés Social" (in Spanish). Bogotá-Colombia, 11 p.

Urrego, H. and Bonett, R.L. (2011). "Performance of post-tensioned dry-stacked masonry". The 11th North American Masonry Conference, Minneapolis, MN.

Walker, P.J. (1987). "A study of the behavior of partially prestressed brick work beams". PhD Thesis, Department of Civil Engineering and Building Science. University of Edinburgh, Scotland.

Walker, P.J. and Sinha, B.P. (1985). "Behaviour of Partially Prestressed Brickwork Beams". Proceedings of the 7th International Brick Masonry Conference, Melbourne, Australia, pp. 1015-1029.
Walker, P.J. (1987). "A Study of the Behaviour of Partially Prestressed Brickwork Beams". Ph. D. Thesis, Department of Civil Engineering and Building Science, The University of Edinburgh, Scotland.

Wallace, M. (1999). "Post-tensioned masonry slashes the need for grout". The Aberdeen Group, a division of Hanley-Wood, Inc. Publication #M980015.

Wang, J.Q., Liu, Z. and Lu, Z.T. (2005). "Stress increment of prestressing tendons based on deflection for unbonded or external prestressed beams." J. Southeast Uni. Vol. 35, N°6, pp. 915–919.

Wee, T.H., Chin, M.S., and Mansur, M.A. (1996). "Stress-strain relationship of high-strength concrete in compression". Journal of Materials in Civil Engineering, Vol. 8, N° 2, pp. 70-76.

Wight, G.D. (2006). "Seismic Performance of a Post-tensioned Concrete Masonry Wall System." PhD. Thesis, University of Auckland. New Zealand.

Wight, G.D. and Ingham, J.M. (2008). "Tendon Stress in Unbonded Posttensioned Masonry Walls at Nominal In-Plane Strength". Journal of Structural Engineering, Vol. 134, No. 6, pp. 938-946.

Wight, G.D. and Ingham, J.M. (2008). "Tendon Stress in Unbonded Posttensioned Masonry Walls at Nominal In-Plane Strength". J. Struct. Eng., pp. 938-946.

Wight, G.D., Ingham, J.M. and Kowalsky, M.J. (2006). "Shaketable testing of rectangular post-tensioned concrete masonry walls". ACI Struct. J., Vol. 103, N°4, pp. 587–595.

Wight, G.D., Ingham, J.M. and Kowalsky, M.J. (2007a). "Direct Displacement-Based Seismic Design of Unbonded Post-Tensioned Masonry Walls". ACI Structural Journal, Vol. 104, N° 5, pp. 560-569.

Wight, G.D., Kowalsky, M.J. and Ingham, J.M. (2007b). “Shake table testing of posttensioned concrete masonry walls with openings”. Journal of Structural Engineering, Vol. 133, N° 11, pp. 1551–1559.

Wight. G.D., Ingham, J.M., and Wilton, A. (2007c). “Innovative seismic design of a post-tensioned concrete masonry house”. Canadian Journal of Civil Engineering, Vol. 34, pp. 1393–1402.

Williams, E.O.L. and Phipps, M. (1982). ”'Bending Behaviour of Prestessed Masonry Box Beams”, Proceedings of the 6th International Brick Masonry Conference, ed. Laterconsult, Rome, pp. 981-994.

Woodham, D.B. (2001). “Construction and monitoring of Post-tensioned masonry sound walls”. Atkinson-Noland & Associates, Inc. Colorado Department of Transportation, Denver, United States of America, 26p.

Woodham, D.B. and Hamilton, H.R. (2003). “Monitoring prestress losses in posttensioned concrete masonry”. Proceedings of the 9th North American Masonry Conference, Clemson, South Carolina, pp. 487-498.

Yaginuma, Y. (1995). “Non-linear analysis of ultimate flexural strength of beams with external tendons.” J. Prestressed Concr., Vol. 37, N°3, pp. 54–65.

Yang, K. H. and Kang, T. H. K. (2011). “Equivalent strain-distribution factor for unbonded tendon stress at ultimate”. ACI Struct. J., Vol. 108, N° 2, pp. 217-226.